The Depositional Record
The journal of the International Association of Sedimentologists
Open Access

ORIGINAL RESEARCH ARTICLE

Intercontinental correlation of organic carbon and carbonate stable isotope records: evidence of climate and sea-level change during the Turonian (Cretaceous)

IAN JARVIS*, JOÃO TRABUCHO-ALEXANDRE†,‡, DARREN R. GRÖCKE†, DAVID ULIČNÝ§ and JIŘÍ LAURIN§

*Department of Geography and Geology, Kingston University London, Kingston upon Thames, KT1 2EE, UK
†Department of Earth Sciences, Durham University, Durham, DH1 3LE, UK
‡Institute of Earth Sciences, Utrecht University, Budapestlaan, 43584 CD, Utrecht, Netherlands
§Institute of Geophysics, Academy of Sciences of the Czech Republic, 141 31, Prague, Czech Republic

Keywords
Carbon isotopes, chemostratigraphy, climate change, Cretaceous, oxygen isotopes, pCO_2, sea-level change.

Manuscript received: 3 August 2015; Accepted: 14 December 2015

The Depositional Record 2015; 1(2): 53–90

doi: 10.1002/dep2.6

ABSTRACT

Carbon ($\delta^{13}C_{org}$, $\delta^{13}C_{carb}$) and oxygen ($\delta^{18}O_{carb}$) isotope records are presented for an expanded Upper Cretaceous (Turonian–Coniacian) hemipelagic succession cored in the central Bohemian Cretaceous Basin, Czech Republic. Geophysical logs, biostratigraphy and stable carbon isotope chemostratigraphy provide a high-resolution stratigraphic framework. The $\delta^{13}C_{carb}$ and $\delta^{13}C_{org}$ profiles are compared, and the time series correlated with published coeval marine and non-marine isotope records from Europe, North America and Japan. All previously named Turonian carbon isotope events are identified and correlated at high-resolution between multiple sections, in different facies, basins and continents. The viability of using both carbonate and organic matter carbon isotope chemostratigraphy for improved stratigraphic resolution, for placing stage boundaries, and for intercontinental correlation is demonstrated, but anchoring the time series using biostratigraphic data is essential. An Early to Middle Turonian thermal maximum followed by a synchronous episode of stepped cooling throughout Europe during the Middle to Late Turonian is evidenced by bulk carbonate and brachiopod shell $\delta^{18}O_{carb}$ data, and regional changes in the distribution and composition of macrofaunal assemblages. The Late Turonian Cool Phase in Europe was coincident with a period of long-term sea-level fall, with significant water-mass reorganization occurring during the mid-Late Turonian maximum lowstand. Falling $\Delta^{13}C$ ($\delta^{13}C_{carb} - \delta^{13}C_{org}$) trends coincident with two major cooling pulses, point to pCO_2 drawdown accompanying cooling, but the use of paired carbon isotopes as a high-resolution pCO_2 proxy is compromised in the low-carbonate sediments of the Bohemian Basin study section by diagenetic overprinting of the $\delta^{13}C_{carb}$ record. Carbon isotope chemostratigraphy is confirmed as a powerful tool for testing and refining intercontinental and marine to terrestrial correlations.

INTRODUCTION

The global carbon cycle constitutes one of the most fundamental biogeochemical systems affecting all surface reservoirs on our planet, with complex biosphere–atmosphere–hydrosphere–lithosphere interactions that modulate and drive climate change on both short and long timescales (Archer, 2010; Ciais *et al.*, 2013; Schlesinger & Berhardt, 2013). Secular variation in stable carbon isotope ratios determined from fossil carbonate and organic matter provides evidence that the sizes of, and fluxes between, global carbon reservoirs have changed significantly throughout the geological record (Veizer *et al.*, 1999). A residence time of *ca* 100 kyr for carbon in the ocean-atmosphere system (Walker, 1986; Kump & Arthur, 1999; Berner, 2006) ensures that the rock record has potential

to capture a robust global signal of palaeo-environmental change affecting the carbon cycle.

Stable carbon isotope ($\delta^{13}C$) chemostratigraphy is increasingly being used as a tool for regional to global correlation of Cretaceous successions (Wendler, 2013 and references therein). It offers higher precision than possible using conventional biostratigraphy (Paul & Lamolda, 2009), potentially down to 10 kyr, and as a result it has been adopted as one of the criteria for the definition of Cretaceous Global Boundary Stratotype Section and Points (GSSPs, Kennedy *et al.*, 2014; Lamolda *et al.*, 2014).

Most stratigraphic studies of Cretaceous carbon isotopes have focussed on $\delta^{13}C$ time series obtained from marine bulk pelagic or hemipelagic carbonates (Scholle & Arthur, 1980; Jenkyns *et al.*, 1994; Weissert *et al.*, 1998, 2008; Herrle *et al.*, 2004; Katz *et al.*, 2005; Sprovieri *et al.*, 2006, 2013; Jarvis *et al.*, 2002, 2006; Wendler, 2013). However, a unique feature of carbon isotope chemostratigraphy is the ability to compare records derived from oxidized carbon (carbonate, $\delta^{13}C_{carb}$) and reduced carbon (organic matter, $\delta^{13}C_{org}$) reservoirs (Jarvis *et al.*, 2011), and between marine and non-marine (terrestrial) environments (Gröcke *et al.*, 1999, 2005; Uramoto *et al.*, 2013).

Multiple complementary $\delta^{13}C$ time series may be produced by analysing a wide range of carbon-bearing materials, including bulk sedimentary carbonate or organic matter, carbonate fine fraction (micrite), early diagenetic cements, fossils (skeletal carbonate, leaves, wood, charcoal) and individual organic compounds (biomarkers). However, particularly in Mesozoic and older sediments, facies variation and diagenesis commonly limit the ability to obtain reliable multiple $\delta^{13}C$ records from the same interval within a single section.

The Cenomanian–Turonian boundary (CTB) interval (*ca* 94 Ma) is characterized by a large global positive excursion of $\delta^{13}C$ spanning *ca* 500 kyr that occurs in marine carbonates (values reaching >5‰ $\delta^{13}C_{carb}$), and both marine and terrestrial organic matter (Schlanger *et al.*, 1983, 1987; Arthur *et al.*, 1988; Jarvis *et al.*, 1988a, b, 2006, 2011; Jenkyns *et al.*, 1994; Hasegawa, 1997; Takashima *et al.*, 2011; Uramoto *et al.*, 2013; Joo & Sageman, 2014). This phenomenon is an expression of Oceanic Anoxic Event 2 (OAE2; Schlanger & Jenkyns, 1976), one of the best developed and geographically most extensive of the Mesozoic OAEs (Jenkyns, 2010), which represents an episode of widespread 'black shale' deposition and a major change in the dynamics of the global carbon cycle. It is generally considered that increased burial of organic matter in black shales and other organic reservoirs during OAE2 sequestered ^{12}C, leading to ^{13}C enrichment of all surface carbon reservoirs, and development of the global positive carbon isotope anomaly preserved in multiple archives.

Following OAE2, $\delta^{13}C$ values declined, but carbon isotopes continued to display greater short-term and long-term variation through the Turonian, 93·89 to 89·75 Ma, than any other Late Cretaceous stage (Jarvis *et al.*, 2006; Wendler, 2013). The earliest Turonian represented one of the highest sea-level stands in the Phanerozoic (Hancock & Kauffman, 1979; Haq *et al.*, 1987; Haq, 2014 and references therein), coincident with the highest ocean water temperatures of the last 110 Myr (Friedrich *et al.*, 2012). Major episodes of sea-level and climate change characterized the later Turonian, and hence, the stage provides an excellent opportunity to evaluate interactions between a range of stable isotope and other palaeo-environmental proxies within an interval representing the most extreme Late Cretaceous super-greenhouse.

In this paper, the first continuous high-resolution paired $\delta^{13}C_{carb}$ and $\delta^{13}C_{org}$ records for the Turonian (uppermost Cenomanian–Lower Coniacian) are presented; the similarities and differences between the two time series are critically assessed and correlated with published coeval marine and non-marine records from Europe, North America and Japan (Fig. 1). The viability of using both carbonate and organic matter carbon isotope chemostratigraphy for improved stratigraphic resolution, for placing stage boundaries and for intercontinental correlation is demonstrated, with calibration of the time series using biostratigraphic data. The uses of bulk-sediment carbonate $\delta^{18}O_{carb}$ as a sea-surface temperature (SST) proxy, and of $\Delta^{13}C$ ($\delta^{13}C_{carb} - \delta^{13}C_{org}$) as a pCO_2 proxy, are critically assessed. In addition, evidence is presented for a Europe-wide Late Turonian cool phase that was associated with a drawdown in pCO_2.

CARBON ISOTOPES AS A STRATIGRAPHIC TOOL

The isotopic composition of all surface global carbon reservoirs is considered to be broadly in equilibrium on geological timescales, with rapid exchange of carbon between atmospheric and oceanic carbon dioxide, marine bicarbonate and carbonate tests, and between carbon dioxide and both marine and terrestrial biota (Kump, 1991; Holser, 1997; Kump & Arthur, 1999). Each reservoir displays different $\delta^{13}C$ values due to fractionation effects. The most extreme of these is associated with plant photosynthesis favouring ^{12}C, which today leads to an offset of around −18‰ between dissolved CO_2 and marine phytoplankton, and about −26‰ between dissolved inorganic carbon (DIC; largely bicarbonate HCO_3^-) and phytoplankton (Killops & Killops, 2005). The amount of

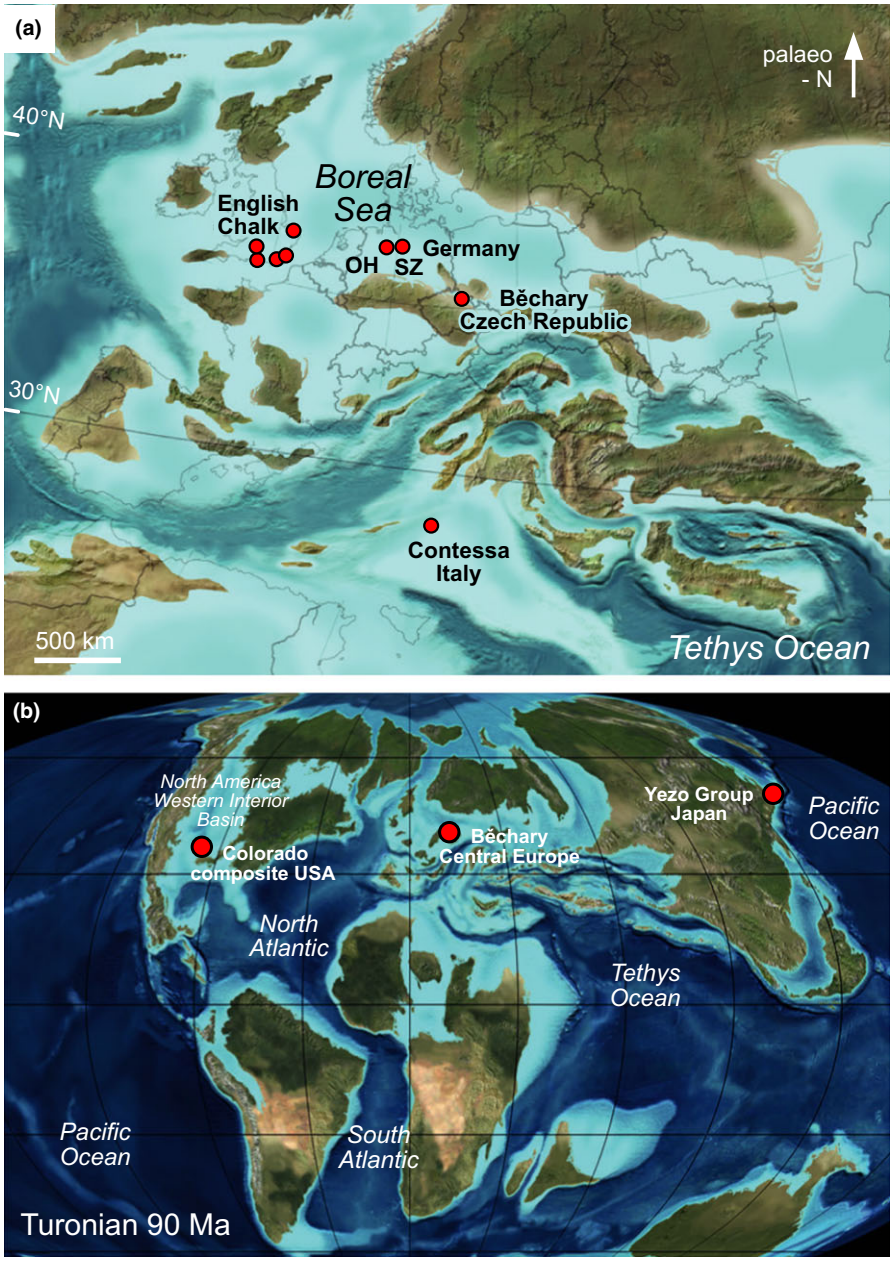

Fig. 1. Turonian palaeogeography and location of sites. (A) Late Cretaceous palaeogeography of Europe showing location of the main regional study sites (filled circles). OH = Oerlinghausen-Halle; SZ = Saltzgitter-Salder. (B) Global palaeogeography at 90 Ma showing location of non-European sections discussed in text. Reconstructions after R.C. Blakey, NAU Geology (http://cpgeosystems.com/75_Cret_EurMap_sm.jpg; http://cpgeosystems.com/90moll.jpg).

isotopic fractionation depends on the photosynthetic 'pathway' (e.g. C3 versus C4 plants; Kump & Arthur, 1999; Gröcke, 2002), on whether photosynthesis takes place in the marine (sea water) or terrestrial (air) environment, on the DIC concentration (or the partial pressure of CO_2), growth rate and on temperature (Rau *et al.*, 1991; Holser, 1997). By contrast, fractionation during precipitation of biogenic or abiogenic calcite from marine bicarbonate (dissolved inorganic carbon) is minor, at around −1‰ (Killops & Killops, 2005).

Carbon isotope chemostratigraphy

Stratigraphic variation in $\delta^{13}C$ values preserved in sedimentary archives is controlled principally by the fraction of carbon that is buried on land and in the oceans rela-

tive to marine carbonate carbon (Kump & Arthur, 1999). An increase in $\delta^{13}C$, for example, implies the burial of a higher fraction of organic carbon or, alternatively, a decrease in the oxidation of organic matter relative to the weathering of carbonate rocks. Variation in the amount of isotopically light authigenic carbonate precipitated in marine sediments has been proposed as an additional mechanism for driving stratigraphic variation (Schrag *et al.*, 2013), although the significance of this remains unproven. However, in addition to stratigraphic changes, geographical variation occurs in the isotopic composition of individual carbon reservoirs. The $\delta^{13}C$ of inorganically precipitated carbonate in the oceans is close to that of DIC, but $\delta^{13}C$ values of modern marine carbonates differ by 1‰ or more, depending on mineralogy, 'vital effects' and water-mass type and 'age' (Rohling & Cooke, 1999).

Different host materials yield different absolute $\delta^{13}C$ values. Upper Cretaceous marine carbonate has typical $\delta^{13}C_{carb}$ values of 1 to 3‰ (Wendler, 2013). By contrast, carbon isotope fractionation during photosynthesis under high pCO_2 conditions has led to Cretaceous marine organic matter exhibiting low $\delta^{13}C_{org}$ values ranging from −26‰ to −28‰ (Hayes *et al.*, 1999; Meyers, 2014), which are lower than coeval land plant or terrestrial organic carbon, with average $\delta^{13}C_{org}$ values of −23‰ to −25‰ (Dean *et al.*, 1986; Gröcke, 2002; Hasegawa, 2003; Uramoto *et al.*, 2013).

Does bulk carbonate preserve a sea water $\delta^{13}C$ record?

The carbonate component of pelagic and hemipelagic Late Cretaceous and younger sediments are typically dominated by mixed assemblages of coccolithophores and other calcareous nannofossils derived from the photic zone (0 to 200 m depth, and with highest abundance around 50 m; Tappan, 1980), which is reflected in positive $\delta^{13}C_{carb}$ values. This condition is a result of the preferential uptake of ^{12}C from surface waters by phytoplankton and the downward export of ^{12}C-enriched marine organic matter out of the photic zone.

Significant isotopic variation between different coccolith species ('vital effects') and between populations living in different environmental conditions (e.g. pH, temperature, nutrient levels) has been observed in laboratory experiments (Ziveri *et al.*, 2003), which raises concerns about stratigraphic variation in bulk-sediment $\delta^{13}C_{carb}$ values being driven by variations in nannofossil assemblage composition or by local environmental changes. However, compared to modern examples, a very small range of vital effects has been observed in Palaeocene coccoliths (Stoll, 2005), which has been attributed to larger cell diameters and more similar carbon acquisition strategies among different fossil species, perhaps in response to higher atmospheric CO_2 concentrations at that time. This condition suggests that bulk carbonate-carbon isotope data from pelagic sediments probably provide reliable records of surface water $\delta^{13}C$ for other Early and pre-Cenozoic sediments (Bolton *et al.*, 2012).

As with all carbonate systems, diagenesis remains a concern (Swart, 2015 and references therein). Carbon isotopes are much less prone to diagenetic alteration than oxygen isotopes in marine carbonates (Hudson, 1977; Anderson & Arthur, 1983; Banner & Hanson, 1990; Marshall, 1992) because porewater in the sediments generally contains little organic matter, the carbon isotope system is rock-dominated, and carbon isotopes show no significant temperature-controlled fractionation during burial. Notable exceptions occur in association with subaerial exposure surfaces where soil zone CO_2 in meteoric porewaters commonly drives bulk-sediment $\delta^{13}C$ to low values, producing local negative excursions of up to several ‰ (Gross, 1964; Allan & Matthews, 1982; Marshall, 1992; Immenhauser *et al.*, 2008). Furthermore, even though the processes that produce these types of excursion are local, they can be synchronously distributed on a global scale as a result of eustatic sea-level fall. Indeed, in some situations, coupled negative excursions in carbonate and organic $\delta^{13}C$ may result from multiple periods of meteoric alteration of the carbonate $\delta^{13}C$ record combined with an increased contribution of isotopically negative terrestrial organic matter to the sediment (Oehlert & Swart, 2014).

Subaerial exposure cannot be invoked for the hemipelagic and pelagic settings considered here. Excellent agreement between the trends of biostratigraphically well-constrained Upper Cretaceous $\delta^{13}C_{carb}$ profiles from hemipelagic and pelagic successions throughout Europe supports the synchroneity of changes in the isotope record, and illustrates the potential of using a composite $\delta^{13}C_{carb}$ reference curve as a primary criterion for transcontinental correlation (Jarvis *et al.*, 2006; Voigt *et al.*, 2010; Wendler, 2013).

The presence of both pervasive and bed-scale diagenesis is clearly discernable in most Cretaceous pelagic and hemipelagic successions. With the exception of synsedimentary sea floor lithification accompanying nodular chalk and hardground formation (Kennedy & Garrison, 1975; Surlyk *et al.*, 2003; Christ *et al.*, 2015), early diagenesis in most Cretaceous pelagic sections is limited by the organic matter-poor, fine-grained, low permeability, low-Mg calcite-dominated composition of the primary sediment and deposition in sub-storm-wave base environments isolated from exposure to meteoric water.

However, during burial, pressure-solution driven redistribution of carbonate typically affects smaller particles

that, in Late Cretaceous pelagic carbonates, consist mainly of coccoliths. These generally have lower $\delta^{13}C$ values than most other co-occurring fossils, so a distinct isotopic pattern that is often observed, with higher $\delta^{13}C$ values in marls than in adjacent chalks (Jarvis *et al.*, 1988a; Frank *et al.*, 1999; Paul *et al.*, 1999; Jeans *et al.*, 2012), may be attributed in part to coccolith depletion in the former lithology. At the same time, pressure-solution driven redistribution of marl-derived carbonate into adjacent chalks as cement (Jarvis *et al.*, 1988a; Mitchell *et al.*, 1997; Jeans *et al.*, 2012) will cause an offset to lower $\delta^{13}C$ values in the chalks, and lead to $\delta^{13}C$ versus $\delta^{18}O$ covariance. However, kinetic fractionation effects during precipitation of the original biogenic calcite may also produce covariance (Wendler *et al.*, 2013), so this is not an unequivocal sign of diagenesis. On the other hand, oxygen isotopes display far greater fractionation than carbon during burial diagenesis, and so offer sensitive indicators of alteration for screening on a sample-by-sample basis (see Anderson & Arthur, 1983; Marshall, 1992).

Can bulk organic matter preserve a primary $\delta^{13}C$ record?

The stable carbon isotope composition of bulk organic matter is affected by changes in the terrestrial contribution to the total organic carbon (TOC) (Kuypers *et al.*, 2004): Cretaceous marine organic matter typically yields $\delta^{13}C$ values that are lower by 3 to 4‰ compared to coeval land plant or terrestrial organic C, so changing ratios of the two components in samples may lead to significant variation in $\delta^{13}C_{org}$ values of bulk organic matter. Varying proportions of different terrestrial constituents such as charcoal (wood), leaf and cuticle may also influence bulk $\delta^{13}C_{org}$ values, although such effects are relatively minor (Heimhofer *et al.*, 2003; Gröcke *et al.*, 2006). Primary chemostratigraphic trends, therefore, will be best obtained from bulk samples where either the contribution of marine or terrestrial organic matter predominates, or the ratio of the two components remains constant.

Regional differences in the degree of carbon isotope fractionation in coeval marine organic matter may be caused by varying rates of productivity. Southern proto-North Atlantic CTB sites, for example, display 2‰ greater amplitude positive $\delta^{13}C_{org}$ excursions than sections elsewhere (Arthur *et al.*, 1988; Sinninghe Damsté *et al.*, 2008). This difference has been interpreted as being a result of higher rates of local CO_2 uptake in surface waters accompanying enhanced primary production, driven by shallowing of the chemocline and increased nutrient input into the photic zone (Laws *et al.*, 1995; Kuypers *et al.*, 2002).

Marine organic matter is also much more reactive than carbonate, a large part of the exported organic material is remineralized in the upper part of the sediment column. Changes in the degree of preservation of components with higher isotope values, such as carbohydrate carbon (Sinninghe Damsté & Köster, 1998; Forster *et al.*, 2008; Zonneveld *et al.*, 2010), may affect the preserved signal. Furthermore, terrestrial organic matter may be preferentially preserved during early diagenesis (de Lange *et al.*, 1994; Hatch & Leventhal, 1997; Prahl *et al.*, 1997), which can produce shifts in $\delta^{13}C_{org}$ records of up to 4 to 5‰, which has implications for the ratio of marine to terrestrial organic matter in bulk deposits, and the subsequent $\delta^{13}C_{org}$ record. Overall, the processes influencing the $\delta^{13}C_{org}$ record are complex and less well understood than those for carbonate (Werne & Hollander, 2004). For stratigraphic purposes, therefore, the form and shape of isotope profiles preserved in geological archives is more reliable than the absolute values, and the potential effects of varying terrestrial versus marine organic matter ratios need to be critically assessed.

The ultimate test for the preservation of a primary signal is whether the same pattern of variation in $\delta^{13}C$ can be recognized in different host materials (e.g. carbonate and organic matter), in different sections, and in different basins, where good stratigraphic constraints are available using biostratigraphy, magnetostratigraphy, astrochronology and/or geochronology. Even then, care is required. For example, Oehlert *et al.* (2012) demonstrated how local carbonate and organic $\delta^{13}C$ covariance may be caused by mixing between pelagic and platform-derived carbonate and organic matter. However, the main focus of the present paper is on European and North American shallow-buried hemipelagic to pelagic carbonate successions that were never subject to subaerial exposure, and lacked adjacent carbonate platforms. These successions should offer optimum conditions for deriving robust primary chemostratigraphic data.

Turonian carbon isotope chemostratigraphy

The most prominent feature of the Late Cretaceous carbon isotope record is the large positive $\delta^{13}C$ excursion representing OAE2, spanning the CTB. The carbon isotope record of the CTB interval has been studied extensively (Schlanger *et al.*, 1987; Jarvis *et al.*, 1988a,b, 2001, 2006, 2011; Arthur *et al.*, 1990; Gale *et al.*, 1993, 2005; Pratt *et al.*, 1993; Jenkyns *et al.*, 1994; Hasegawa, 1997, 2003; Voigt & Hilbrecht, 1997; De Cabrera *et al.*, 1999; Hasegawa & Hatsugai, 2000; Voigt, 2000a; Keller *et al.*, 2001; Wang *et al.*, 2001; Tsikos *et al.*, 2004; Amédro *et al.*, 2005; Bowman & Bralower, 2005; Erbacher *et al.*, 2005; Kolonic *et al.*, 2005; Kuhnt *et al.*, 2005; Li

et al., 2006; Parente *et al.*, 2007; Scopelliti *et al.*, 2008; Elrick *et al.*, 2009; Takashima *et al.*, 2011; van Bentum *et al.*, 2012; Hasegawa *et al.*, 2013; Elderbak *et al.*, 2014; Eldrett *et al.*, 2014; Joo & Sageman, 2014; Nagm *et al.*, 2014; Wohlwend *et al.*, 2015) since the pioneering work of Scholle and Arthur (1980).

By marked contrast, a review of carbon isotope stratigraphy from the Archaean to present-day by Saltzman and Thomas (2012) showed an absence of data from almost the entire Turonian. This major gap is due to a paucity of Turonian data from deep-sea isotope records (Katz *et al.*, 2005). Nonetheless, a carbon isotope stratigraphy for the Turonian, based on bulk carbonate records from the English Chalk, was erected by Jarvis *et al.* (2006), who reviewed earlier work on CTB sections in England (Jarvis *et al.*, 1988a,b, 2001; Jeans *et al.*, 1991; Gale *et al.*, 1993, 2005; Lamolda *et al.*, 1994; Paul *et al.*, 1999; Keller *et al.*, 2001; Tsikos *et al.*, 2004), and broader isotopic studies of the Turonian in England (Jenkyns *et al.*, 1994; Pearce *et al.*, 2003), Germany (Voigt & Hilbrecht, 1997; Wiese, 1999; Wiese & Kaplan, 2001), northern Spain (Wiese, 1999) and Italy (Corfield *et al.*, 1991; Jenkyns *et al.*, 1994; Stoll & Schrag, 2000).

Subsequent work has included new carbonate $\delta^{13}C$ data for the Turonian of Germany (Voigt *et al.*, 2007, 2008; Richardt & Wilmsen, 2012) and Italy (Sprovieri *et al.*, 2013; Gambacorta *et al.*, 2015). Turonian $\delta^{13}C_{carb}$ profiles have also been presented from southern Tethyan sections in Tibet (Li *et al.*, 2006; Wendler *et al.*, 2009, 2011), although these display generally lower values and more erratic patterns in the Lower and Middle Turonian than European successions (Wendler, 2013). Most recently, complete Turonian organic carbon $\delta^{13}C$ records have been published from the Czech Republic (Uličný *et al.*, 2014; Olde *et al.*, 2015a) and the US Western Interior Basin (Joo & Sageman, 2014).

MATERIAL AND METHODS

The isotope data presented in this paper were obtained from a research core drilled during 2010 through a thick (405 m) uppermost Cenomanian to Lower Coniacian hemipelagic succession in the Bohemian Cretaceous Basin (Fig. 1; Uličný *et al.*, 2014). This NW–SE oriented 280 km long elongate basin extends between Saxony, Bohemia and Moravia (Czech Republic).

The Bch-1 core site (50·31506°N 15·29497°E), located in the village of Běchary, is situated in the central basin between two depocentres, one adjacent to the Most-Teplice High and Western Sudetic Island in the north-west, the other bordering the Bohemian Massif to the south-east (Uličný *et al.*, 2014, fig. 1). These terrestrial source areas contributed varying amounts of sediment through the Turonian, with the Western Sudetic Island being by far the most prominent. Fine-grained siliciclastic sediment transported via basin-margin deltas and shorefaces became mixed with autochthonous pelagic carbonate to generate calcareous hemipelagic successions in the central basin. No carbonate platform facies are developed within the region, which was dominated by siliciclastic sand facies in near-shore settings.

Bch-1 study core

The main lithofacies at Běchary (Fig. 2) consists of very dark grey marlstones and calcareous mudstones with a varying proportion of quartz silt (coarsest intervals occurring between 360 to 380 m and 140 to 220 m). The mean percentage of $CaCO_3$ through the core is *ca* 35% (range: 4 to 71%), and carbonate is generally represented by a micritic component, some mm-scale bioclasts and microspar in horizons with concretionary cement. These are mostly prominently developed in the low to mid-Upper Turonian (Fig. 2). TOC contents average 0·42% (range: 0·17 to 0·80%) in the bulk sediments (TOC_{WR}) and 0·68% (0·18 to 1·28%) in the acid insoluble residues (TOC_{IR}). Turonian lithofacies show abundant bioturbation throughout the core, dominated by a distal *Cruziana* ichnofacies (cf. MacEachern *et al.*, 2010).

The core was described by Uličný *et al.* (2014), who used geophysical logs combined with lithological and biostratigraphic data to correlate the succession to neighbouring cores and outcrops. The section has been placed in a regional famework via a basin-scale correlation grid developed using well-log correlation (gamma-ray, resistivity, neutron porosity logs) and core data from >700 boreholes, where possible, calibrated by outcrop sedimentology and gamma-ray logging (Uličný *et al.*, 2009, 2014).

The Turonian–Coniacian of the Bohemian Cretaceous Basin has been subdivided into a number of genetic sequences, termed TUR1–TUR7, CON1 and CON2, which were detailed by Uličný *et al.* (2009). The sequences record long-term cycles of regression and subsequent transgression, within which there are multiple smaller scale events; the positions of these sequences in the Bch-1 core are shown in Fig. 2, revised from Uličný *et al.* (2014), following Olde *et al.* (2015a,b). Basin-wide sediment geometries and transgressive-regressive (shore proximity) curves have additionally been used to construct an inferred eustatic sea-level curve, which has been correlated with the Bch-1 well (Uličný *et al.*, 2014).

A precise chronostratigraphic framework for Bch-1 has been developed using macrofossil, calcareous nannofossil and dinoflagellate cyst records from the core (Fig. 2; Uličný *et al.*, 2014; Olde *et al.*, 2015a), combined with

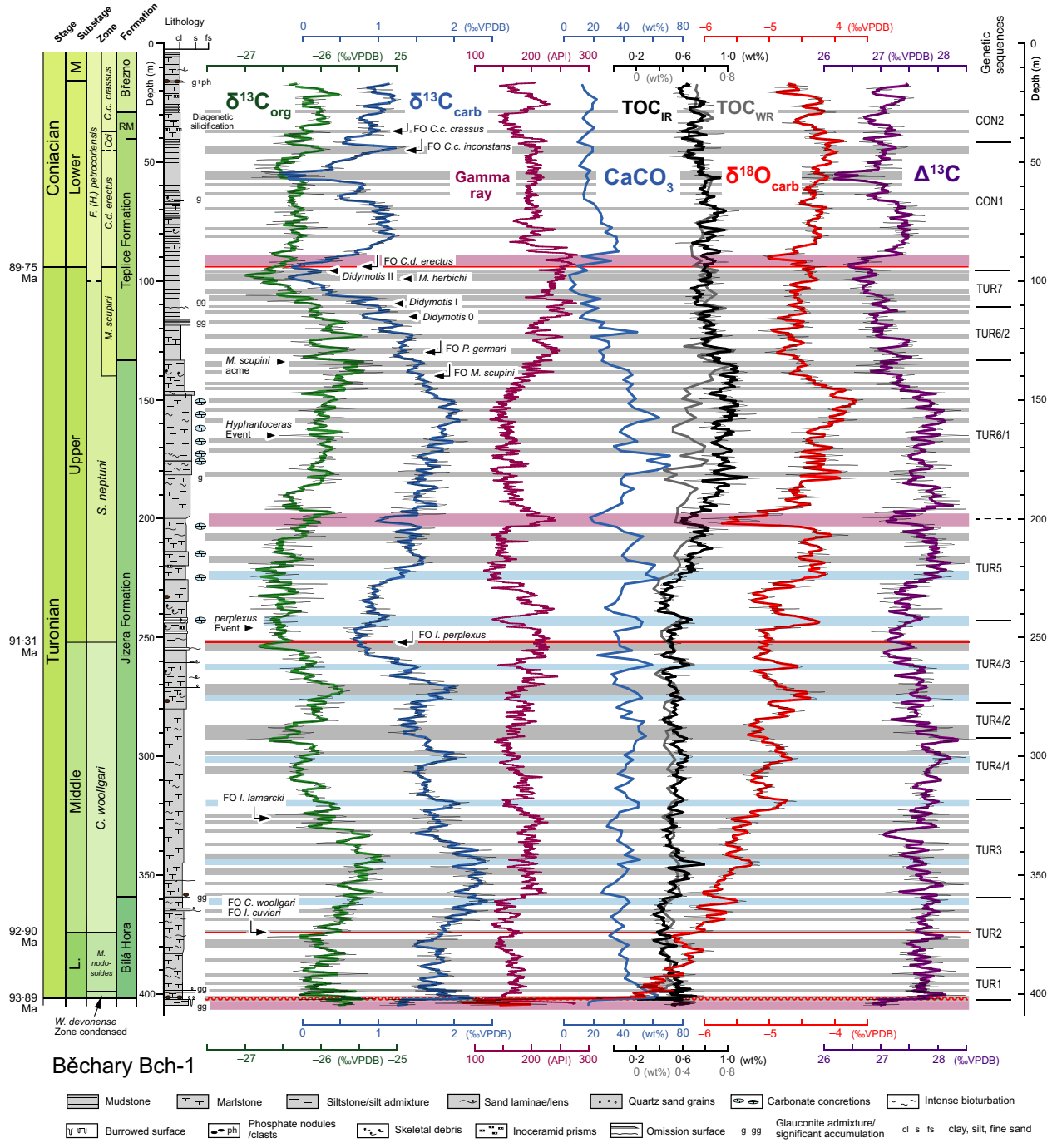

Fig. 2. Lithology, stratigraphy and geochemistry of the Bch-1 well. Carbon isotopes of bulk organic matter ($\delta^{13}C_{org}$) and bulk carbonate ($\delta^{13}C_{carb}$), gamma ray, $CaCO_3$, insoluble residue total organic carbon (TOC_{IR}; black high-resolution profile and black numerals) and whole-rock TOC (TOC_{WR}; grey low-resolution profile and grey numerals), bulk carbonate oxygen isotopes ($\delta^{18}O_{carb}$), and the offset between $\delta^{13}C_{org}$ and $\delta^{13}C_{carb}$ ($\Delta^{13}C$) are shown. Thin black lines represent all data; associated smoothed coloured curves are three-point moving averages. Gamma ray, $CaCO_3$ and TOC_{WR} curves are unsmoothed. Ages of stage and substage boundaries derived from Ogg *et al*. (2012), Laurin *et al*. (2014) and Sageman *et al*. (2014). Biostratigraphy and fossils datum levels after Olde *et al*. (2015b); lithostratigraphic terminology after Čech *et al*. (1980). Basin-scale genetic sequences are modified from Uličný *et al*. (2014), following Olde *et al*. (2015b). Grey bands highlight coincident peaks and troughs in the paired $\delta^{13}C$ profiles. Blue bars are carbonate-rich intervals displaying positive $\delta^{18}O_{carb}$ values. Purple bands highlight levels with a significant diagenetic overprint (see text for details). FO = first occurrence.

geophysical log correlation of key macrofossil biostratigraphic datum levels from adjacent cores and outcrops. Biostratigraphic tie points and age controls are summarized in Appendix S1. The CTB near the base of the core (402 m) is marked by an omission surface. A major hiatus at this level (Uličný *et al*., 1993, 2014) is confirmed by the absence of calcareous nannofossil zones UC 5a-b, which correlates to the upper part of the *Metoicoceras geslinianum* and *Neocardioceras juddii* ammonite zones (Burnett *et al*., 1998). This hiatus has been attributed to a major flooding episode (Valečka & Skoček, 1991).

The first occurrence (FO) of the ammonite *Collignoceras woollgari* (Mantell), which marks the base of the Middle Turonian, occurs in the middle of Sequence TUR2, and is correlated with 374 m in Bch-1 (Uličný *et al*., 2014). This level corresponds to a major regional sea-level lowstand, which was followed by a marked early Middle Turonian transgression. The FO of *Inoceramus perplexus* Whitfield, the Upper Turonian index taxon, is correlated with 252 m (Uličný *et al*. 2014). The end-Middle Turonian marks a long-term regressive maximum, following a general Middle Turonian sea-level fall.

A transgressive event at the base of TUR5 (243 m in Bch-1) in the lowest Upper Turonian is prominent basin wide, and marks a shift to intervals with higher carbonate contents and more widespread cementation in all facies (Fig. 2; Uličný *et al*., 2014). This event correlates to an acme of *I. perplexus* (= *perplexus* Event). A coarsening-upward trend within TUR6/1, above, provides evidence of shallowing, with high-energy and probably very shallow-water (close to fair-weather wave base) conditions. Subsequent drowning during the latest Turonian, is indicated by a fining-upwards trend accompanying sharply falling $CaCO_3$ contents towards the top of Sequence TUR6/2, but starting from around from 135 m (Fig. 2). Uppermost Turonian Sequence TUR7 is marked by low-carbonate contents (Fig. 2) that fall to a minimum at the top of the sequence, immediately below the stage boundary. The FO of *Cremnoceramus deformis erectus* (Meek), the base Coniacian marker (Kauffman *et al*. 1996), is found towards the bottom of Sequence CON1, correlated with 94 m in Bch-1, with specimens recorded from the core a short distance above (Uličný *et al*., 2014).

Analytical methods

Samples of *ca* 20 g were taken every 50 cm through the 406 m Bch-1 core for bulk carbonate ($\delta^{13}C_{carb}$, $\delta^{18}O_{carb}$) and bulk organic matter ($\delta^{13}C_{org}$) stable isotope analysis, and TOC determination. New $\delta^{13}C_{carb}$, $\delta^{18}O_{carb}$ data are reported here (803 samples); $\delta^{13}C_{org}$ and TOC results for the same samples were presented previously by Uličný *et al*. (2014). Analytical methodologies are described in Appendix S2. Isotopic ($\delta^{13}C_{carb}$, $\delta^{13}C_{org}$, $\delta^{18}O_{carb}$) and TOC data are provided in Appendix S3. Based on an average compacted sedimentation rate for the Middle and Upper Turonian of 9 cm kyr^{-1} (Uličný *et al*., 2014), sampling resolution is on the order of 5·6 kyr.

The elemental geochemistry and palynology of the section were studied by Uličný *et al*. (2014) and Olde *et al*. (2015a,b) using a larger size (50 g) lower resolution sample set taken at 2 m intervals (22 kyr) through the core. The isotope data presented here include results from splits of these larger samples, they do not constitute a separate sample set.

GEOCHEMICAL VARIATION IN BCH-1

Stable isotope ($\delta^{13}C_{org}$, $\delta^{13}C_{carb}$, $\delta^{18}O_{carb}$) and TOC data are plotted as chemostratigraphic profiles in Fig. 2, together with the gamma-ray log and a carbonate curve from the lower resolution data set. It is evident that the organic-carbon and carbonate-carbon isotope profiles show very similar long-term trends, offset by 26 to 28‰ ($\Delta^{13}C = \delta^{13}C_{carb} - \delta^{13}C_{org}$), with low-Middle Turonian and mid-Upper Turonian maxima, and lowest Upper Turonian and Turonian–Coniacian boundary minima. Neither carbon isotope curve bears any similarity to the long-term trend of $\delta^{18}O_{carb}$, which displays generally rising values from the base upwards, peaking in the mid-Upper Turonian, followed by a basal *M. scupini* Zone minimum, and then rises again thereafter.

Predictably, $CaCO_3$ shows an inverse correlation with downhole gamma-ray (sourced from K, Th, U radionuclides located principally in the aluminosilicate fraction) values, the lower resolution profile of the former capturing the main stratigraphic patterns seen in the high-resolution (5 cm; 500 years) gamma-ray data (Fig. 2; Uličný *et al*., 2014). The TOC_{WR} and TOC_{IR} contents are both low throughout the Lower and Middle Turonian. They rise through the Upper Turonian to coincident long-term maxima at the top of the Jizera Formation (around the level of a $\delta^{13}C_{org}$ maximum), then remain at higher levels throughout the remainder of the section; TOC_{WR} contents are generally low, rarely exceeding those of average shale (0·8%; Mason & Moore, 1982). The $\Delta^{13}C$ profile displays a relatively flat long-term trend with values of *ca* 27·7‰ through most of the Turonian, but with an interval of lower values spanning the Middle–Upper Turonian boundary interval. The $\Delta^{13}C$ values fall to *ca* 27·1‰ towards the top of the Upper Turonian, at the summit of the Jizera Formation.

In addition to the long-term (>400 kyr) interrelationships described above, several noteworthy medium-term correlations are evident; these are considered below.

Carbon and oxygen isotopes

There is good correspondence between many short-term (10 to 50 kyr) peaks and troughs developed in the $\delta^{13}C_{carb}$ and $\delta^{13}C_{org}$ curves; these are highlighted by the grey shaded bands in Fig. 2. These coincident peaks and troughs probably reflect an original palaeo-environmental signal, and offer the greatest potential to provide robust datum levels in carbon isotope chemostratigraphy.

In a few cases, the correspondence between the $\delta^{13}C_{carb}$ and $\delta^{13}C_{org}$ curves is poor, or the curves are anti-correlated. Three levels (purple shaded bands in Fig. 2) in particular show major discrepancies: (1) the Cenomanian section at the base of the core below 402 m; (2) a low-carbonate interval in the Upper Turonian around 200 m; (3) the basal Coniacian section below 90 m. All three intervals are characterized by low-carbonate contents with coincident gamma-ray peaks, and exhibit negative excursions in $\delta^{13}C_{carb,}$ $\delta^{18}O_{carb}$ and $\Delta^{13}C$. The low absolute values of $\delta^{13}C_{carb,}$ $\delta^{18}O_{carb}$ and coincident depletion in both isotopes, point to significant local diagenetic overprinting of carbonate at these levels. This condition was probably caused by carbonate dissolution and the addition of burial microspar precipitated under elevated pore-fluid temperatures (cf. Choquette & James, 1987) or late stage interaction with freshwater aquifer fluids (see below for discussion).

A second type of divergence between the carbon isotope profiles occurs in the Middle Turonian and lower Upper Turonian section. Here, a series of *ca* 0·5‰ positive excursion in $\delta^{18}O_{carb}$ correspond to carbonate-rich levels with small increases in $\delta^{13}C_{carb}$ that are not matched exactly by corresponding peaks in $\delta^{13}C_{org}$ (blue shaded bands in Fig. 2). In many cases this manifests as a small peak offset (e.g. peaks around 320 m), while in others, the disparity is large (e.g. peaks around 300 m). Some of these horizons correlate to concretionary horizons identified in the core (Fig. 2). It is likely, therefore, that the locally elevated values in $\delta^{18}O_{carb}$ and $\delta^{13}C_{carb}$ reflect the addition of early diagenetic calcite cements that have protected the host sediment from later diagenetic alteration. The possibility of significant interaction with organic-derived bicarbonate, which characterizes many concretion carbonates (Hudson, 1977), is excluded by the modest changes observed in $\delta^{13}C_{carb}$.

Geochemical interrelationships

Stratigraphic and diagenetic interrelationships in the geochemical data may be visualized using bivariate plots (Figs 3 and 4). The Al_2O_3 versus $CaCO_3$ plot (Fig. 3A to D) illustrates an inverse relationship between carbonate and clay mineral contents that control the bulk-sediment composition. A linear 'dilution' trend is well displayed by the Upper Turonian interval (Fig. 3C) that contains the widest range of carbonate contents. These data produce a well-defined mixing line between a non-calcareous mudrock with 15% Al_2O_3 and a marly limestone with 80% carbonate (green line in Fig. 3A to D). The line parallels the mixing line between 'average shale' (Wedepohl, 1971) and a pure carbonate end-member (dashed line in Fig. 3A to D). The same regression lines plotted on the other stratigraphic intervals reveals similar tends but with greater scatter below the line, particularly in the Lower Coniacian (Fig. 3D). This phenomenon is attributed to the presence of varying amounts of biogenic silica and/or detrital quartz in the samples; both calcitized silicisponge spicules and detrital quartz grains are visible in thin sections from several intervals.

The TOC_{WR} is positively correlated with Al_2O_3 but with considerable scatter around the 'average shale' mixing line (Fig. 3E to H). This correlation is characteristic of modern shelf sediments and is attributed to the high surface area of the clay mineral fraction (represented here by the Al proxy) favouring the adsorption and preservation of organic matter (Keil *et al.*, 1994; Mayer, 1994; Hedges & Keil, 1995; Hedges *et al.*, 1997). Iron minerals also enhance the preservation of organic matter in marine sediments (Berner, 1970; Lalonde *et al.*, 2012); this may be an additional factor, since Fe is positively correlated with Al in Bch-1 (R^2 = 0·88, data presented in Olde *et al.*, 2015b). The top Cenomanian–Lower Turonian and Middle Turonian intervals are distinguished by having lower whole-rock TOC contents and being TOC-depleted relative to their Al contents (Figs 2 and 3E to F), when compared to the stratigraphically higher parts of the section. This condition is consistent with lower sedimentation rates (Uličný *et al.*, 2014; see footnote in Table S2), greater sea floor oxidation, and reduced burial efficiency driving a lower organic matter burial flux (Hedges & Keil, 1995; Hedges *et al.*, 1999).

With the exception of the Cenomanian–Turonian boundary interval, $\delta^{13}C_{org}$ is generally positively correlated with $\delta^{13}C_{carb}$ throughout the succession (Fig. 4) but with considerable scatter. A reference regression line calculated for the Middle Turonian samples (Fig. 4B) and transposed onto the other three age groups (Fig. 4A and C to D), illustrates a shift to lower $\delta^{13}C_{carb}$ values (<0·5‰) for low-carbonate samples in the uppermost Upper Turonian and Lower Coniacian intervals (Fig. 4C and D). This phenomenon is attributed to the addition of isotopically lighter cement associated with the microbial decomposition of organic matter in this part of the section (cf. Hudson, 1977). Samples in this category display significant shifts to lower $\delta^{13}C_{carb}$ compared to their corresponding $\delta^{13}C_{org}$ and $\delta^{18}O_{carb}$ values, which are compa-

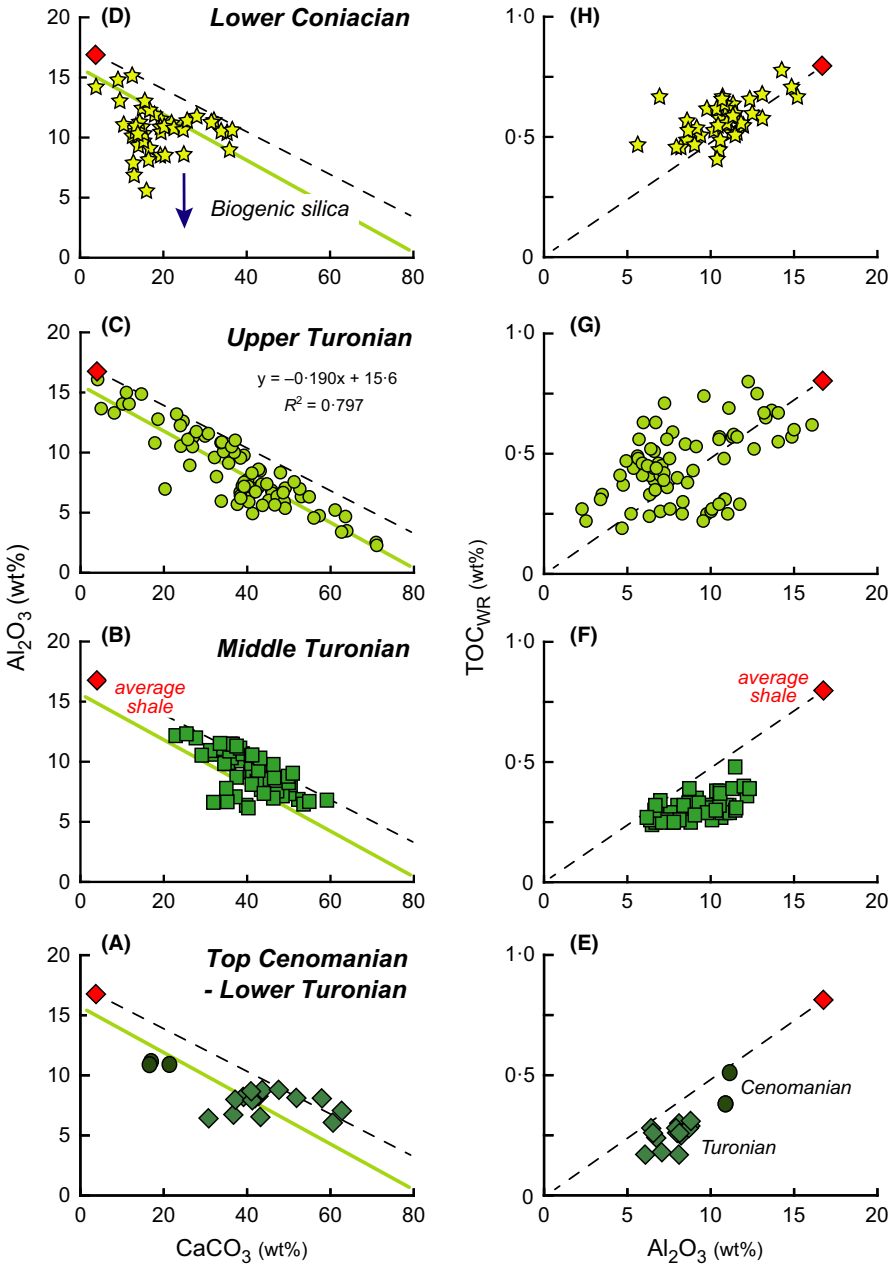

Fig. 3. Elemental cross-plots showing inter-relationships and stratigraphic trends in Bch-1 samples. (A to D) Al_2O_3 versus $CaCO_3$ for the: (A) top Cenomanian–Lower Turonian; (B) Middle Turonian; (C) Upper Turonian; (D) Lower Coniacian intervals. (E to F) Whole-rock total organic carbon (TOC_{WR}) versus Al_2O_3 for the: (E) top Cenomanian–Lower Turonian; (F) Middle Turonian; (G) Upper Turonian; (H) Lower Coniacian intervals. Green filled circles in (A) and (E) are top Cenomanian; green filled diamonds are Lower Turonian samples. Red-filled diamonds show the composition of average shale (Wedepohl, 1971). Green lines in (A to D) are the least squares regression line derived from the Upper Turonian sample set (C). Black dashed lines are mixing lines between average shale and a pure carbonate end-member. Blue arrow in (D) indicates trend offset towards lower Al_2O_3 values caused by the addition of biogenic silica.

rable to values of less altered samples within the same stratigraphic interval (Fig. 4C to D and G to H). The lack of a corresponding shift to lower $\delta^{18}O_{carb}$ values coincident with $\delta^{13}C_{carb}$ depletion (e.g. Fig. 4H) points to an early burial origin for these organic matter-derived cements.

The carbonate carbon versus oxygen isotope plots (Fig. 4) emphasize the stratigraphic trends noted from

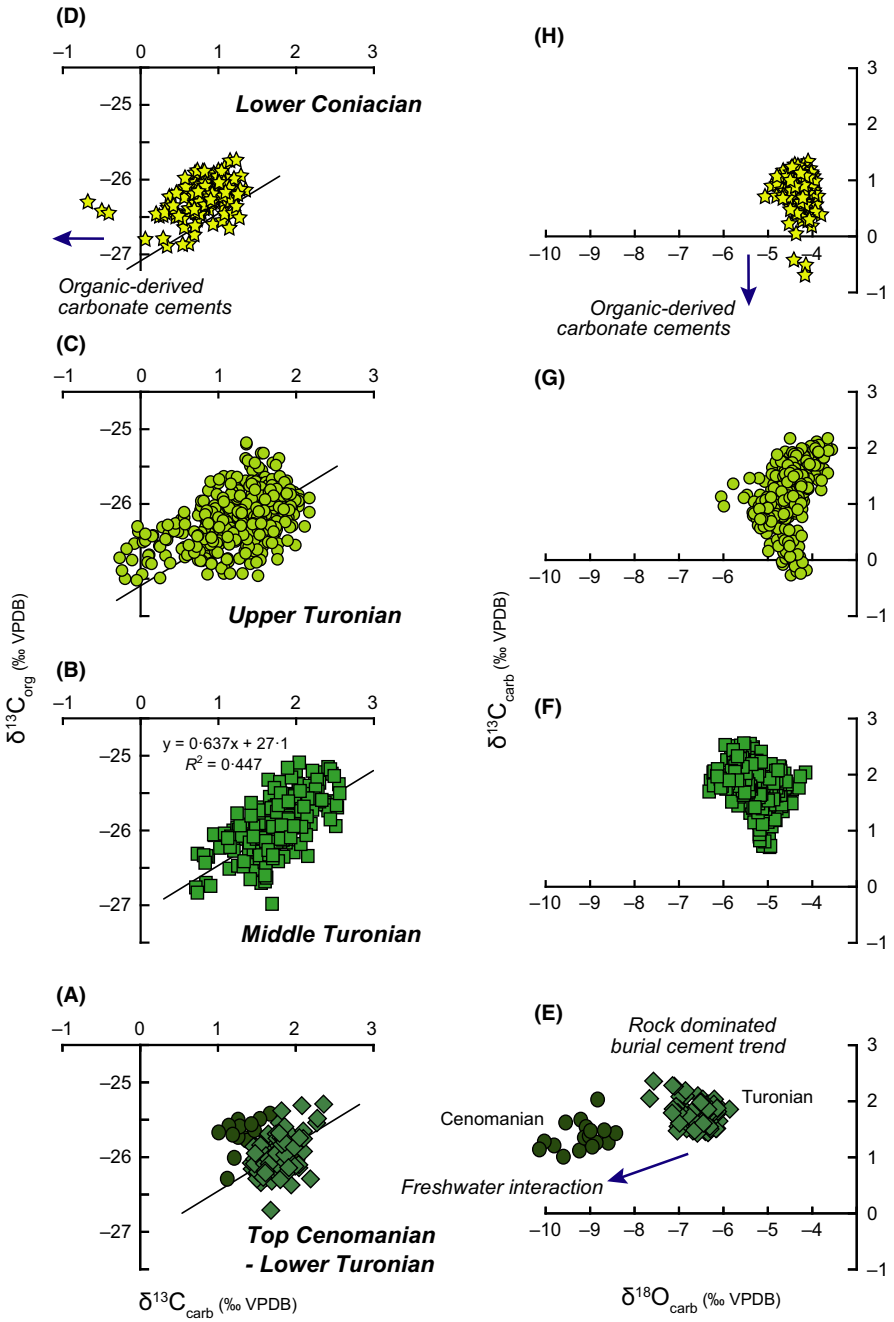

Fig. 4. Isotope cross-plots showing inter-relationships and stratigraphic trends in Bch-1 samples. (A to D) Organic-carbon versus carbonate-carbon stable isotopes ($\delta^{13}C_{org}$ versus $\delta^{13}C_{carb}$) for the: (A) top Cenomanian–Lower Turonian; (B) Middle Turonian; (C) Upper Turonian; (D) Lower Coniacian intervals. (E to F) Carbonate carbon versus oxygen isotopes ($\delta^{13}C_{carb}$ versus $\delta^{18}O_{carb}$) for the: (E) top Cenomanian–Lower Turonian; (F) Middle Turonian; (G) Upper Turonian; (H) Lower Coniacian intervals. Green filled circles in (A) and (E) are top Cenomanian; green filled diamonds are Lower Turonian samples. Black least squares regression lines in (A to D) are derived from the Middle Turonian sample set (B). Major diagenetic trends (blue arrows) are indicated; see text for discussion.

the isotope profiles (Fig. 2), with increasing $\delta^{18}O_{carb}$ values stratigraphically upwards (Fig. 4E to H), and extremely low values (−6 to −10‰ $\delta^{18}O_{carb}$ and *ca* 1‰ $\delta^{13}C_{carb}$) at the base of the section in the uppermost Cenomanian and Lower Turonian (Fig. 4E). No covariance is apparent between $\delta^{18}O_{carb}$ and $\delta^{13}C_{carb}$ in any of the four stratigraphic intervals. Interpretation of these signatures is discussed further below.

CARBON ISOTOPE STRATIGRAPHY AND EUROPEAN CORRELATION

Uličný *et al.* (2014) presented a $\delta^{13}C_{org}$ curve for Bch-1 that was used to place the positions of key named Turonian–Coniacian carbon isotope events (CIEs) in the section. Biostratigraphic data, predominantly macrofossil and nannofossil records from the core and correlated FO datum levels of macrofossils, were employed to pin the isotope curve to a time framework, principally using the bases of the Lower, Middle and Upper Turonian and the base Lower Coniacian (Fig. 2). The placement of named CIEs was based on the recognition of key positive and negative excursions, and inflection and turning points on the $\delta^{13}C_{org}$ curve, and the correlation of these to corresponding features on the English Chalk $\delta^{13}C_{carb}$ reference curve of Jarvis *et al.* (2006), taking into account available biostratigraphic data. Good correlations were demonstrated between the Běchary $\delta^{13}C_{org}$ curve and $\delta^{13}C_{carb}$ curves and faunal records from England, Liencres northern Spain and Salzgitter-Salder NW Germany (Uličný *et al.*, 2014, fig. 3), except for a divergence of trends in the upper part of the Upper Turonian, which was attributed to the more expanded nature of the Běchary section.

The placement of CIEs at Běchary may be re-evaluated using the new $\delta^{13}C_{carb}$ results obtained during the present study (Fig. 5). The $\delta^{13}C_{carb}$ and $\delta^{13}C_{org}$ profiles show generally good agreement and both compare well to the English Chalk reference curve (Jarvis *et al.*, 2006). Confidence in the assignment of the CIEs is further demonstrated by detailed correlation with $\delta^{13}C_{carb}$ curves from corresponding sections at Oerlinghausen-Halle and Saltzgitter-Salder in Germany (Wiese, 1999; Voigt *et al.*, 2007) and Contessa Quarry in Italy (Stoll & Schrag, 2000), where additional biostratigraphic data are available (Figs 1 and 5). The four $\delta^{13}C_{carb}$ curves display parallel trends but varying offsets in absolute values, with Běchary being the lowest by *ca* 1‰. Good correlation has also been achieved to stratigraphically less complete or biostratigraphically less well-constrained $\delta^{13}C_{carb}$ curves from: Anröchte (Richardt & Wilmsen, 2012), Söhlde (Voigt & Hilbrecht, 1997) and Wunstorf (Voigt *et al.*, 2008), Germany; Bottaccione (Corfield *et al.*, 1991; Jenkyns *et al.*, 1994; Sprovieri *et al.*, 2013) and Gubbio (Tsikos *et al.*, 2004) Italy; Santa Ines (Stoll & Schrag, 2000), Spain; and even beyond Europe to Gongzha (Li *et al.*, 2006) and Guru (Wendler *et al.*, 2011), Tibet (data not shown; see Wendler, 2013 for a review).

Precise placement of the CIEs at Běchary is hampered by greater sample-to-sample $\delta^{13}C_{carb}$ variation than exhibited by the smoother $\delta^{13}C_{carb}$ curves obtained from more carbonate-rich and diagenetically more uniform successions elsewhere (Fig. 5). As is generally the case, the complementary $\delta^{13}C_{org}$ curve is even noisier due the greater number of factors influencing bulk organic matter isotopic composition. Using the data from both curves, however, and giving the greatest confidence to features that are coincident in both, it is possible to confirm the placements of Uličný *et al.* (2014) for the Holywell, Pewsey, Navigation, Beeding and Light Point CIEs, and many unnamed correlatable excursions. Taking into account the new $\delta^{13}C_{carb}$ data, which in some intervals show much less variance and closer agreement with the correlative carbonate curves than $\delta^{13}C_{org}$ (Fig. 5), the Round Down and Low-woollgari CIEs are placed one carbon peak lower (equivalent to *ca* 125 kyr), and small shifts upwards or downwards (equivalent to *ca* 50 kyr) are applied to the placement of the Lulworth, Glynde, Caburn, Bridgewick and Hitch Wood CIEs (as adopted previously by Olde *et al.*, 2015a,b; compare Fig. 4 to Uličný *et al.* 2014, fig. 3).

The greatest divergence between the Běchary $\delta^{13}C_{carb}$ and $\delta^{13}C_{org}$ profiles is seen in the Upper Turonian above the Hitch Wood CIE. This CIE, which corresponds to a small positive excursion and turning point at peak $\delta^{13}C_{carb}$ values in the Upper Turonian (Jarvis *et al.* 2006), is immediately preceded by the *Hyphantoceras* faunal Event at Běchary, Saltzgitter-Salder and in southern England (Fig. 5), and elsewhere in Europe. A turning point at an equivalent stratigraphic level (based on biostratigraphy) is not present in the $\delta^{13}C_{org}$ curve, which continues to rise to a stratigraphically higher maximum at the HW2 CIE of Uličný *et al.* (2014). Those authors recognized the lack of correspondence between the Běchary $\delta^{13}C_{org}$ profile and published $\delta^{13}C_{carb}$ curves from elsewhere and, taking into account the biostratigraphic data, placed the Hitch Wood CIE at a minor peak in the organic carbon curve which was designated HW1. This placement falls a short distance below the Hitch Wood Event defined here using the $\delta^{13}C_{carb}$ profile, and coincides with the *Hyphantoceras* Event.

The amplitude of $\delta^{13}C_{carb}$ variation through the Upper Turonian–Lower Coniacian boundary interval is greater at Běchary than in the other European sections illustrated here (Fig. 5), which is attributed to greater diagenetic overprinting of the carbonate-poor sediments in Bch-1. Nonetheless, the general shape of the curve agrees closely with those from elsewhere, and corresponds well to the $\delta^{13}C_{org}$ curve. In this interval, the Běchary $\delta^{13}C_{org}$ curve shows lower amplitude medium-term variation than $\delta^{13}C_{carb}$, and the former is closer to the scale of variation seen in $\delta^{13}C_{carb}$ curves in other sections. Minor Upper Turonian $\delta^{13}C$ excursions (including HW2 and HW3 of Uličný *et al.*, 2014) that are well-constrained by biostratigraphy show good correspondence to peaks identified at other localities (Fig. 5).

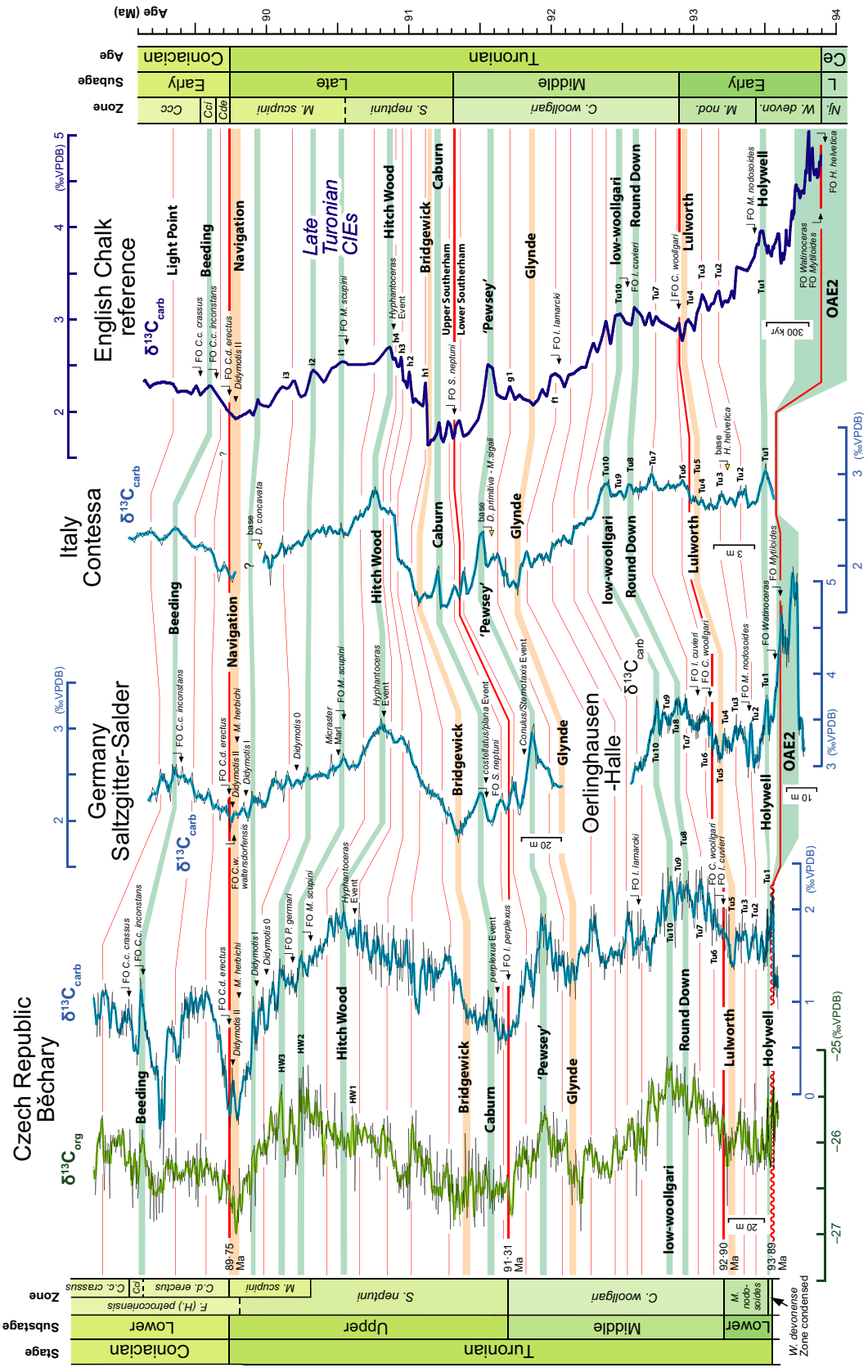

Fig. 5. Chemostratigraphic correlation of European Turonian sections using bulk-sediment carbonate-carbon stable isotopes. Location of the sites is shown in Fig. 1. High-resolution paired $\delta^{13}C_{carb}$ and $\delta^{13}C_{org}$ data from the Bèchary core illustrate generally good agreement between the two profiles. Thin black lines represent all data; associated smoothed coloured curves are three-point moving averages. The English Chalk reference curve displays smoothed data only. Isotope data sources: Bèchary $\delta^{13}C_{carb}$, this study; $\delta^{13}C_{org}$, Uličný *et al.* (2014); Saltzgitter-Salder (Voigt and Hilbrecht, 1997); Oerlinghausen-Halle, Voigt *et al.* (2007); Contessa, Stoll and Schrag (2000); English Chalk, Jarvis *et al.* (2006), recalibrated to GTS2012 after Laurin *et al.* (2014). Ages of stage and substage boundaries derived from Ogg *et al.* (2012), Laurin *et al.* (2014) and Sageman *et al.* (2014). Placement of Contessa biostratigraphic datum levels based on Sprovieri *et al.* (2013). Break in the Contessa profile represents an unsampled section correlated with immediately below the Navigation CIE (Sprovieri *et al.*, 2013). Correlation of positive (green) and negative (cream) carbon isotope excursions defining named carbon isotope events (Jarvis *et al.*, 2006) is shown by horizontal coloured bands. Thin red horizontal lines indicate other isotope correlations; thick red horizontal lines are stage and substage boundaries.

Jeans *et al.* (2012) have argued that the CIEs defined by Jarvis *et al.* (2006) from the English Chalk might be attributed largely to diagenesis, driven by the presence of varying proportions of fine-grained (<2 μm) cements having $\delta^{13}C_{carb}$ values ranging from 3·5 to −8‰. A lack of correlation between carbonate and organic matter $\delta^{13}C$ trends in a short section of English Lower Campanian Chalk was offered as evidence that the carbonate is diagenetically altered, despite the well-preserved nature of the sediments and their enclosed fossils. As a result, most previously defined Upper Cretaceous CIEs (Jarvis *et al.*, 2006) were considered to be untenable by Jeans *et al.* (2012). However, the new high-resolution carbon isotope data presented here fully support our previous work and assumptions.

Our correlations confirm the utility of carbon isotope stratigraphy, even in sections that have been overprinted by significant diagenesis, but they demonstrate that it is essential to have complementary biostratigraphic data to anchor the chemostratigraphic framework. Correlation precision is limited by sample-to-sample variability in the isotope data, but robust correlations may still be achieved when both $\delta^{13}C_{carb}$ and $\delta^{13}C_{org}$ curves are available. Despite the inherent differences expected between $\delta^{13}C_{carb}$ and $\delta^{13}C_{org}$ profiles obtained from successions showing a significant diagenetic overprint, correlation using a $\delta^{13}C_{org}$ curve from such sections, compared to $\delta^{13}C_{carb}$ curves from elsewhere, is able to achieve a precision for the correlation of major CIEs of better than 40 kyr, in most cases.

OXYGEN ISOTOPES AND THE LATE TURONIAN COOL PHASE

Cretaceous pelagic and hemipelagic carbonate bulk sediment and carbonate fine-fraction oxygen isotopes commonly preserve consistent stratigraphic trends that have been used to interpret variation in past SST (Ditchfield & Marshall, 1989; Jenkyns *et al.*, 1994; Schrag *et al.*, 1995; Clarke & Jenkyns, 1999; Stoll & Schrag, 2000). The suitability of $\delta^{18}O$ trends derived from bulk-sediment analyses as a palaeo-environmental proxy, is supported by compatible $\delta^{18}O$ data obtained from pristine brachiopod shells (Voigt, 2000b; Voigt *et al.*, 2004, 2006) and planktonic foraminifera (Voigt *et al.*, 2010) enclosed in the same sediments, and from coincident changes in macrofossil assemblages (Jarvis *et al.*, 2011).

Bulk pelagic carbonate $\delta^{18}O$ data for the Cretaceous generally exhibit the lowest values around the CTB extending into the Lower Turonian, pointing to a SST maximum and associated climate optimum, followed by general long-term cooling through the remainder of the Late Cretaceous (Scholle & Arthur, 1980; Jenkyns *et al.*, 1994; Clarke & Jenkyns, 1999). This interpretation is supported by isotopic analysis of pristine benthic and planktonic foraminifera in deep-sea sediments, and by TEX_{86} biomarker studies (Huber *et al.*, 2002; Friedrich *et al.*, 2012; MacLeod *et al.*, 2013; Linnert *et al.*, 2014).

Běchary oxygen isotope record

The long-term oxygen isotope profile at Bch-1 displays background rising values from −7 to −5‰ $\delta^{18}O$ through the Lower to mid-Middle Turonian, then a relatively flat background but with high-amplitude *ca* 1‰ medium-term peaks and troughs through the upper Middle to low Upper Turonian (Fig. 2). A shift to higher values of −4·5‰ $\delta^{18}O$ occurs in the Upper Turonian, reaching a maximum of −3·6‰ immediately above the Hitch Wood CIE and *Hyphantoceras* Event (Fig. 6). Falling values characterize the uppermost Upper Turonian, with a minimum of around −5‰ $\delta^{18}O$ in the mid-*M. scupini* Zone, then values rise again through the uppermost Turonian–Lower Coniacian. They reach a maximum of −3·8‰ $\delta^{18}O$ above the Beeding CIE, followed by a decline in the uppermost Lower Coniacian. The amplitude of medium-term $\delta^{18}O$ variation is generally lower (*ca* 0·5‰) in the upper half of the section (Fig. 2).

The CTB sediments at the base of the cored section in the Bch-1 well (402 to 405 m) display anomalously low $\delta^{18}O$ values of −8 to −10‰ (Figs 2 and 4E; Appendix S3). Similar low values have been reported for CTB sediments from other sections in the Bohemian Cretaceous Basin (Uličný *et al.*, 1993). These indicate a substantial diagenetic overprint when compared to values of −3 to −4‰ $\delta^{18}O$ that characterize most shallow-buried CTB pelagic carbonates elsewhere (Jenkyns *et al.*, 1994; Jarvis *et al.*, 2006, 2011). Carbonate in this interval also has $\delta^{13}C$ values that are up to 1‰ lower than the overlying Lower Turonian sediments (Figs 2 and 4E; Appendix S3), despite lying at a stratigraphic level characterized by a global positive $\delta^{13}C$ excursion of *ca* 2‰ amplitude (Jarvis *et al.*, 2006; Figs 4 and 5), generating $\delta^{13}C_{carb}$ values of up to 5‰ elsewhere. These isotope trends (Figs 2 and 4E) and values of coincident $\delta^{13}C_{carb}$ and $\delta^{18}O_{carb}$ depletion are consistent with substantial carbonate recrystallization and cementation occurring in a rock-dominated semi-closed porewater system (Hudson, 1977; Choquette & James, 1987; Marshall, 1992). Thin-section and SEM studies of equivalent levels at other localities in the area (Uličný *et al.*, 1993) provide evidence of significant dissolution of biogenic calcite and precipitation of microspar cement.

The cored interval in Bch-1 is underlain by an Upper Cenomanian calcareous sandstone aquifer with high fluid pressures that provides a major groundwater resource in

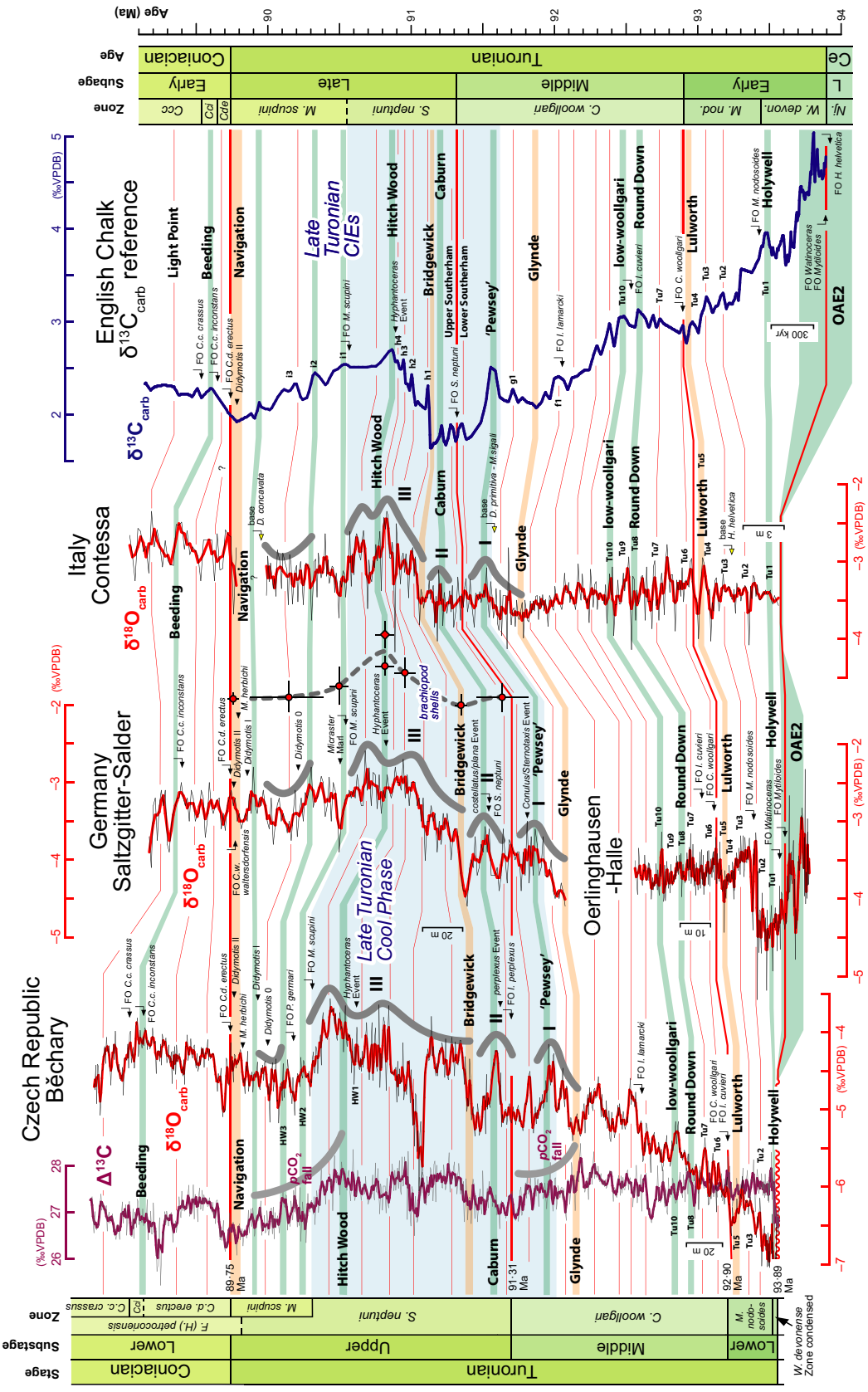

Fig. 6. Oxygen isotope profiles of European Turonian sections derived from bulk-sediment carbonate and brachiopod shells. Correlation of sections follows the carbon isotope stratigraphy illustrated in Fig. 5 (English Chalk $\delta^{13}C_{carb}$ reference curve shown on far right of diagram). Note coherent cooling tends (thick grey curves) towards higher $\delta^{18}O_{carb}$ values in the Mid-Turonian to Upper Turonian of the Czech Republic, Germany and Italy. Crosses (mean values with error bars) and red-filled symbols are brachiopod shell data from southern England (circles) and NW Germany (diamond), after Voigt (2000b). Brachiopod shells are typically offset to *ca* 1‰ higher values than their enclosing sediment but display identical trends (Voigt, 2000b, fig. 8). The three cooling intervals (I to III) of Voigt and Wiese (2000) are shown. Sediment isotope data sources: Bĕchary, this study; Saltzgitter-Salder (Voigt & Hilbrecht, 1997); Oerlinghausen-Halle, Voigt *et al.* (2007); Contessa, Stoll and Schrag (2000); English Chalk, Jarvis *et al.* (2006). Break in the Contessa profile represents an unsampled section correlated with immediately below the Navigation CIE (Sprovieri *et al.*, 2013). See Fig. 5 for explanation of other symbols.

the Bohemian Cretaceous Basin (Paces *et al.*, 2008). Fluid mixing of groundwater with porewaters in the overlying sediments would be limited by the low permeability of the carbonate-poor (17 to 21% $CaCO_3$) fine-grained calcareous mudstones (an aquiclude) at the base of the section. However, diffusional exchange with the aquifer waters and enhanced pressure solution (cf. Bloomfield, 1997) might be invoked to explain extensive carbonate recrystallization and the resetting of isotope values in the CTB section. A similar pattern of extreme $\delta^{18}O_{carb}$ depletion, with values of −10 to −14‰ and $\delta^{13}C_{carb}$ values *ca* 2‰, has been previously reported from Upper Cenomanian calcareous sandstones and overlying calcareous siltstones by Voigt and Hilbrecht (1997) in the Dresden-Blasewitz borehole of Saxony, northern Germany.

Present-day groundwater in Bohemian Cenomanian aquifers has $\delta^{18}O_{water}$ VSMOW values of around −10‰ (Jiráková *et al.*, 2010), close to the mean annual value of regional precipitation (−9·4‰ IAEA, 2009). Groundwater temperatures in the aquifer are of the order of 30°C which, using the equation of Anderson and Arthur (1983), generates a calcite equilibrium value of −13‰ ($\delta^{18}O_{carb}$ VPDB), or lower if higher temperatures developed in the geothermally influenced aquifer system (cf. Jiráková *et al.*, 2011). The isotopic composition of total dissolved inorganic carbon in the aquifer waters is also significantly lower than the host sediment, but is much more variable than for oxygen (−4·5 to −16·3‰ $\delta^{13}C_{carb}$, Jiráková *et al.*, 2010). For carbon, the potential impact of these very low values on sediment $\delta^{13}C_{carb}$ during recrystallization is limited by high rock: fluid inorganic carbon ratios.

Salinity in the Bohemian Cretaceous Basin

The Turonian $\delta^{18}O$ profile in Bch-1 shows a steeply rising trend from −8 to −5‰ VPDB through the Lower to mid-Middle Turonian (Figs 2 and 6). Sharp rises in $\delta^{18}O$ of *ca* 1·5‰ following a lowest Turonian minimum (Early Turonian thermal maximum) occur at the level of the Lower Turonian Tu2 CIE at Halle North Germany (Fig. 5; Voigt *et al.*, 2007) and at Dover England (Jenkyns *et al.*, 1994, fig. 4), but in those sections background values above Tu2 are relatively constant through the remainder of the Lower–Middle Turonian (Fig. 6). The background $\delta^{18}O$ trend at Contessa Italy remains flat throughout the Lower–Middle Turonian interval (Fig. 6), falling slightly in the upper Middle Turonian below the Glynde CIE.

The anomalous sharply rising $\delta^{18}O$ profile through the Lower–Middle Turonian at Bch-1 (Fig. 6), which is also evident in the record from the Dresden-Blasewitz (Voigt & Hilbrecht, 1997, fig. 4), might be attributed to carbonate recrystallization and cementation accompanying diffusion exchange with the underling aquifer waters and/or enhanced pressure-solution effects in the deeper buried section. However, this would require isotopic exchange over an 80 m section of low permeability claystones, which is unlikely. It is notable that spar-filled moulds after silicisponge spicules are common in the Lower Turonian section, decreasing in abundance upwards. A falling proportion of coarse burial-cement filled mouldic pores through the Lower to mid-Middle Turonian may partly explain the observed upward increase in $\delta^{18}O$.

An alternative explanation is that the increasing $\delta^{18}O$ trend reflects rising salinity of the Bohemian Cretaceous Basin and waters bordering the Bohemian Massif through the early to mid-Middle Turonian. Oxygen isotope values in the Upper Turonian–Coniacian section at Běchary are lower by *ca* 1‰ than equivalent sections in North Germany (Lower Saxony Basin) and Italy (Fig. 6). This depletion may be attributed to greater effect of diagenesis on bulk carbonate $\delta^{18}O$ in the relative carbonate-lean sediments. The Lower Turonian section, by contrast, is offset by −2·5‰ compared to the other sections. Taking into account a −1‰ $\delta^{18}O$ diagenetic offset, leaves −1·5‰ unaccounted for; this might potentially be attributed to reduced salinity of Bohemian Cretaceous Basin surface water compared to NW Germany Boreal and central Italy Tethyan waters.

The Bohemian Cretaceous Basin was surrounded by landmasses that during the Turonian sourced substantial volumes of siliciclastic sediments via prograding delta systems to the NW and SE of the study section (Uličný *et al.*, 2009, 2014). Although strongly tidally influenced with vigorous circulation (Mitchell *et al.*, 2010), basin waters received substantial freshwater input, and the occurrence of shallow-water dinoflagellate cyst species in the central basin points to transport by hypopycnal flows carrying low-salinity surface water across the basin (Olde *et al.*, 2015b). Water depths of <50 m are estimated for most of the basin area.

Results from a parallel ocean climate model for the Middle Cretaceous suggests salinities of *ca* 31·5 g kg^{-1} for the European area, a value that is 3 g kg^{-1} below the assumed global average of 34·7 g kg^{-1} (Poulsen *et al.*, 1998). Shackleton and Kennett (1975) estimated a mean $\delta^{18}O$ value of −1·0‰ VSMOW for sea water of a Cretaceous ice-free world. In the northern hemisphere where freshwater runoff was high, open-ocean sea water isotope values may have been lowered to less than −4‰ in the Arctic, while modelled Tethyan surface water has been estimated at +0·3 to +0·5‰ (Zhou *et al.*, 2008). A general value of −1·5‰ $\delta^{18}O$ has been proposed by Turonian epicontinental sea water in Western European basins (Voigt, 2000a).

At the assumed Turonian palaeolatitude of Central Europe *ca* 35°N (Fig. 1), mean annual zonal average precipitation is estimated to have been around −6‰ (Zhou *et al.*, 2008). The amount of altitude-effect $\delta^{18}O$ depletion in runoff is probably to have been modest due to the restricted topography on the adjacent landmasses. A simple mass balance calculation shows that addition of *ca* 22% freshwater of −6‰ $\delta^{18}O$ is required to generate the −1‰ offset observed in the earliest Turonian $\delta^{18}O$, with surface waters becoming progressive more saline thereafter. Using this estimate and assuming mixing freshwater of 0·5 g kg^{-1} with sea water of 31·5 g kg^{-1} generates a mildly brackish salinity of 24·7 g kg^{-1} for the earliest Turonian Bohemian Cretaceous Basin surface water. A lower volume of freshwater is required and the salinity would have been correspondingly higher if local runoff was more enriched in the light isotope.

A problem with invoking increasing salinity to explain rising $\delta^{18}O$ values through the Early–mid-Middle Turonian is that this period corresponds to a period of medium-term to long-term sea-level fall rather than sea-level rise (Uličný *et al.*, 2014). Lowest sea-levels are projected for the mid-Late Turonian. Increased marine water influence would be expected to accompany sea-level rise not fall.

The cause of rising $\delta^{18}O$ values through the Lower–Middle Turonian in Bch-1 remains uncertain. Oxygen isotope data from other sections in the Bohemian Cretaceous Basin are required to assess the potential influence of diagenetic versus salinity effects on the $\delta^{18}O$ records.

The Late Turonian Cool Phase

By contrast to the lower beds, oxygen isotope records from the upper Middle Turonian–Lower Coniacian at Běchary (Fig. 6) show very similar medium-term to long-term trends to published $\delta^{18}O_{carb}$ records from Salzgitter-Salder (Voigt & Hilbrecht, 1997) and Söhlde NW Germany (Voigt & Hilbrecht, 1997), Dover England (Jenkyns *et al.*, 1994, fig. 4), Liencres northern Spain (Wiese, 1999), and Contessa Italy (Stoll & Schrag, 2000). The oxygen stable isotope profile for the Upper Turonian at Běchary shows a strong trend of increasing values upwards to a maximum immediately above the *Hyphantoceras* Event and Hitch Wood CIE in the Upper Turonian mid-*S. neptuni* Zone (Figs 2 and 6). A $\delta^{18}O$ maximum at the same level is displayed by a less stratigraphically extensive low-resolution $\delta^{18}O$ curve for the mid-Upper Turonian at Úpohlavy (Wiese *et al.*, 2004), located on the NW margin of the Bohemian Cretaceous Basin, 90 km NW of Běchary.

Bulk-sediment oxygen isotope profiles for the Upper Turonian of the Bohemian Cretaceous Basin and elsewhere in Europe exhibit punctuated multi-stage increases in $\delta^{18}O$ interpreted to represent a marine cooling trend (Wiese, 1999; Voigt, 2000b; Wiese & Voigt, 2002), starting with a $\delta^{18}O$ rise in the upper Middle Turonian around the 'Pewsey' CIE (Fig. 6). Values increase sharply by *ca* 1‰ above the Bridgewick CIE, and peak above and below the Hitch Wood CIE, representing maximum Late Turonian cooling, before decreasing again to a minimum, indicative of temporarily warmer conditions in the latest Turonian *M. scupini* Zone. Oxygen isotope values increase above this, demonstrating continued cooling into the Early Coniacian.

Bulk $\delta^{18}O$ curves are inherently noisy due to the susceptibility of oxygen isotopes to diagenetic overprinting (Marshall, 1992; Schrag *et al.*, 1995; Frank *et al.*, 1999) and commonly display a strong lithological control. Unsurprising, therefore, unlike carbon isotopes, short-term peaks and troughs in $\delta^{18}O$ show relatively poor agreement between different sections (Fig. 6). In addition, $\delta^{18}O$ values in the Bohemian Cretaceous Basin hemipelagic successions are lower by *ca* 1‰ than those at equivalent levels in the pelagic German and Italian sections, and show high-amplitude (up to 1‰) short-term variation, evidencing more extensive and more variable lithology-controlled diagenesis in the relatively carbonate-poor sediments (Fig. 2; 4 to 71% $CaCO_3$, average 35%). Lower $\delta^{18}O$ values and higher amplitude isotopic variation are also observed in other low-carbonate Upper Turonian hemipelagic sections (e.g. at Liencres, Voigt & Wiese, 2000).

An anomalous large negative excursion of *ca* 2‰ $\delta^{18}O$ occurs in the lower *S. neptuni* Zone at the facies change marking the boundary between Sequences TUR 5 and TUR6/1 in Bch-1. This excursion is confined to a low-carbonate interval (18% $CaCO_3$), and corresponds to a $\delta^{13}C_{carb}$ negative excursion that coincides with a $\delta^{13}C_{org}$ peak (Fig. 2). The level marks a significant lithological and geochemical facies change upwards to coarser grained silty and more calcareous marlstones (Fig. 2) with high Si/Al, Ti/Al and Zr/Al ratios (Uličný *et al.*, 2014; Olde *et al.*, 2015b). No comparable negative $\delta^{18}O$ isotope excursion is observed in equivalent oxygen isotope profiles from elsewhere in Europe (Fig. 6). Coupled oxygen and carbon isotope depletion in bulk carbonate points to a diagenetic origin for this feature, probably caused by enhanced pressure solution and potentially fluid flow focussed along the facies boundary. A similar but much lower amplitude (*ca* 0·5‰ $\delta^{18}O$) negative excursion occurs in low-carbonate claystones (9% $CaCO_3$), immediately below the transition to marlstones (35% $CaCO_3$) near the base of the Lower Coniacian, above the Navigation CIE (Figs 2 and 6).

Identical medium-term to long-term Middle Turonian–Lower Coniacian $\delta^{18}O$ trends, constrained by a combination of high-quality biostratigraphy, tephrostratigraphy and carbon isotope stratigraphy, are seen not only at Běchary, Saltzgitter-Salder and Contessa (Fig. 6), but also in curves from Dover southern England (Jenkyns *et al.*, 1994), Söhlde NW Germany (Voigt & Hilbrecht, 1997), Dubivtsi western Ukraine (Dubicka & Peryt, 2012), Liencres northern Spain (Wiese, 1999), and Santa Ines southern Spain (Stoll & Schrag, 2000), with variable values and amplitudes reflecting varying lithological compositions, and different burial and diagenetic histories. The remarkable consistency of the stratigraphic trends mediates against them being purely a diagenetic artefact. Essentially synchronous diagenetic effects in multiple sections might be invoked if diagenesis were linked to eustatic sea-level change via an influence on the amount of authigenic cements (cf. the carbon isotope argument of Schrag *et al.*, 2013), or via sediment coarsening and associated higher permeability (and thus susceptibility to diagenesis) of sediments deposited during periods of lower eustatic sea-level. However, it is difficult to envisage how so similar $\delta^{18}O$ trends and values might be generated in such a wide range of depositional settings, from tidally influenced shallow-water epicontinental basins (e.g. Běchary) to pelagic slope environments at 1 to 1·5 km water depth (e.g. Contessa; Premoli Silva & Sliter, 1995).

Three stages of Mid-Turonian to Late Turonian medium-term (*ca* 250 kyr) stepped cooling were postulated by Voigt and Wiese (2000) using $\delta^{18}O$ data from England, Germany and Spain, which they designated as 'Phases' I to III (termed 'Intervals' I to III here, Fig. 6). These intervals peak around the 'Pewsey', Caburn, and Hitch Wood positive CIEs, with significant $\delta^{18}O$ increases starting above the Glynde (Interval I) and Bridgewick (Interval III) negative CIEs. Significantly, oxygen isotope analysis of well-preserved brachiopod shells from southern England and NW Germany follow bulk-rock $\delta^{18}O$ trends in their enclosing sediments (Fig. 5; Voigt, 2000b), with *ca* 1‰ lower values in the latter attributable to the addition of a pervasive isotopically lighter cement, and/or kinetic 'vital' effects influencing brachiopod shell values. Brachiopod data indicate *ca* 2°C of bottom-water cooling from 18·2° to 16·0°C during Interval III, with lower minimum temperatures attained in NW Germany (14·2°C) than in southern England (Fig. 5; Voigt, 2000b). Voigt (2000b) attributed this to a greater influence of cool northern Boreal North Sea waters in Germany compared to the proto-Atlantic influenced Anglo-Paris Basin.

The palaeo-environmental significance of the medium-term and long-term $\delta^{18}O$ isotope trends is demonstrated by temporary influxes of Boreal and temperate taxa into the 'Northern Transitional Subprovince' during peak cooling of Intervals I and III (Voigt & Wiese, 2000; Wiese & Voigt, 2002; Wiese *et al.*, 2004). This area extended from northern Spain, through southern France, SE Germany, and the Czech Republic to Austria, and is characterized by faunal assemblages that are a hybrid of northern and southern affinity ammonites, bivalves and echinoids (Wiese & Voigt, 2002).

Interval I terminated with the short-term immigration of northern affinity echinoids and ammonites into the Spanish North Cantabrian Basin (Voigt & Wiese, 2000). Contemporaneous with the southward spread of collignoniceratid ammonites into northern Spain, taxa more indicative of southern areas (*Romaniceras*, *Coilopoceras*) migrated northwards, suggesting weakening of former provincialism. Interval III is characterized by the progressive establishment of typical northern echinoid and inoceramid assemblages in northern and central Europe; in northern Spain these assemblages become dominant within the interval of highest $\delta^{18}O$ values above the Hitch Wood CIE. Collignoniceratid ammonites occur in southern France at the same level (Devalque *et al.*, 1982). The combination of isotopic and faunal evidence for Late Turonian cooling throughout Europe, points to a temporary shift of northern waters southwards during Intervals I and III, together with other water-mass reorganization (Voigt & Wiese, 2000; Wiese & Voigt, 2002; Wiese *et al.*, 2004). Coincident faunal changes during Interval III include the migration of the North American ammonite *Prionocyclus* into Europe and North Africa.

The Bohemian Cretaceous Basin was a key area sensitive to climate change during the Turonian, as it represented a gateway between northern Tethys and the southern Boreal Sea (Fig. 1A). Faunally, the area lay at the northern limit of the Northern Transitional Subprovince. The ammonite assemblage or '*reussianum* fauna' characterizing the *Hyphantoceras* Event [Fig. 6; named after the distinctive heteromorph ammonite *Hyphantoceras reussianum* (d'Orbigny)] and peak Interval III cooling, is widely distributed in the Czech Republic, England, parts of France, Germany, Poland and, to some extent, Kazakhstan (Wiese *et al.*, 2004). However, the relative rarity of allocrioceratids and collignoniceratids in the Bohemian faunas point to a southern affinity for the ammonite assemblage there (Wiese *et al.*, 2004).

In Bohemia, warm-water Nerineacean gastropod assemblages of the Cenomanian–Middle Turonian are replaced by a Boreal Pleurotomariacean fauna at the level of the *Hyphantoceras* Event (Kollmann *et al.*, 1998), along with an influx of rare Boreal belemnites from North America via Greenland and Scandinavia

(Košťák *et al.*, 2004; Wiese *et al.*, 2004; Košťák & Wiese, 2011). The nautiloid *Deltocymatoceras rugatum* (Fritsch & Schönbach) is recorded solely from the *Hyphantoceras* Event, and is restricted to shallow-water facies on the northern margins of the Bohemian Massif, and in the vicinity of the adjacent Lausitz and Sudetic blocks (Frank *et al.*, 2013). Bohemian Cretaceous Basin records, therefore, provide strong evidence of regional faunal changes accompanying the Late Turonian Cool Phase.

LINKED CLIMATE AND SEA-LEVEL CHANGE

A tentative eustatic sea-level curve for the Turonian based on the analysis of sediment geometries and the delineation of transgressive/regressive maxima across the Bohemian Cretaceous Basin was presented by Uličný *et al.* (2014). The medium-term to long-term transgressive–regressive framework and inferred sea-level model (Fig. 7) is supported by complementary chemostratigraphic and palynological studies (Olde *et al.*, 2015b). For example, well-defined maxima in bulk-sediment manganese content are associated with maximum flooding zones, and troughs with intervals of lowstand; falling Mn contents accompany regression and rising values transgression (Jarvis *et al.*, 2001, 2008; Olde *et al.*, 2015b, fig. 11). The most prominent feature of the Mn profile is a major long-term symmetrical trough centred on the *Hyphantoceras* Event and Hitch Wood CIE, interpreted to represent a peak regional lowstand on a long timescale. The Si/Al, Ti/Al and Zr/Al ratios, tracers for input of a more proximal siliciclastic fine fraction, display the opposite trend to Mn, with rising values accompany long-term sea-level fall, and declining values following sea-level rise, as exemplified by the Ti/Al profile in Fig. 7.

Dinoflagellate cyst species richness provides another excellent sea-level proxy in the Bohemian Cretaceous Basin (Olde *et al.*, 2015b). Intervals yielding low-diversity dinocyst assemblages in the Běchary succession correlate to sea-level minima. Sharp increases in species richness accompany transgression, with maxima coincident with periods of maximum flooding. The majority of well-defined short-term transgressive–regressive sea-level cycles in the Middle–Upper Turonian at Běchary (Fig. 7) are clearly expressed by peaks and troughs in the dinocyst species richness record (Olde *et al.*, 2015b, fig. 10).

The Late Turonian Cool Phase coincided, therefore, with evidence of a major third-order fall of sea-level that started in the early-Middle Turonian and terminated in the mid-Late Turonian (Fig. 7). The hardground complexes of the Chalk Rock were deposited at that time in England (Bromley & Gale, 1982; Hancock, 1989; Gale, 1996), massively bedded, in-part nodular, limestones formed in northern Germany (Wood *et al.*, 1984), and nodular glauconitic limestones and turbidite successions were deposited in northern Spain (Wiese, 1997).

Interval I, around the level of the 'Pewsey' CIE, represents an initial period of medium-term shallowing (e.g. Fig. 7). Coarser grained, silty marlstones with common skeletal debris and sand laminae characterize this level at Běchary (270 to 276 m, Fig. 2). The onset of massive stacked hardground development on basin margins occurred in southern England, a thinning upwards sequence of nodular and bedded limestones terminating in the *Conulus*/*Sternotaxis* Event was deposited in northern Germany (Fig. 6), and glauconitic turbidite sequences, hardgrounds and regional hiatuses characterize the interval in northern Spain (Voigt & Wiese, 2000; Wiese & Voigt, 2002).

Increased sedimentation in all areas characterizes Interval II, reflecting a medium-term transgression. In Bohemia, a transgression at the base of Upper Turonian Sequence TUR 5 is prominent basin wide, and marks the onset of higher carbonate contents and more widespread cementation in all facies that culminate around the level of the *Hyphantoceras* Event (Fig. 2). An acme of *Inoceramus perplexus* Whitfield in the Bohemian sections (*perplexus* Event) correlates to the *costellatus/plana* Event in NW Germany (cf. Richardt & Wilmsen, 2012), at the base of the Caburn CIE (Fig. 6).

Interval III is associated with evidence of progressive shallowing in many European basins: a regressive maximum is seen throughout the Bohemian Cretaceous Basin, corresponding to the summit of the coarsening-upward succession at Běchary (Fig. 2). The uppermost hardgrounds of the English Chalk Rock developed at this time, terminating in the Hitch Wood Hardground (Bromley & Gale, 1982; Gale, 1996). There is an increased abundance of benthic carbonate producers, and the development of nodular limestones with regional hiatuses in northern Germany, and in northern Spain, a calciturbidite sequence occurs, terminated by calcarenitic channel-fill deposits (Voigt & Wiese, 2000; Wiese & Voigt, 2002). In Bohemia and western Ukraine, a transition to more calcareous dinoflagellate cyst-rich (principally pithonellids) sediments and the temporary disappearance of keeled planktonic foraminifera further indicate shallower water and more oligotrophic conditions (Wiese *et al.*, 2004; Dubicka & Peryt, 2012).

Renewed transgression characterized the latest Turonian basal *M. scupini* Zone throughout Europe, and the biota of the Northern Transitional Subprovince retained a more Boreal affinity thereafter. Sedimentological evidence suggests, therefore, a relation between regional cooling of bottom and surface waters, the southward spread of Bor-

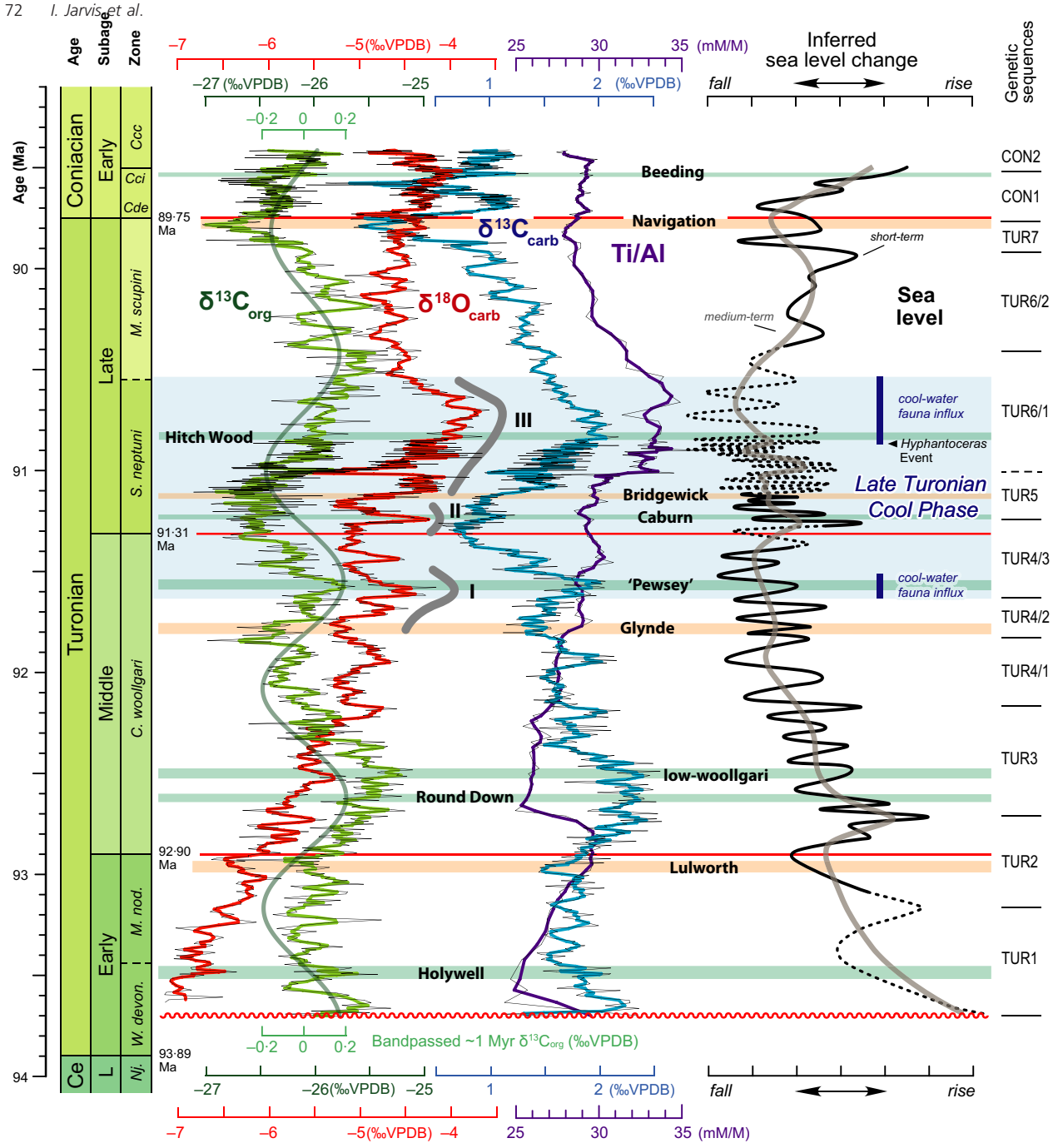

Fig. 7. Stable isotope profiles for the Turonian–Coniacian at Běchary compared to an inferred sea-level curve. Sea-level trends derived from transgressive–regressive maxima and basin-scale sediment geometries in the Bohemian Cretaceous Basin (Uličný *et al*., 2014). Late Turonian cooling intervals after Voigt and Wiese (2000). A bandpassed *ca* 1 Myr signal in $\delta^{13}C_{org}$ interpreted as a signature of axial-obliquity modulation (Laurin *et al*., 2015) is indicated by a thick green curve. Data were calibrated in the time domain using a modified age model from Laurin *et al*. (2015): the stratigraphic position of the Hitch Wood Event was reinterpreted based on new $\delta^{13}C_{carb}$ data (this study); the FO *P. germari* was not used as an age control point due to uncertainties in the local distribution of this taxon (cf. Laurin *et al*. 2014); for the Lower Turonian, a 200 kyr hiatus was applied at the base of the Turonian, above this hiatus, sedimentation rates were linearly increased from 0 cm kyr^{-1} to 7·5 cm kyr^{-1} (mean sedimentation rate for the Middle Turonian) at the top of the substage. Ages of stage and substage boundaries derived from Ogg *et al*. (2012), Laurin *et al*. (2014) and Sageman *et al*. (2014); age controls are summarized in Appendix S1. Ti/Al ratio curve, a potential sea-level proxy, from Olde *et al*. (2015b). Basin-scale genetic sequences are modified from Uličný *et al*. (2014), following Olde *et al*. (2015b). Note that Late Turonian cooling Intervals I and III observed in the oxygen isotope profiles throughout Europe (Fig. 5), correspond to packages displaying influxes of cool-water fauna in the Bohemian Cretaceous Basin, and more widely across the Northern Transitional faunal Subprovince (Voigt & Wiese, 2000; Wiese & Voigt, 2002). Cool-water faunal influxes occurred during episodes of short-term transgression, approaching levels of maximum regression and inferred sea-level lowstand.

eal taxa and low-order transgressions following sea-level falls.

The wider impact of the Late Turonian Cool Phase in Europe in relation to global climate and palaeoceanography remains to be adequately tested. However, northern hemisphere-wide water-mass reorganization is indicated by the a temporary influx during Interval III of *Prionocyclus* ammonites from the North American Western Interior Seaway (WIS), which are widely distributed in northern Germany and the Czech Republic, through southern Spain to Tunisia (Robaszynski *et al.*, 2000). At the same time, several belemnite taxa migrated eastwards from Greenland (Košťák & Wiese, 2011), and a connection to Japan is suggested by the occurrence of *Mytiloides incertus* Jimbo in both Europe and Japan (Voigt, 1995; Takahashi, 2005; Hayakawa & Hirano, 2013).

Pronounced Late Turonian cooling is indicated by $\delta^{18}O$ trends in the fine-fraction curves from the Southern Hemisphere Exmouth Plateau (Clarke & Jenkyns, 1999). However, the Late Turonian cooling discussed above appears to be significantly younger than a 'middle' Turonian glacial episode and sea-level lowstand postulated by Miller *et al.* (2004) in New Jersey, by Bornemann *et al.* (2008) from Demerara Rise western Equatorial Atlantic, and by Galeotti *et al.* (2009) on the Apulian margin Italy. Unfortunately, in all of these cases, age control is poor compared to the high-resolution multi-stratigraphic correlations achievable in European pelagic and hemipelagic sections.

Biostratigraphic correlation from northern European to Atlantic and Italian sections remains ambiguous: the correspondences between Turonian CC and UC calcareous nannofossil zones (Sissingh, 1977; Burnett *et al.*, 1998), planktonic foraminiferal zones, regional macrofossil zones, and CIEs are all relatively poorly constrained (Lees, 2008; Švábenická, 2012). The correlation by Bornemann *et al.* (2008) of a $\delta^{18}O$ peak and inferred sea-level lowstand at western equatorial Atlantic ODP Site 1259 with the 'Pewsey' CIE is probably erroneous (see Uličný *et al.*, 2014 for discussion). The possibility of a Middle Turonian glacial episode was rejected by MacLeod *et al.* (2013), based on the uniformity of $\delta^{18}O$ values obtained from multiple benthic and planktonic foraminifera species collected through a Lower to Middle Turonian section in Tanzania. However, their data do not extend into the Upper Turonian, so the possibility of a glacial influence on Late Turonian global cooling and sea-level fall remains untested.

Possible inter-relationships between climate and sea-level change remain controversial for a greenhouse climate system. In the absence of evidence for significant polar ice in the Turonian, Wendler and Wendler (2016) suggested that aquifer-eustatic (cf. Hay & Leslie, 1990) rather than glacio-eustatic forcing of sea-level might occur. This condition challenges the general assumption, based on changes in polar ice volume, that transgression will necessarily accompany warming (with falling sea water $\delta^{18}O$), and regression will accompany cooling (rising sea water $\delta^{18}O$). In an aquifer-eustatic system, an enhanced hydrological cycle during periods of climate warming may lead to increased aquifer storage volumes, sea-level fall and rising sea water $\delta^{18}O$ values. Our Bohemian Cretaceous Basin records, however, show a clear association between medium-term to long-term sea-level fall, inferred from detailed analysis of sediment sequence geometries, and a Europe-wide southward spread of cooler water masses with elevated $\delta^{18}O$ values. In the short term, however, major influxes of cool-water faunas appear to accompany transgression. Clearly, comparable high-resolution data sets from other basins with independently derived sea-level curves are needed to address these issues further.

CARBON ISOTOPES AS A pCO_2 PROXY

Photosynthetic carbon stable isotope fractionation (ε_p) by marine phytoplankton increases with ocean conditions that promote high CO_2 availability in surface waters, such as elevated atmospheric CO_2 concentrations (Dean *et al.*, 1986). This phenomenon explains why Cretaceous marine organic matter typically has $\delta^{13}C$ values that are up to 5 to 7‰ lower than its modern equivalent (Arthur *et al.*, 1985). It has been proposed that the larger amplitude of the CTB $\delta^{13}C_{org}$ excursion (as much as 4 to 6‰) compared to the $\delta^{13}C_{carb}$ excursion (typically *ca* 2‰) in sections worldwide may be attributed to reduced isotopic fractionation between dissolved inorganic carbon and marine organic matter as a consequence of lower atmospheric carbon dioxide (CO_2 drawdown) and increased marine productivity during OAE2 (Arthur *et al.*, 1988; Freeman & Hayes, 1992; Kuypers *et al.*, 1999, 2002; Tsikos *et al.*, 2004; Sinninghe Damsté *et al.*, 2008; Jarvis *et al.*, 2011).

Given the relationship between ε_p and pCO_2, stratigraphic variation in the offset between covarying $\delta^{13}C_{carb}$ and $\delta^{13}C_{org}$ curves, expressed by $\Delta^{13}C$, offers a potential tool for tracing palaeo-pCO_2 change (cf. Kump & Arthur, 1999; Jarvis *et al.*, 2011), assuming: (1) no significant diagenetic alteration of the carbonate or organic carbon $\delta^{13}C$ values, or a uniform systematic overprinting of these; (2) an overwhelmingly marine or terrestrial organic matter fraction, or a constant proportion of these; and (3) limited temporally restricted productivity effects.

Paired carbonate and organic matter $\delta^{13}C$ records have been reported from several CTB sections (Freeman & Hayes, 1992; Tsikos *et al.*, 2004; Sageman *et al.*, 2006; Voigt *et al.*, 2006, 2007; Scopelliti *et al.*, 2008; Jarvis *et al.*,

2011). However, in many cases, the reliability of one of the data sets is questionable due to: (1) an absence of carbonate in the most organic-rich layers and/or insufficient organic matter in some limestones (e.g. the Bonarelli Level at Bottaccione); (2) the occurrence of erratic anomalously low values in $\delta^{13}C_{carb}$ profiles, indicative of locally precipitated organic matter-derived carbonate cements (e.g. Tarfaya) and (3) uniform low $\delta^{13}C_{carb}$ values, suggesting pervasive overprinting by recrystallization or the addition of extensive homogenous calcite cement (e.g. Bonarelli equivalent, Novara di Sicilia). However, stratigraphic variation in paired records presented by Jarvis *et al.* (2011) from a CTB section in the Vocontian Basin of SE France, compare favourably to the data across the same interval in England (Paul *et al.*, 1999; Gale *et al.*, 2005) and Germany (Voigt *et al.*, 2006), and offsets between the carbonate and organic curves ($\Delta^{13}C = \delta^{13}C_{carb} - \delta^{13}C_{org}$) were used to interpret a pCO_2 record for the interval.

Turonian $\Delta^{13}C$ values at Běchary are relatively constant at 27·7 ± 0·3‰ up to the level of the Hitch Wood CIE (Fig. 6) and then fall to a minimum of *ca* 26·4‰ at the Navigation CIE and Turonian–Coniacian boundary. This fall is initiated at the main influx of cool-water fauna around the *Hyphantoceras* Event. The ensuing medium-term $\Delta^{13}C$ falling trend spans an interval of falling then rising $\delta^{18}O$ values at Běchary (temporary warming), although a comparable $\delta^{18}O$ minimum is less clearly expressed at Saltzgitter-Salder and Contessa (Fig. 6). In these cases, the main feature of the long-term $\delta^{18}O$ trends is a step change to cooler temperatures by the later Late Turonian. This phenomenon implies that the main pCO_2 fall followed rather than preceded cooling. Significantly, a less marked $\Delta^{13}C$ fall occurs in the upper Middle Turonian at the level of the Glynde CIE, immediately preceding the first influx of cool-water biota around the 'Pewsey' CIE and the first step upwards in $\delta^{18}O$ (Fig. 6).

Any interpretation of $\Delta^{13}C$ trends at Běchary as a pCO_2 proxy must be treated with caution, given the observed diagenetic modification of primary $\delta^{18}O$ values, and the coincidence of the main $\Delta^{13}C$ shift with a facies change to finer-grained less-calcareous sediments (Fig. 2). The decreasing offset between $\delta^{13}C_{carb}$ and $\delta^{13}C_{org}$ records might be related to an increased proportion of authigenic carbonate, either locally at Běchary, or more generally in the oceans (cf. Schrag *et al.*, 2013). An increase in the proportion of organically influenced isotopically lighter carbonate cement will lower $\Delta^{13}C$. This fall would be amplified if marine organic matter was preferentially oxidized, leaving a higher proportion of isotopically heavier terrestrial organic matter. However, this is unlikely to be the case in Bch-1, where the terrestrial/marine palynomorph ratio falls significantly through the uppermost Turonian–lowest Coniacian (Olde *et al.*, 2015b); this would be expected to increase rather than decrease $\Delta^{13}C$ values. Nonetheless, the coincidence between the faunal and geochemical proxies of climate change is intriguing and warrants further investigation in other sections.

CARBON ISOTOPE RECORDS AND SEA-LEVEL CHANGE

A number of short-term, basin-wide regressions in the Bohemian Cretaceous Basin, most probably reflecting eustatic falls, have been documented with a recurrence interval of 100 kyr or less (Uličný *et al.*, 2009, 2014; Mitchell *et al.*, 2010). The estimated magnitude of these sea-level falls is typically 10 to 20 m and generally <40 m. The correspondence between $\delta^{13}C_{org}$ at Běchary and an inferred sea-level curve for the Basin was examined by Uličný *et al.* (2014). They noted that a long-term 'background' cycle of $\delta^{13}C_{org}$ (Fig. 7), shows a duration close to the 2·4 Myr long-eccentricity cycle, and shorter-term (1 Myr scale) highs and lows in $\delta^{13}C_{org}$ appear to broadly correspond to intervals characterized by more pronounced short-term sea-level highs and lows, respectively. However, despite a number of individual matches, neither a systematic in-phase nor out-of-phase correlation with interpreted sea-level cycles could be demonstrated at the level of either short-term (≤100 kyr) or intermediate-term (100 to 500 kyr) $\delta^{13}C_{org}$ fluctuations.

Comparison of the new $\delta^{13}C_{carb}$ and published $\delta^{13}C_{org}$ profiles to the sea-level model of Uličný *et al.* (2014) indicates a better correlation for the former than for the latter (Fig. 7), with approximately two-thirds of the inflection points on the short-term sea-level curve (transgressive surfaces) corresponding to the bases of $\delta^{13}C_{carb}$ peaks, and over half of the regressive maxima corresponding to $\delta^{13}C_{carb}$ minima. However, only half of the positive correlations of $\delta^{13}C_{carb}$ to sea-level show coincident shifts in $\delta^{13}C_{org}$, so a clear relationship with the global carbon cycle remains unproven.

A number of factors may influence the differing relationships between $\delta^{13}C_{carb}$ and $\delta^{13}C_{org}$ at Běchary and the sea-level record. First, both isotope records are relatively noisy, prejudicing the exact placement of maxima and minima. Second, uncertainty remains in the correlation of transgressive/regressive maxima between the NW and SE basin fills and the Bch-1 core; the sea-level model requires further refinement. Third, elemental chemostratigraphy (Olde *et al.*, 2015b) demonstrates short-term changes in sediment composition that accompany transgressive pulses, exemplified by intervals with increased Ti/Al (Fig. 7), Si/Al and Zr/Al ratios in the core. The combination of physical and mineralogical changes at these levels would probably affect carbonate diagenesis, which

impacts $\delta^{13}C_{carb}$. At the same time, subtle changes in organic matter provenance, composition or preservation might also cause a divergence between the $\delta^{13}C_{org}$ versus $\delta^{13}C_{carb}$ records. Additional work is required to rigorously test relationships between carbon isotope records and sea-level change.

The main interval of divergence between the $\delta^{13}C_{carb}$ and $\delta^{13}C_{org}$ profiles lies in the higher part of the Upper Turonian where falling $\delta^{13}C_{carb}$ accompanies a rising $\delta^{13}C_{org}$ trend. Declining $\delta^{13}C_{carb}$ values might be interpreted to indicate increasing carbonate diagenesis accompanying falling carbonate values (Fig. 2). However, an identical trend is seen in carbonate isotope curves throughout Europe (Fig. 5), so it is unlikely to be a diagenetic artefact. Declining isotopic fractionation in marine organic matter due to falling pCO_2 (Fig. 5) offers a possible explanation for the divergence between $\delta^{13}C_{org}$ and $\delta^{13}C_{carb}$ trends (cf. Jarvis *et al.*, 2011).

CARBONATE AND ORGANIC CARBON FLUXES

Simplistically, the long-term Turonian carbon isotope record at Bch-1 (Figs 5 and 7) implies a moderately high organic matter versus carbonate burial flux in the Early Turonian, a period of enhanced burial of organic matter in the early-Middle Turonian, then a falling burial flux through the remainder of the Middle Turonian to a minimum during the earliest Late Turonian. The Late Turonian shows distinct rising then falling organic matter burial, peaking in the middle of the subzone and with a period of minimum burial spanning the Turonian–Coniacian boundary then a modest recovery thereafter.

Laurin *et al.* (2015) employed spectral analysis of $\delta^{13}C_{org}$ data from the Bch-1 core, together with $\delta^{13}C_{carb}$ data from other European Cretaceous sections, to propose that transfers between surface carbon reservoirs may be controlled by external forcing, principally *ca* 1 Myr changes in the amplitude of axial obliquity. The authors argued that the astronomical control causes transient storage of organic matter or methane in quasi-stable reservoirs such as terrestrial peat, soils and lakes, marginal zones of marine euxinic strata and, potentially, permafrost. These reservoirs responded nonlinearly to obliquity-driven changes in high-latitude insolation and/or the meridional insolation gradient, resulting in the *ca* 1 Myr cyclic $\delta^{13}C$ pattern observed in the Turonian–Coniacian (e.g. Figs 5 and 7), and potentially driving the multi-Myr-scale cyclicity observed in the Cenozoic (Boulila *et al.*, 2012).

The balance between the carbonate-carbon and organic-carbon burial fluxes is not controlled solely by the efficiency of organic matter preservation; both fluxes must balance the terrestrial carbon input flux on a 10^6 timescale and longer due to the small size of the ocean-atmosphere reservoir in comparison with the observed flux rates. At steady state, with a constant terrestrial carbon input by chemical weathering, an increase in inorganic carbon burial will lead to decreased organic carbon burial. This condition will release CO_2 to the ocean–atmosphere system and decrease $\delta^{13}C$ values. The marked expansion of chalk sedimentation in the Early Turonian (Voigt, 2000a, fig. 5) might explain the long-term $\delta^{13}C$ decline evident in Lower and Middle Turonian records (Fig. 5).

GLOBAL CORRELATION OF TURONIAN CARBON ISOTOPE CURVES

US Western Interior Basin: a $\delta^{13}C_{org}$ correlation

The Cretaceous Western Interior Basin of North America (Fig. 1B) has a well-established inoceramid bivalve and ammonite biostratigraphy (Kauffman *et al.*, 1993; Cobban *et al.*, 2006), has excellent geochonological control from radiometrically dated volcanic ash bands (Obradovich, 1993; Meyers *et al.*, 2012; Sageman *et al.*, 2014), includes key intervals with astrochronological time scales (Sageman *et al.*, 2006; Meyers *et al.*, 2012), and hosts the GSSP for the base Turonian Stage (Kennedy *et al.*, 2005). The occurrence of common bentonites throughout the Western Interior succession offers unique potential for geochronological calibration of the Cretaceous timescale using paired $^{40}Ar/^{39}Ar$ sanidine and U–Pb zircon ages.

Unfortunately, intercontinental correlation of Western Interior successions has been hampered by: taxonomic issues with inoceramid assemblages; a dominance of endemic ammonite faunas in the post-Cenomanian section; the general absence of echinoderms and other stenohaline taxa; and basin restriction and the presence of siliciclastic sediments in many intervals limiting the use of planktonic foraminifera and calcareous nannofossil biostratigraphy. However, carbon isotope chemostratigraphy has been successfully applied for high-resolution correlation of the base Turonian GSSP to Europe (Gale *et al.*, 1993; Kennedy *et al.*, 2005), and offers great potential to develop more refined Turonian correlations between North America and other successions globally.

A composite $\delta^{13}C_{org}$ reference curve for Cenomanian–Campanian of the United States Western Interior Basin was published by Joo and Sageman (2014), based on analysis of three cored boreholes and correlation of macrofossil biostratigraphic datum levels to these from outcrop. in addition, a temporal framework was developed by correlation with current geochronological and astrochronological timescales (Meyers *et al.*, 2012). However,

biostratigraphic control is limited above the CTB interval, and inter-core correlation and the placement of zonal boundaries was based largely on lithostratigraphy. The Turonian section of the North American composite curve is compared to the age-calibrated English Chalk $\delta^{13}C_{carb}$ reference curve and age-calibrated $\delta^{13}C_{carb}$ and $\delta^{13}C_{org}$ curves from Běchary in Fig. 8.

Correlation of the CTB interval between the Western Interior and Europe is well-established (Kennedy *et al.*, 2005). The boundary section at Běchary is thin and incomplete (Fig. 2), and cannot be compared to the expanded North American succession in detail. The Lower Turonian in the Western Interior can be anchored by the FO *Watinoceras devonense* and *Mytiloides puebloensis* at the bottom and FO *C. woollgari* at the top of the substage, with the base of the *Mammites nodosoides* Zone coincident with the top of the Holywell CIE (Fig. 7; = excursion T1 of Joo & Sageman, 2014).

The Western Interior Basin Middle Turonian composite curve shows a characteristic rising trend to the Low-woollgari CIE maximum, and declines above. A step increase of 1‰ at the base of the *Collignoniceras praecox-Prionocyclus hyatti/Inoceramus howellii* Zones (lower profile break in Fig. 8) is almost certainly an artefact caused by stacking data from the CL-1 core on top of the Portland core. The profile across the interval in the Portland core alone shows progressively declining values upwards with no offset (Joo & Sageman, 2014, fig. 2).

Placement of the base Upper Turonian in the Western Interior is uncertain compared to its equivalent level in Europe (i.e. first appearance of *I. perplexus*). It is conventionally placed at the base of the *Scaphites whitfieldi* Zone (Joo & Sageman, 2014) in the Western Interior, but the carbon isotope correlation with the CL-1 core indicates that positioning the substage boundary lower, at the base of the *Inoceramus dimidius* Zone offers better consistency (Fig. 8). This positioning conforms to the base Upper Turonian as defined by Kauffman *et al.* (1993), although those authors did not indicate their reason for placing it at that level. The recorded FO of *I. dimidius* in the CL-1 core (Ball *et al.*, 2010), used to construct this part of the composite curve, is consistent with the position of the Upper Turonian substage boundary based on our carbon isotope correlation (Fig. 8). Records of *I.* aff. *perplexus* in the mid-*I. dimidius* Zone of CL-1 (Ball *et al.*, 2010) also support this interpretation, although these are above the $\delta^{13}C_{org}$ minimum marking the Bridgewick CIE. The shape of the Late Turonian Western Interior curve corresponds very closely to the Běchary record (Fig. 8), but the best-fit isotope correlation shows an apparent age offset of around 300 kyr at the level of the HW3 CIE. This condition is a consequence of the age model used by Joo and Sageman (2014), who pinned the base Coniacian to the bottom of a $\delta^{13}C_{org}$ minimum (which they interpreted to represent the Navigation CIE) below their Co1 negative excursion. A different interpretation of the CIE stratigraphy is proposed here (see below).

The Western Interior $\delta^{13}C_{org}$ curve lacks resolution across the Turonian–Coniacian boundary interval (Joo & Sageman, 2014). The composite curve is based on splicing the uppermost Turonian of the CL-1 core to the basal Coniacian in the Aristocrat Angus core. Data from the former section does not extend to the base Coniacian, which corresponds to a minor disconformity surface at the base of the Niobrara Formation (Fort Hayes Limestone Member; Ball *et al.*, 2010). The Fort Hays Limestone in the Aristocrat Angus core rests on a major disconformity surface, and represents a thin, highly condensed and probably incomplete, Upper Turonian to basal Coniacian succession, as documented more generally for the US Western Interior (Walaszczyk *et al.*, 2014). The exact placement of the base of the Lower Coniacian *Scaphites preventricosus* ammonite zone with respect to the isotope curve is therefore uncertain.

The FO of *S. preventricosus* coincides with the FO of *C. deformis erectus* in the Western Interior (Walaszczyk & Cobban, 2000). This inoceramid is first recorded at the top of the Navigation CIE in Europe (Fig. 5), placing the Turonian–Coniacian boundary at the top of the negative isotope excursion, not at its base, as indicated by Joo and Sageman (2014, fig. 4). It is probably that either the base of the *S. preventricosus* Zone has been misplaced on their isotope curve, or the identification of the Navigation CIE immediately below their isotope peak Co1 is incorrect. Overall, the isotope profile indicates the presence of a significant hiatus spanning the Turonian–Coniacian boundary interval in the Western Interior composite curve.

Within the constraints of the available data, there is excellent agreement between both long-term and short-term variation in the Turonian $\delta^{13}C_{org}$ curves from Central Europe and North America (Fig. 8). It is particularly noteworthy that the long-term reversal of rising to falling $\delta^{13}C_{org}$ values lies within the mid-*M. scupini* Zone in both sections, rather than the turning point occurring lower in the mid-*S. neptuni* Zone, as seen universally in $\delta^{13}C_{carb}$ records (Fig. 5), which supports our previous argument that the divergence in paired carbon isotope trends with falling $\Delta^{13}C$ in the Late Turonian, may be attributed to pCO_2 drawdown rather than regional differences or diagenetic factors.

Correlation with the terrestrial record: Yezo Group, Japan

The isotopic linkage between marine and terrestrial carbon reservoirs means that carbon isotope stratigraphy is

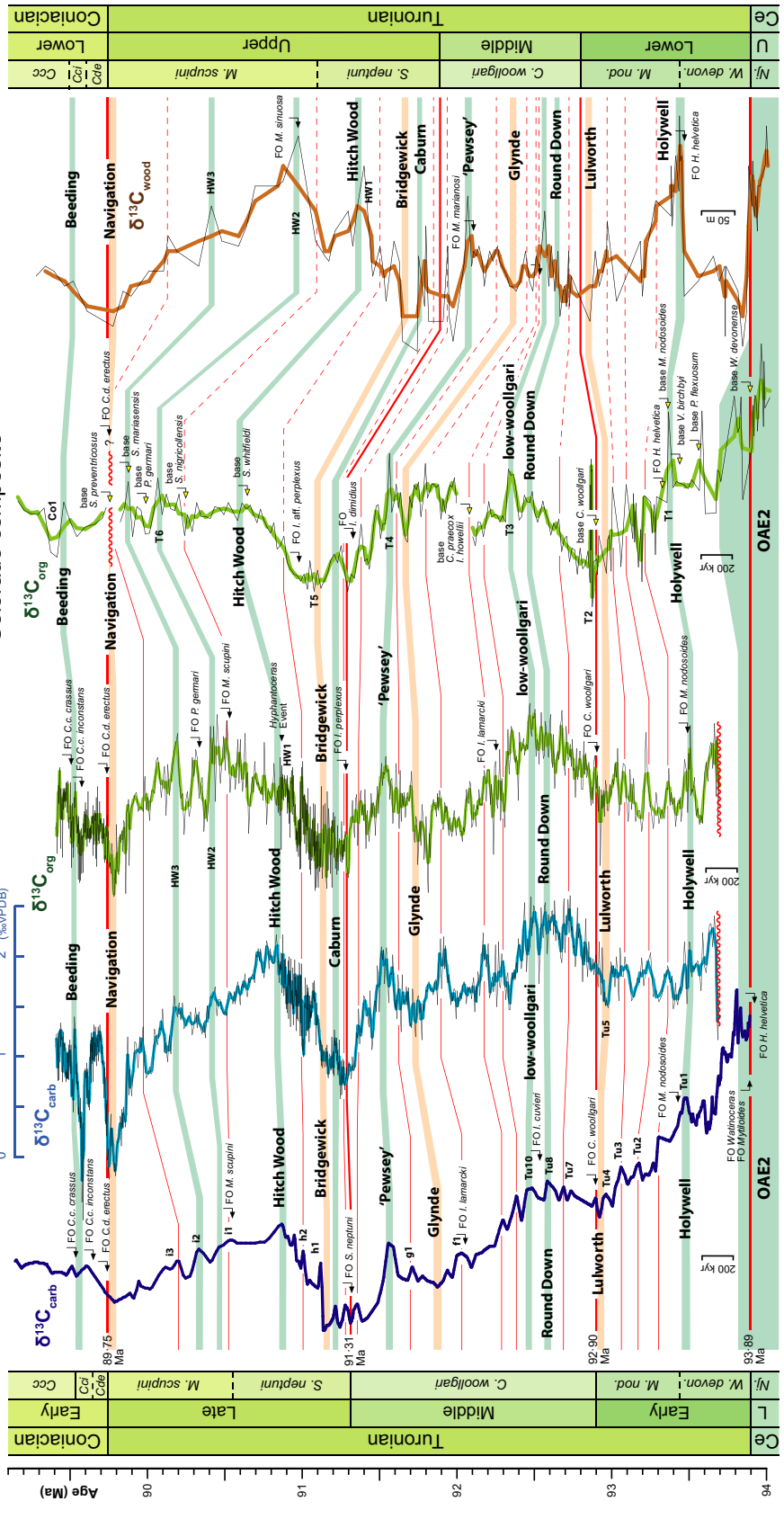

Fig. 8. Correlation of age-calibrated Turonian $\delta^{13}C_{carb}$ profiles for Europe (English Chalk reference curve and Běchary) and North America (US Western Interior Basin composite), and the terrestrial wood record ($\delta^{13}C_{wood}$) from the NW Pacific (Yezo Group, Japan). Locations of the sites are shown in Fig. 1. Breaks in the North America profile in the mid-Middle Turonian and at the Turonian–Coniacian boundary indicate positions of core changes in the stacked composite profile (see text for discussion). Data sources: Běchary, Uličný *et al.* (2014), age calibration as in Fig. 7; US WIS composite, isotope data and zonal bases (yellow arrows) from Joo and Sageman (2014), faunal records (black arrows) from Ball *et al.* (2010); Japan, Takashima *et al.* (2010); English Chalk, Jarvis *et al.* (2006), age recalibrated after Laurin *et al.* (2014). Ages of stage and substage boundaries derived from Ogg *et al.* (2012), Laurin *et al.* (2014) and Sageman *et al.* (2014). For the Lower Turonian at Běchary, a 200 kyr hiatus was applied at the base of the Turonian, above this hiatus, sedimentation rates were linearly increased from 0 cm kyr^{-1} to 7·5 cm kyr^{-1} (mean sedimentation rate for the Middle Turonian) at the top of the substage.

potentially a powerful tool for high-resolution correlation between marine and non-marine successions. Extensive work has been undertaken on characterizing $\delta^{13}C$ trends in bulk terrestrial organic matter in the Turonian Yezo Group of Japan (Hasegawa & Saito, 1993; Hasegawa, 1997, 2003; Hasegawa & Hatsugai, 2000; Hasegawa *et al.*, 2003; Tsuchiya *et al.*, 2003; Uramoto *et al.*, 2009, 2013, 2015; Hayakawa & Hirano, 2013; Takashima *et al.*, 2010, 2011), enabling comparison to marine $\delta^{13}C$ records.

The Upper Cenomanian–Lower Coniacian Yezo Group crops out widely along the NW Pacific margin, constituting the sedimentary fill of a forearc basin (Fig. 1B; Uramoto *et al.*, 2013, 2015). Elevated sedimentation rates (20 to 40 cm kyr^{-1}) offer high stratigraphic resolution through the Turonian but, with the exception of the CTB interval, biostratigraphic control is poor. The most detailed Turonian terrestrial $\delta^{13}C$ record available to date has been derived from the analysis of wood fragments ($\delta^{13}C_{wood}$), sampled at 5 to 20 m intervals throughout *ca* 1 km thickness of a section at Kotanbetsu, northern Hokkaido, Japan (Takashima *et al.*, 2010). Wood was chosen in an attempt to overcome possible limitations of previous work using bulk organic matter ($\delta^{13}C_{TOM}$), in which the inclusion of variable amounts of marine organic material, the presence of varying floral components (e.g. leaf, stem, root) or material originating from different environments with different isotopic signatures, might have overprinted global stratigraphic trends (see Gröcke *et al.*, 2005 for discussion).

Tethyan planktonic foraminifera marker species are rare or absent from the Yezo Group, necessitating the application of a regional foraminifera biostratigraphy (Nishi *et al.*, 2003), calibrated using records of occasional international markers. The regional macrofossil biostratigraphy principally employs endemic inoceramid bivalve assemblages, calibrated to the international timescale using occasional co-occurring Tethyan ammonites and inoceramid species (Toshimitsu *et al.*, 1995; Hayakawa & Hirano, 2013). The latter have only been recorded sporadically from any of the carbon isotope study sections. In addition, Turonian stable isotope values of bulk wood fluctuate widely between −26 and −21‰ (Takashima *et al.*, 2010, 2011), with an average value of −24‰ $\delta^{13}C_{wood}$, producing a very noisy isotope profile (Fig. 8). Similar values have been obtained by lower resolution $\delta^{13}C_{TOM}$ studies of the Turonian aged Yezo Group (Uramoto *et al.*, 2013, 2015).

The base of the Turonian at Kotanbetsu is relatively well-constrained by a + 4‰ positive $\delta^{13}C_{wood}$ isotope excursion located a short distance above the LO *Rotalipora cushmani* (Morrow) (Fig. 7; Takashima *et al.*, 2010). The CTB interval is similarly characterized by a + 3‰ excursion in complementary $\delta^{13}C_{TOM}$ profiles (Uramoto *et al.*, 2013, 2015). The exact placement of the stage boundary within the Yezo Group has been confirmed recently by osmium isotope stratigraphy and U–Pb geochronology (Du Vivier *et al.*, 2015).

Takashima *et al.* (2010, fig. 4) highlighted a number of other planktonic foraminifera ranges as being of stratigraphic value in the Yezo Group, which were used to pin the $\delta^{13}C_{wood}$ isotope curve. The FO *Helvetoglobotruncana helvetica* (Bolli) occurs at a second large positive $\delta^{13}C_{wood}$ excursion (Fig. 8) below the base of the Saku Formation. The FO of this species has been widely used as a Lower Turonian biostratigraphic marker, but this has proven problematic due to an apparently diachronous FO (Desmares *et al.*, 2007; Robaszynski *et al.*, 2010). This diachroneity is attributable to a number of factors, including inconsistency in the taxonomic concept of the nominate species, its rarity in the lower part of its stratigraphic range, its rarity in or absence from higher latitude and nearshore settings, and its high degree of morphological variability (Huber & Petrizzo, 2014). At the GSSP site for the base of the Turonian at Pueblo, following the concept of Caron *et al.* (2006), the FO of *H. helvetica* occurs just above the base of the *M. nodosoides* Zone (Sageman *et al.*, 2006), at the level of the Holywell CIE (Fig. 8).

A short total range of *Marginotruncana marianosi* Douglas within to the mid-*H. helvetica* Zone has been documented at Kotanbetsu (Takashima *et al.*, 2010). These records are of little stratigraphic value. At the Exmouth Plateau, offshore NW Australia, the species appears in the Coniacian and extends into the lower Santonian (Wonders, 1992; Petrizzo, 2000, 2002). In the tropical western Tethyan Realm it extends through the lower Turonian to a LO at the top of the Middle Turonian (Robaszynski & Caron, 1979a,b; Caron, 1985). In Tibet, *M. marianosi* is also present in the lower and middle Turonian (Wendler *et al.*, 2011) but extends well into the Coniacian. The species has been recorded from the Upper Turonian in the Western Interior (Sikora *et al.*, 2004; note modified age assignment of Wagon Mound section by Walaszczyk *et al.*, 2012).

Takashima *et al.* (2010) documented the FO *Marginotruncana sinuosa* Porthault in the Kotanbetsu section, which they placed in the uppermost Turonian. This taxon was proposed as a base Coniacian marker by Walaszczyk and Peryt (1998), but the species has subsequently been recorded from the higher Upper Turonian *M. scupini* Zone at Saltzgitter–Salder, and at similar levels in the base Coniacian proposed GSSP of Słupia Nadbrzeżna (Walaszczyk *et al.*, 2010), and in the Western Interior (Walaszczyk *et al.*, 2012). It appears to be a consistent higher Upper Turonian marker, based on the current inoceramid definition for the base Coniacian.

Takashima *et al.* (2010) recorded the LO *H. helvetica* above the FO *Marginotruncana sinuosa* at Kotanbetsu,

which is potentially problematic because of recent suggestions (Huber & Petrizzo, 2014) that the LO *H. helvetica* is a reliable Middle Turonian marker, which is supported by the $\delta^{13}C_{carb}$ records and planktonic foraminifera ranges reported by Wendler (2013, fig. 7). The data presented by Takashima *et al.* (2010) points to a diachronous LO between Tethys and the NW Pacific. Similarly in the WIS, *H. helvetica* has been observed towards the top of the Iona-1 core, well into the Lower Coniacian (Eldrett *et al.*, 2015). The FO *Dicarinella concavata* Brotzen was recorded at Kotanbetsu in the Santonian (Takashima *et al.*, 2010, fig. 4), considerably above the stratigraphic interval being discussed here. The index species of the *D. concavata* Zone first appears in the Upper Turonian, but it is usually more abundant and consistently present in the Coniacian, making it a relatively unreliable stratigraphic marker (Robaszynski & Caron, 1995; Wendler, 2013).

Biostratigraphic constraints on the Yezo Group $\delta^{13}C_{wood}$ Turonian curve are therefore ambiguous. This situation is not improved by comparison with low-resolution regional $\delta^{13}C_{TOM}$ profiles (Uramoto *et al.*, 2013, 2015). These are similarly poorly constrained, with calibration attempted using published macrofossil records from the study sections. Ages derived from these when placed within the lithostratigraphic framework agree poorly with the planktonic foraminifera data. Interpretation is complicated further by evidence of sediment condensation and local slumping of the Middle Turonian interval (Uramoto *et al.*, 2015). Further work is required to integrate microfossil data and macrofossil data with the $\delta^{13}C_{wood}$ and $\delta^{13}C_{TOM}$ curves.

Despite the stratigraphic limitations discussed above, a coherent correlation between the terrestrial and marine $\delta^{13}C$ records may be achieved using the limited age constraints provided by planktonic foraminiferal ranges (Takashima *et al.*, 2010), combined with matching medium-term and long-term trends in the $\delta^{13}C$ profiles. The resulting correlation (Fig. 8) differs from previous work (Takashima *et al.*, 2010; Hayakawa & Hirano, 2013; Uramoto *et al.*, 2013, 2015) in recognizing a higher Upper Turonian turning point in isotope profiles from organic matter compared to $\delta^{13}C_{carb}$ curves, and correlating the turning point at Kotanbetsu to the Běchary HW2 CIE, rather than the older Hitch Wood CIE. This reinterpretation is supported by the FO *M. sinuosa*, a high Upper Turonian marker, coincident with HW2.

Synchronous isotope excursions in marine and terrestrial organic matter that diverge from marine carbonate trends would be predicted by the fundamental observation that carbon isotope fractionation increases in both marine plankton (Dean *et al.*, 1986; Kump & Arthur, 1999) and terrestrial C_3 land plants (Schubert & Jahren, 2013) in response to increasing pCO_2 levels. Other terrestrial photosynthetic pathways are not believed to be important here, because classical C_4 photosynthesis is a recent evolutionary innovation, becoming significant only in the Miocene, since 13 Ma (Edwards *et al.*, 2001), and CAM photosynthesis is largely limited to aqueous and desert environments. It is notable that the post-Hitch Wood pCO_2 fall interpreted from our Central European high-resolution $\Delta^{13}C$ curve (Fig. 5) is consistent with low-resolution Turonian terrestrial organic matter-based $\Delta^{13}C$ trends derived from the NW Pacific (Uramoto *et al.*, 2013), and general models indicating a long-term Late Cretaceous $_pCO_2$ fall (Tajika, 1999; Berner, 2006).

The recognition of key Turonian carbon CIEs in the terrestrial carbon record offers an opportunity to further refine the calibration of the biostratigraphy of the endemic mollusc faunas in the NW Pacific to the international timescale (cf. Hayakawa & Hirano, 2013). In addition, there is potential for dating fully non-marine Turonian successions barren of fossils, although here a long and detailed time series will be required, and an absence of major hiatuses is essential to correctly identify major isotope shifts that can be assigned to specific CIEs.

CONCLUSIONS

Trends in Turonian carbon isotope curves derived from hemipelagic sediments sampled at 5·6 kyr average resolution enable the recognition of 10 major Turonian CIEs and more than 20 secondary correlation levels in the Bohemian Cretaceous Basin. Mismatches between the $\delta^{13}C_{carb}$ versus $\delta^{13}C_{org}$ profiles are attributed principally to diagenesis and compositional variation in the two fractions, except for a divergence of the medium-term trends in the Upper Turonian interval, where atmospheric CO_2 drawdown may have been responsible.

Carbonate-carbon isotope curves allow the precise correlation of Turonian successions throughout Europe, despite diagenetic overprinting in some low-carbonate sections. Calibration using biostratigraphic datum levels is essential to ensure the robust unambiguous correlation of $\delta^{13}C$ profiles; following calibration, a correlation resolution of around 40 kyr is achievable where sampling density is sufficient.

Bulk-sediment oxygen isotopes provide evidence of Turonian climate change. Sea-surface temperatures were highest in the Early to Middle Turonian, coincident with high eustatic sea-levels. Medium-term to long-term trends in $\delta^{18}O_{carb}$ profiles indicate a Europe-wide trend of stepped cooling that accompanied long-term sea-level fall, beginning in the late-Middle Turonian and culminating in the mid-Late Turonian – the *Late Turonian Cool Phase*.

Brachiopod $\delta^{18}O_{carb}$ shell data indicate up to 4°C cooling of bottom waters. Coincident faunal changes include the southward spread of Boreal taxa in Europe, and evidence of major water-mass reorganization accompanying a eustatic lowstand, prior to renewed sea-level rise in the latest Turonian.

Turonian marine carbonate $\delta^{13}C$ records have been successfully correlated with marine organic matter and terrestrial wood carbon isotope records from Europe ($\delta^{13}C_{org}$), the North American Western Interior Basin ($\delta^{13}C_{org}$) and the NW Pacific ($\delta^{13}C_{wood}$), which offers opportunities for the improved intercalibration of regional biostratigraphic schemes, necessitated by the presence of endemic faunas, and for the correlation of marine to fully terrestrial records.

Correlation of $\delta^{13}C_{org}$ profiles from Central Europe to the North American Western Interior Basin demonstrates consistent trends, with the identification of key CIEs in both records, but with a hiatus spanning the Turonian–Coniacian boundary in the North American composite section.

Consistent marine carbonate and organic carbon isotope records on two continents, and comparable trends in terrestrial wood, evidence strong coupling of isotope signatures in the ocean–atmosphere–biosphere carbon reservoirs during the Late Cretaceous. Convergence in $\delta^{13}C_{carb}$ and $\delta^{13}C_{org}$ values (falling $\Delta^{13}C_{org}$) during the latest Turonian may represent a period of pCO_2 decline, beginning during the final stages of the Late Turonian Cool Phase.

ACKNOWLEDGEMENTS

This paper benefited from detailed reviews by Amanda Oehlert and Ines Wendler, and comments from Editor Peter Swart. IJ and DRG acknowledge funding by UK Natural Environment Research Council (NERC) grants NE/H020756/1 and NE/H021868/1, respectively. This research was supported by the Czech Science Foundation (GACR) grant P210/10/1991 and research programme AV0Z30120515 of the Academy of Sciences of the Czech Republic. JL acknowledges support from KONTAKT II Programme, grant LH12041.

References

Allan, J.R. and **Matthews, R.K.** (1982) Isotope signatures associated with early meteoric diagenesis. *Sedimentology*, **29**, 797–817.

Amédro, F., Accarie, H. and **Robaszynski, F.** (2005) Position de la limite Cénomanien – Turonien dans la Formation Bahloul de Tunisie centrale: apports intégrés des ammonites et des isotopes du carbone ($\delta^{13}C$). *Eclogae Geol. Helv.*, **98**, 151–167.

Anderson, T.F., and **Arthur M.A.** (1983) Stable isotopes of oxygen and carbon and their application to sedimentologic and environmental problems. In: *Stable Isotopes in Sedimentary Geology* (Eds M.A. Arthur, T.F. Anderson, I.R. Kaplan, J. Veizer and L.S. Land), *Short Course, Soc. Econ. Paleontol. Mineral.*, **10**, 1–151.

Archer, D. (2010) *The Global Carbon Cycle*. Princeton University Press, Princeton, 205 pp.

Arthur, M.A., Dean, W.E. and **Schlanger, S.O.** (1985) Variations in the global carbon cycle during the Cretaceous related to climate, volcanism and changes in atmospheric CO_2. In: *The Carbon Cycle and Atmospheric CO2: Natural Variations Archean to Present* (Eds E.T. Sundquist and W.S. Broecker), *Am. Geophys. Union Monogr.*, **32**, 504–529. Washington, DC.

Arthur, M.A., Dean, W.E. and **Pratt, L.M.** (1988) Geochemical and climatic effects of increased marine organic carbon burial at the Cenomanian/Turonian boundary. *Nature*, **335**, 714–717.

Arthur, M.A., Jenkyns, H.C., Brumsack, H.J. and **Schlanger, S.O.** (1990) Stratigraphy, geochemistry, and paleoceanography of organic carbon-rich Cretaceous sequences. In: *Cretaceous Resources Events and Rhythms: Background and Plans for Research* (Eds R.N. Ginsburg and B. Beaudoin), *NATO Sci. Ser. C Math. Phys. Sci.*, **304**, 75–119. Kluwer Academic Publishers, Dordrecht, The Netherlands.

Ball, B.A., Cobban, W.A., Merewether, E.A., Grauch, R.I., McKinney, K.C. and **Livo, K.E.** (2010) *Fossils, Lithologies, and Geophysical Logs of the Mancos Shale from Core Hole USGS CL-1 in Montrose County, Colorado*. U.S. Geol. Surv., Reston, Virginia, 38 pp.

Banner, J.L. and **Hanson, G.N.** (1990) Calculation of simultaneous isotopic and trace-element variations during water-rock interaction with applications to carbonate diagenesis. *Geochim. Cosmochim. Acta*, **54**, 3123–3137.

van Bentum, E.C., Reichart, G.J., Forster, A. and **Sinninghe Damsté, J.S.** (2012) Latitudinal differences in the amplitude of the OAE-2 carbon isotopic excursion: pCO_2 and paleo productivity. *Biogeoscience*, **9**, 717–731.

Berner, R.A. (1970) Sedimentary pyrite formation. *Am. J. Sci.*, **268**, 1–23.

Berner, R.A. (2006) GEOCARBSULF: a combined model for Phanerozoic atmospheric O_2 and CO_2. *Geochim. Cosmochim. Acta*, **70**, 5653–5664.

Bloomfield, J.P. (1997) The role of diagenesis in the hydrogeological stratification of carbonate aquifers: an example from the Chalk at Faircross, Berkshire, UK. *Hydrol. Earth Syst. Sci.*, **1**, 19–33.

Bolton, C.T., Stoll, H.M. and **Mendez-Vicente, A.** (2012) Vital effects in coccolith calcite: cenozoic climate-pCO_2 drove the diversity of carbon acquisition strategies in coccolithophores? *Paleoceanography*, **27**, PA4204, doi:10.1029/2012PA002339.

Bornemann, A., Norris, R.D., Friedrich, O., Beckmann, B., Schouten, S., Damste, J.S.S., Vogel, J., Hofmann, P. and **Wagner, T.** (2008) Isotopic evidence for glaciation during the Cretaceous supergreenhouse. *Science*, **319**, 189–192.

Boulila, S., Galbrun, B., Laskar, J. and **Paelike, H.** (2012) A ~9 myr cycle in Cenozoic $\delta^{13}C$ record and long-term orbital eccentricity modulation: is there a link? *Earth Planet. Sci. Lett.*, **317**, 273–281.

Bowman, A.R. and **Bralower, T.J.** (2005) Paleoceanographic significance of high-resolution carbon isotope records across the Cenomanian-Turonian boundary in the Western Interior and New Jersey coastal plain, USA. *Mar. Geol.*, **217**, 305–321.

Bromley, R.G. and **Gale, A.S.** (1982) The lithostratigraphy of the English Chalk Rock. *Cret. Res.*, **3**, 273–306.

Burnett, J.A., Gallagher, L.T. and **Hampton, M.J.** (1998) Upper Cretaceous. In: *Calcareous Nannofossil Biostratigraphy* (Ed. P.R. Bown), *Br. Micropalaeontol. Soc. Publ. Ser.*, 132–199. Kluwer, Dordrecht.

Caron, M. (1985) Cretaceous planktonic foraminifera. In: *Plankton Stratigraphy* (Eds H.M. Bolli, M. Saunders and K. Perch-Nielsen), pp. 17–86. Cambridge University Press, Cambridge.

Caron, M., Dall'Agnolo, S., Accarie, H., Barrera, E., Kauffman, E.G., Amédro, F. and **Robaszynski, F.** (2006) High-resolution stratigraphy of the Cenomanian-Turonian boundary interval at Pueblo (USA) and wadi Bahloul (Tunisia) stable isotope and bio-events correlation. *Geobios*, **39**, 171–200.

Čech, S., Klein, V., Kříž, J. and **Valečka, J.** (1980) Revision of the Upper Cretaceous stratigraphy of the Bohemian Cretaceous Basin. *Věst. Ústřed. Úst. Geol. (Bull. Geol. Surv. Prague)*, **55**, 277–296.

Choquette, P.W. and **James, N.P.** (1987) Diagenesis #12. Diagenesis in limestones 3. The deep burial environment. *Geosci. Canada*, **14**, 3–35.

Christ, N., Immenhauser, A., Wood, R.A., Darwich, K. and **Niedermayr, A.** (2015) Petrography and environmental controls on the formation of Phanerozoic marine carbonate hardgrounds. *Earth-Sci. Rev.*, **151**, 176–226.

Ciais, P., Sabine, C., Bala, G., Bopp, L., Brovkin, V., Canadell, J., Chhabra, A., DeFries, R., Galloway, J., Heimann, M., Jones, C., Le Quéré, C., Myneni, R.B., Piao, S. and **Thornton, P.** (2013) Carbon and other biogeochemical cycles. In: *Climate Change 2013: The Physical Science Basis. Contribution of Working Group I to the Fifth Assessment Report of the Intergovernmental Panel on Climate Change* (Eds T.F. Stocker, D. Qin, G.-K. Plattner, M. Tignor, S.K. Allen, J. Boschung, A. Nauels, Y. Xia, V. Bex and P.M. Midgley), pp. 465–570. Cambridge University Press, Cambridge.

Clarke, L.J. and **Jenkyns, H.C.** (1999) New oxygen isotope evidence for long-term Cretaceous climatic change in the Southern Hemisphere. *Geology*, **27**, 699–702.

Cobban, W.A., Walaszczyk, I., Obradovich, J.D. and **McKinney, K.C.** (2006) *A USGS Zonal Table for the Upper Cretaceous Middle Cenomanian–Maastrichtian of the Western Interior of the United States Based on Ammonites, Inoceramids, and Radiometric Ages*. U.S. Geological Survey, Reston, Virginia, 45 pp.

Corfield, R.M., Cartlidge, J.E., Premoli Silva, I.P. and **Housley, R.A.** (1991) Oxygen and carbon isotope stratigraphy of the Palaeogene and Cretaceous limestones in the Bottaccione Gorge and the Contessa Highway sections, Umbria, Italy. *Terra Nova*, **3**, 414–422.

De Cabrera, S.C., Sliter, W.V. and **Jarvis, I.** (1999) Integrated foraminiferal biostratigraphy and chemostratigraphy of the Querecual Formation (Cretaceous), Eastern Venezuela. *J. Foram. Res.*, **29**, 487–499.

Dean, W.E., Arthur, M.A. and **Claypool, G.E.** (1986) Depletion of ^{13}C in Cretaceous marine organic matter: source, diagenetic or environmental signal? *Mar. Geol.*, **70**, 119–157.

Desmares, D., Grosheny, D., Beaudoin, B., Gardin, S. and **Gauthier-Lafaye, F.** (2007) High resolution stratigraphic record constrained by volcanic ash beds at the Cenomanian-Turonian boundary in the Western Interior Basin, USA. *Cret. Res.*, **28**, 561–582.

Devalque, C., Amédro, F., Philip, J. and **Robaszynski, F.** (1982) État des corrélation litho et biostratigraphiques dans le Turonien supérieur des massifs d'Uchaux et de la Céze. Les zones d'ammonites et de rudistes. *Mém. Mus. Nation. Hist. Nat. C Sci. Terre*, **49**, 57–69.

Ditchfield, P. and **Marshall, J.D.** (1989) Isotopic variation in rhythmically bedded chalks: paleotemperature variation in the Upper Cretaceous. *Geology*, **17**, 842–845.

Du Vivier, A.D.C., Selby, D., Condon, D.J., Takashima, R. and **Nishi, H.** (2015) Pacific $^{187}Os/^{188}Os$ isotope chemistry and U-Pb geochronology: synchroneity of global Os isotope change across OAE 2. *Earth Planet. Sci. Lett.*, **428**, 204–216.

Dubicka, Z. and **Peryt, D.** (2012) Foraminifers and stable isotope record of the Dubivtsi chalk (upper Turonian, Western Ukraine): palaeoenvironmental implications. *Geol. Q.*, **56**, 199–214.

Edwards, G.E., Furbank, R.T., Hatch, M.D. and **Osmond, C.B.** (2001) What does it take to be C4? Lessons from the evolution of C4 photosynthesis. *Plant Physiol.*, **125**, 46–49.

Elderbak, K., Leckie, R.M. and **Tibert, N.E.** (2014) Paleoenvironmental and paleoceanographic changes across the Cenomanian-Turonian Boundary Event (Oceanic Anoxic Event 2) as indicated by foraminiferal assemblages from the eastern margin of the Cretaceous Western Interior Sea. *Palaeogeogr. Palaeoclimatol. Palaeoecol.*, **413**, 29–48.

Eldrett, J.S., Minisini, D. and **Bergman, S.C.** (2014) Decoupling of the carbon cycle during Ocean Anoxic Event 2. *Geology*, **42**, 567–570.

Eldrett, J.S., Ma, C., Bergman, S.C., Lutz, B., Gregory, F.J., Dodsworth, P., Phipps, M., Hardas, P., Minisini, D.,

Ozkan, A., Ramezani, J., Bowring, S.A., Kamo, S.L., Ferguson, K., Macaulay, C. and **Kelly, A.E.** (2015) An astronomically calibrated stratigraphy of the Cenomanian, Turonian and earliest Coniacian from the Cretaceous Western Interior Seaway, USA: implications for global chronostratigraphy. *Cret. Res.*, **56**, 316–344.

Elrick, M., Molina-Garza, R., Duncan, R. and **Snow, L.** (2009) C-isotope stratigraphy and paleoenvironmental changes across OAE2 (mid-Cretaceous) from shallow-water platform carbonates of southern Mexico. *Earth Planet. Sci. Lett.*, **277**, 295–306.

Erbacher, J., Friedrich, O., Wilson, P.A., Birch, H. and **Mutterlose, J.** (2005) Stable organic carbon isotope stratigraphy across Oceanic Anoxic Event 2 of Demerara Rise, western tropical Atlantic. *Geochem. Geophys. Geosyst.*, **6**, Q06010. doi:10.1029/2004GC000850.

Forster, A., Kuypers, M.M.M., Turgeon, S.C., Brumsack, H.J., Petrizzo, M.R. and **Sinninghe Damsté, J.S.** (2008) The Cenomanian/Turonian oceanic anoxic event in the South Atlantic: new insights from a geochemical study of DSDP Site 530A. *Palaeogeogr. Palaeoclimat. Palaeoecol.*, **267**, 256–283.

Frank, T.D., Arthur, M.A. and **Dean, W.E.** (1999) Diagenesis of Lower Cretaceous pelagic carbonates, North Atlantic: paleoceanographic signals obscured. *J. Foram. Res.*, **29**, 340–351.

Frank, J., Wilmsen, M. and **Košťák, M.** (2013) The endemic and morphologically remarkable nautilid genus *Deltocymatoceras* Kummel, 1956 from the Late Cretaceous of Central Europe. *Bull. Geosci.*, **88**, 793–812.

Freeman, K.H. and **Hayes, J.M.** (1992) Fractionation of carbon isotopes by phytoplankton and estimates of ancient CO_2 levels. *Biogeochem. Cycles*, **6**, 185–198.

Friedrich, O., Norris, R.D. and **Erbacher, J.** (2012) Evolution of middle to Late Cretaceous oceans – a 55 m.y. record of Earth's temperature and carbon cycle. *Geology*, **40**, 107–110.

Gale, A.S. (1996) Turonian correlation and sequence stratigraphy of the Chalk in southern England. In: *Sequence Stratigraphy in British Geology* (Eds S.P. Hesselbo and D.N. Parkinson), *Geol. Soc. London. Spec. Publ.*, **103**, 177–195. Geological Society of London, Bath.

Gale, A.S., Jenkyns, H.C., Kennedy, W.J. and **Corfield, R.M.** (1993) Chemostratigraphy versus biostratigraphy: data from around the Cenomanian-Turonian boundary. *J. Geol. Soc. London*, **150**, 29–32.

Gale, A.S., Kennedy, W.J., Voigt, S. and **Walaszczyk, I.** (2005) Stratigraphy of the Upper Cenomanian – Lower Turonian Chalk succession at Eastbourne, Sussex, UK: ammonites, inoceramid bivalves and stable carbon isotopes. *Cret. Res.*, **26**, 460–487.

Galeotti, S., Rusciadelli, G., Sprovieri, M., Lanci, L., Gaudio, A. and **Pekar, S.** (2009) Sea-level control on facies architecture in the Cenomanian-Coniacian Apulian margin (Western Tethys): a record of glacio-eustatic fluctuations during the Cretaceous greenhouse? *Palaeogeogr. Palaeoclimatol. Palaeoecol.*, **276**, 196–205.

Gambacorta, G., Jenkyns, H.C., Russo, F., Tsikos, H., Wilson, P.A., Faucher, G. and **Erba, E.** (2015) Carbon- and oxygen-isotope records of mid-Cretaceous Tethyan pelagic sequences from the Umbria–Marche and Belluno Basins (Italy). *Newsl. Stratigr.*, **48**, 299–323.

Gröcke, D.R. (2002) The carbon isotope composition of ancient CO_2 based on higher-plant organic matter. *Phil. Trans. R. Soc. Lond. Ser. A Math. Phys. Eng. Sci.*, **360**, 633–658.

Gröcke, D.R., Hesselbo, S.P. and **Jenkyns, H.C.** (1999) Carbon-isotope composition of Lower Cretaceous fossil wood: ocean-atmosphere chemistry and relation to sea-level change. *Geology*, **27**, 155–158.

Gröcke, D.R., Price, G.D., Robinson, S.A., Baraboshkin, E.Y., Mutterlose, J. and **Ruffell, A.H.** (2005) The Upper Valanginian (Early Cretaceous) positive carbon-isotope event recorded in terrestrial plants. *Earth Planet. Sci. Lett.*, **240**, 495–509.

Gröcke, D.R., Ludvigson, G.A., Witzke, B.L., Robinson, S.A., Joeckel, R.M., Ufnar, D.F. and **Ravn, R.L.** (2006) Recognizing the Albian-Cenomanian (OAE1d) sequence boundary using plant carbon isotopes: Dakota Formation, Western Interior Basin, USA. *Geology*, **34**, 193–196.

Gross, M.G. (1964) Variations in the $^{18}O/^{16}O$ and $^{13}C/^{12}C$ ratios of diagenetically altered limestones in the Bermuda islands. *J. Geol.*, **72**, 172–193.

Hancock, J.M. (1989) Sea-level changes in the British region during the Late Cretaceous. *Proc. Geol. Assoc.*, **100**, 565–594.

Hancock, J.M. and **Kauffman, E.G.** (1979) The great transgressions of the Late Cretaceous. *J. Geol. Soc. London*, **136**, 175–186.

Haq, B.U. (2014) Cretaceous eustasy revisited. *Glob. Planet. Change*, **113**, 44–58.

Haq, B.U., Hardenbol, J. and **Vail, P.R.** (1987) Chronology of fluctuating sea levels since the Triassic. *Science*, **235**, 1156–1167.

Hasegawa, T. (1997) Cenomanian-Turonian carbon isotope events recorded in terrestrial organic matter from northern Japan. *Palaeogeogr. Palaeoclimatol. Palaeoecol.*, **130**, 251–273.

Hasegawa, T. (2003) A global carbon-isotope event in the Middle Turonian (Cretaceous) sequences in Japan and Russian Far East. *Proc. Jpn. Acad. Ser. B Phys. Biol. Sci.*, **79**, 141–144.

Hasegawa, T. and **Hatsugai, T.** (2000) Carbon-isotope stratigraphy and its chronostratigraphic significance for the Cretaceous Yezo Group, Kotanbetsu area, Hokkaido, Japan. *Paleontol. Res.*, **4**, 95–106.

Hasegawa, T. and **Saito, T.** (1993) Global synchroneity of a positive carbon isotope excursion at the Cenomanian/Turonian boundary: validation by calcareous microfossil biostratigraphy of the Yezo Group, Hokkaido, Japan. *Island Arc.*, **3**, 181–191.

Hasegawa, T., Pratt, L.M., Maeda, H., Shigeta, Y., Okamoto, T., Kase, T. and **Uemura, K.** (2003) Upper Cretaceous stable carbon isotope stratigraphy of terrestrial organic matter from Sakhalin, Russian Far East: a proxy for the isotopic composition of paleoatmospheric CO_2. *Palaeogeogr. Palaeoclimatol. Palaeoecol.*, **189**, 97–115.

Hasegawa, T., Crampton, J.S., Schioler, P., Field, B., Fukushi, K. and **Kakizaki, Y.** (2013) Carbon isotope stratigraphy and depositional oxia through Cenomanian/Turonian boundary sequences (Upper Cretaceous) in New Zealand. *Cret. Res.*, **40**, 61–80.

Hatch, J.R. and **Leventhal, J.S.** (1997) Early diagenetic partial oxidation of organic matter and sulfides in the Middle Pennsylvanian (Desmoinesian) Excello Shale Member of the Fort Scott Limestone and equivalents, northern Midcontinent region, USA. *Chem. Geol.*, **134**, 215–235.

Hay, W.W. and **Leslie, M.A.** (1990) Could possible changes in global groundwater reservoir cause eustatic sea level fluctuations? In: *Sea Level Change: Studies in Geophysics* (Ed. R. Ravelle), pp. 161–170. National Academy Press, Washington, DC.

Hayakawa, T. and **Hirano, H.** (2013) A revised inoceramid biozonation for the Upper Cretaceous based on high-resolution carbon isotope stratigraphy in northwestern Hokkaido, Japan. *Acta Geol. Pol.*, **63**, 239–263.

Hayes, J.M., Strauss, H. and **Kaufman, A.J.** (1999) The abundance of ^{13}C in marine organic matter and isotopic fractionation in the global biogeochemical cycle of carbon during the past 800 Ma. *Chem. Geol.*, **161**, 103–125.

Hedges, J.I. and **Keil, R.G.** (1995) Sedimentary organic matter preservation – an assessment and speculative synthesis. *Mar. Chem.*, **49**, 81–115.

Hedges, J.I., Keil, R.G. and **Benner, R.** (1997) What happens to terrestrial organic matter in the ocean? *Org. Geochem.*, **27**, 195–212.

Hedges, J.I., Hu, F.S., Devol, A.H., Hartnett, H.E., Tsamakis, E. and **Keil, R.G.** (1999) Sedimentary organic matter preservation: a test for selective degradation under oxic conditions. *Am. J. Sci.*, **299**, 529–555.

Heimhofer, U., Hochuli, P.A., Burla, S., Andersen, N. and **Weissert, H.** (2003) Terrestrial carbon-isotope records from coastal deposits (Algarve, Portugal): a tool for chemostratigraphic correlation on an intrabasinal and global scale. *Terra Nova*, **15**, 8–13.

Herrle, J.O., Kossler, P., Friedrich, O., Erlenkeuser, H. and **Hemleben, C.** (2004) High-resolution carbon isotope records of the Aptian to Lower Albian from SE France and the Mazagan Plateau (DSDP Site 545): a stratigraphic tool for paleoceanographic and paleobiologic reconstruction. *Earth Planet. Sci. Lett.*, **218**, 149–161.

Holser, W.T. (1997) Geochemical events documented in inorganic carbon isotopes. *Palaeogeogr. Palaeoclimatol. Palaeoecol.*, **132**, 173–182.

Huber, B.T. and **Petrizzo, M.R.** (2014) Evolution and taxonomic study of the Cretaceous planktic foraminiferal genus *Helvetoglobotruncana* Reiss, 1957. *J. Foram. Res.*, **44**, 40–57.

Huber, B.T., Norris, R.D. and **MacLeod, K.G.** (2002) Deep-sea paleotemperature record of extreme warmth during the Cretaceous. *Geology*, **30**, 123–126.

Hudson, J.D. (1977) Stable isotopes and limestone lithification. *J. Geol. Soc. London*, **133**, 637–660.

IAEA (2009) *Czech Republic*. Global Network of Isotopes in Precipitation (GNIP), International Atomic Energy Agency, Vienna. Available at: http://www.univie.ac.at/cartography/project/wiser/.

Immenhauser, A., Holmden, C. and **Patterson, W.P.** (2008) Interpreting the carbon-isotope record of ancient shallow epeiric seas: lessons from the recent. In: *Dynamics of Epeiric Seas* (Eds B.R. Pratt and C. Holmden), *Geol. Assoc. Canada Spec. Pap.*, **48**, 137–174. Geological Association of Canada.

Jarvis, I., Carson, G.A., Cooper, M.K.E., Hart, M.B., Leary, P.N., Tocher, B.A., Horne, D. and **Rosenfeld, A.** (1988a) Microfossil assemblages and the Cenomanian – Turonian (late Cretaceous) oceanic anoxic event. *Cret. Res.*, **9**, 3–103.

Jarvis, I., Carson, G.A., Hart, M.B., Leary, P.N. and **Tocher, B.A.** (1988b) The Cenomanian – Turonian (late Cretaceous) anoxic event in SW England: evidence from Hooken Cliffs near Beer, SE Devon. *Newsl. Stratigr.*, **18**, 147–164.

Jarvis, I., Murphy, A.M. and **Gale, A.S.** (2001) Geochemistry of pelagic and hemipelagic carbonates: criteria for identifying systems tracts and sea-level change. *J. Geol. Soc. London*, **158**, 685–696.

Jarvis, I., Mabrouk, A., Moody, R.T.J. and **De Cabrera, S.C.** (2002) Late Cretaceous (Campanian) carbon isotope events, sea-level change and correlation of the Tethyan and Boreal realms. *Palaeogeogr. Palaeoclimatol. Palaeoecol.*, **188**, 215–248.

Jarvis, I., Gale, A.S., Jenkyns, H.C. and **Pearce, M.A.** (2006) Secular variation in Late Cretaceous carbon isotopes and sea-level change: evidence from a new $\delta^{13}C$ carbonate reference curve for the Cenomanian – Campanian (99.6 – 70.6 Ma). *Geol. Mag.*, **143**, 561–608.

Jarvis, I., Mabrouk, A., Moody, R.T.J., Murphy, A.M. and **Sandman, R.I.** (2008) Applications of carbon isotope and elemental (Sr/Ca, Mn) chemostratigraphy to sequence analysis: sea-level change and the global correlation of pelagic carbonates. In: *Geology of East Libya* (Eds M.J. Salem and A.S. El-Hawat), *Earth Sci. Soc. Libya Tripoli*, **I**, 369–396.

Jarvis, I., Lignum, J.S., Groecke, D.R., Jenkyns, H.C. and **Pearce, M.A.** (2011) Black shale deposition, atmospheric CO_2 drawdown, and cooling during the Cenomanian-Turonian Oceanic Anoxic Event. *Paleoceanography*, **26**, Pa3201. doi:10.1029/2010pa002081.

Jeans, C.V., Long, D., Hall, M.A., Bland, D.J. and **Cornford, C.** (1991) The geochemistry of the Plenus Marls at Dover, England: evidence of fluctuating oceanographic conditions

and of glacial control during the development of the Cenomanian-Turonian $\delta^{13}C$ anomaly. *Geol. Mag.*, **128**, 603–632.

Jeans, C.V., Hu, X. and **Mortimore, R.** (2012) Calcite cements and the stratigraphical significance of the marine delta $\delta^{13}C$ carbonate reference curve for the Upper Cretaceous Chalk of England. *Acta Geol. Pol.*, **62**, 173–196.

Jenkyns, H.C. (2010) Geochemistry of oceanic anoxic events. *Geochem. Geophys. Geosyst.*, **11**, Q03004. doi:10.1029/2009GC002788.

Jenkyns, H.C., Gale, A.S. and **Corfield, R.M.** (1994) Carbon- and oxygen-isotope stratigraphy of the English Chalk and Italian Scaglia and its palaeoclimatic significance. *Geol. Mag.*, **131**, 1–34.

Jiráková, H., Huneau, F., Hrkal, Z., Celle-Jeanton, H. and **Le Coustumer, P.** (2010) Carbon isotopes to constrain the origin and circulation pattern of groundwater in the north-western part of the Bohemian Cretaceous Basin (Czech Republic). *Appl. Geochem.*, **25**, 1265–1279.

Jiráková, H., Procházka, M., Dědeček, P., Kobr, M., Hrkal, Z., Huneau, F. and **Le Coustumer, P.** (2011) Geothermal assessment of the deep aquifers of the northwestern part of the Bohemian Cretaceous basin, Czech Republic. *Geothermics*, **40**, 112–124.

Joo, Y.J. and **Sageman, B.B.** (2014) Cenomanian to Campanian carbon isotope chemostratigraphy from the Western Interior Basin, U.S.A. *J. Sed. Res.*, **84**, 529–542.

Katz, M.E., Wright, J.D., Miller, K.G., Cramer, B.S., Fennel, K. and **Falkowski, P.G.** (2005) Biological overprint of the geological carbon cycle. *Mar. Geol.*, **217**, 323–338.

Kauffman, E.G., Sageman, B.B., Elder, W.P., Kirkland, J.I. and **Villamil, T.** (1993) Cretaceous molluscan biostratigraphy and biogeography, Western Interior Basin, North America. In: *Evolution of the Western Interior Basin* (Eds W.G.E. Caldwell and E.G. Kauffman), *Spec. Pap. Geol. Assoc. Canada*, **39**, 397–434.

Kauffman, E.G., Kennedy, W.J. and **Wood, C.J.** (1996) The Coniacian stage and substage boundaries. In: *Proceedings "Second International Symposium on Cretaceous Stage Boundaries" Brussels 8-16 September 1995* (Eds P.F. Rawson, A.V. Dhondt, J.M. Hancock and W.J. Kennedy), *Bulletin de l'Institut Royal des Sciences Naturelles de Belgique Sciences de la Terre*, **66** (Suppl), 81–94.

Keil, R.G., Hu, F.S., Tsamakis, E.C. and **Hedges, J.I.** (1994) Pollen in marine sediments as an indicator of oxidation of organic matter. *Nature*, **369**, 639–641.

Keller, G., Han, Q., Adatte, T. and **Burns, S.J.** (2001) Palaeoenvironment of the Cenomanian-Turonian transition at Eastbourne, England. *Cret. Res.*, **22**, 391–422.

Kennedy, W.J. and **Garrison, R.E.** (1975) Morphology and genesis of nodular chalks and hardgrounds in the Upper Cretaceous of southern England. *Sedimentology*, **22**, 311–386.

Kennedy, W.J., Walaszczyk, I. and **Cobban, W.A.** (2005) The Global Boundary Stratotype Section and Point for the base of the Turonian Stage of the Cretaceous: Pueblo, Colorado, U.S.A. *Episodes*, **28**, 93–104.

Kennedy, W.J., Gale, A.S., Huber, B.T., Petrizzo, M.R., Bown, P., Barchetta, A. and **Jenkyns, H.C.** (2014) Integrated stratigraphy across the Aptian/Albian boundary at Col de Pre-Guittard (southeast France): a candidate Global Boundary Stratotype Section. *Cret. Res.*, **51**, 248–259.

Killops, S. and **Killops, V.** (2005) *Introduction to Organic Geochemistry*. Blackwell, Oxford, 393 pp.

Kollmann, H.A., Peza, L.H. and **Čech, S.** (1998) Upper Cretaceous Nerineacea of the Bohemian Basin (Czech Republic) and the Saxonian Basin (Germany) and their significance for Tethyan environments. *Abh. Staat. Mus. Mineral. Geol. Dresden*, **43/44**, 151–172.

Kolonic, S., Wagner, T., Forster, A., Sinninghe Damsté, J.S.S., Walsworth-Bell, B., Erba, E., Turgeon, S., Brumsack, H.-J., Chellai, E.H., Tsikos, H., Kuhnt, W. and **Kuypers, M.M.M.** (2005) Black shale deposition on the northwest African Shelf during the Cenomanian/Turonian oceanic anoxic event: climate coupling and global organic carbon burial. *Paleoceanography*, **20**, PA1006. doi:10.1029/2003PA000950.

Košťák, M. and **Wiese, F.** (2011) Extremely rare Turonian belemnites from the Bohemian Cretaceous Basin and their palaeogeographical importance. *Acta Geol. Pol.*, **56**, 433–437.

Košťák, M., Čech, S., Ekrt, B., Mazuch, M., Wiese, F., Voigt, S. and **Wood, C.J.** (2004) Belemnites of the Bohemian Cretaceous Basin in a global context. *Acta Geol. Pol.*, **54**, 511–533.

Kuhnt, W., Luderer, F., Nederbragt, S., Thurow, J. and **Wagner, T.** (2005) Orbital-scale record of the late Cenomanian-Turonian oceanic anoxic event (OAE-2) in the Tarfaya Basin (Morocco). *Int. J. Earth Sci. (Geol. Rundsch.)*, **94**, 147–159.

Kump, L.R. (1991) Interpreting carbon-isotope excursions – Stangelove oceans. *Geology*, **19**, 299–302.

Kump, L.R. and **Arthur, M.A.** (1999) Interpreting carbon-isotope excursions: carbonates and organic matter. *Chem. Geol.*, **161**, 181–198.

Kuypers, M.M.M., Pancost, R.D. and **Sinninghe Damsté, J.S.** (1999) A large and abrupt fall in atmospheric CO_2 concentration during Cretaceous times. *Nature*, **399**, 342–345.

Kuypers, M.M.M., Pancost, R.D., Nijenhuis, I.A. and **Sinninghe Damsté, J.S.** (2002) Enhanced productivity led to increased organic carbon burial in the euxinic North Atlantic basin during the late Cenomanian oceanic anoxic event. *Paleoceanography*, **17**, 1051. doi:10.1029/2000PA000569.

Kuypers, M.M.M., Lourens, L.J., Rijpstra, W.R.C., Pancost, R.D., Nijenhuis, I.A. and **Sinninghe Damsté, J.S.** (2004) Orbital forcing of organic carbon burial in the proto-North Atlantic during oceanic anoxic event 2. *Earth Planet. Sci. Lett.*, **228**, 465–482.

Lalonde, K., Mucci, A., Ouellet, A. and **Gelinas, Y.** (2012) Preservation of organic matter in sediments promoted by iron. *Nature*, **483**, 198–200.

Lamolda, M.A., Gorostidi, A. and **Paul, C.R.C.** (1994) Quantitative estimates of calcareous nannofossil changes across the Plenus Marls (latest Cenomanian), Dover, England – implications for the generation of the Cenomanian-Turonian boundary event. *Cret. Res.*, **15**, 143–164.

Lamolda, M.A., Paul, C.R.C., Peryt, D. and **Pons, J.M.** (2014) The Global Boundary Stratotype and Section Point (GSSP) for the base of the Santonian Stage, "Cantera de Margas", Olazagutia, northern Spain. *Episodes*, **37**, 2–13.

de Lange, G.J., van Os, B., Pruysers, P.A., Middelburg, J.J., Castradori, D., van Santvoort, P., Müller, P.J., Eggenkanp, H. and **Prahl, F.G.** (1994) Possible early diagenetic alteration of palaeo proxies. In: *Carbon Cycling in the Glacial Ocean: Constraints on the Ocean's Role in Global Change* (Eds R. Zahn, T.F. Pederson, M.A. Kaminski and L. Labeyrie), *NATO ASI Ser.*, **117**, 225–258. Springer-Verlag, Berlin, Heidelberg.

Laurin, J., Čech, S., Uličný, D., Štaffen, Z. and **Svobodová, M.** (2014) Astrochronology of the Late Turonian: implications for the behavior of the carbon cycle at the demise of peak greenhouse. *Earth Planet. Sci. Lett.*, **394**, 254–269.

Laurin, J., Meyers, S.R., Uličný, D., Jarvis, I. and **Sageman, B.B.** (2015) Axial obliquity control on the greenhouse carbon budget through middle- to high-latitude reservoirs. *Paleoceanography*, **30**, 133–149. doi:10.1002/2014PA002736.

Laws, E.A., Popp, B.N., Bidigare, R.R., Kennicutt, M.C. and **Macko, S.A.** (1995) Dependence of phytoplankton carbon isotope composition on growth rate and $(CO_2)_{aq}$: theoretical considerations and experimental results. *Geochim. Cosmochim. Acta*, **59**, 1131–1138.

Lees, J.A. (2008) The calcareous nannofossil record across the Late Cretaceous Turonian/Coniacian boundary, including new data from Germany, Poland, the Czech Republic and England. *Cret. Res.*, **29**, 40–64.

Li, X., Jenkyns, H.C., Wang, C., Hu, X., Chen, X., Wei, Y., Huang, Y. and **Cui, J.** (2006) Upper Cretaceous carbon- and oxygen-isotope stratigraphy of hemipelagic carbonate facies from southern Tibet, China. *J. Geol. Soc. London*, **163**, 375–382.

Linnert, C., Robinson, S.A., Lees, J.A., Bown, P.R., Perez-Rodriguez, I., Petrizzo, M.R., Falzoni, F., Littler, K., Antonio Arz, J. and **Russell, E.E.** (2014) Evidence for global cooling in the Late Cretaceous. *Nat. Comm.*, **5**, 1–7.

MacEachern, J.A., Pemberton, S.G., Gingras, M.K. and **Bann, K.L.** (2010) Ichnology and facies models. In: *Facies Models 4* (Eds N.P. James and R.W. Dalrymple), pp. 19–58. Geol. Assoc. Canada, St John's, Newfoundland.

MacLeod, K.G., Huber, B.T., Jimenez Berrocoso, A. and **Wendler, I.** (2013) A stable and hot Turonian without glacial $\delta^{18}O$ excursions is indicated by exquisitely preserved Tanzanian foraminifera. *Geology*, **41**, 1083–1086.

Marshall, J.D. (1992) Climatic and oceanographic isotopic signals from the carbonate rock record and their preservation. *Geol. Mag.*, **129**, 143–160.

Mason, B. and **Moore, C.B.** (1982) *Principles of Geochemistry*. Wiley, New York, 344 pp.

Mayer, L.M. (1994) Surface-area control of organic-carbon accumulation in continental-shelf sediments. *Geochim. Cosmochim. Acta*, **58**, 1271–1284.

Meyers, P.A. (2014) Why are the $\delta^{13}C_{org}$ values in Phanerozoic black shales more negative than in modern marine organic matter? *Geochem. Geophys. Geosyst.*, **15**, 3085–3106.

Meyers, S.R., Siewert, S.E., Singer, B.S., Sageman, B.B., Condon, D.J., Obradovich, J.D., Jicha, B.R. and **Sawyer, D.A.** (2012) Intercalibration of radioisotopic and astrochronologic time scales for the Cenomanian-Turonian boundary interval, Western Interior Basin, USA. *Geology*, **40**, 7–10.

Miller, K.G., Sugarman, P.J., Browning, J.V., Kominz, M.A., Olsson, R.K., Feigenson, M.D. and **Hernandez, J.C.** (2004) Upper Cretaceous sequences and sea-level history, New Jersey Coastal Plain. *GSA Bull.*, **116**, 368–393.

Mitchell, S.F., Ball, J.D., Crowley, S.F., Marshall, J.D., Paul, C.R.C., Veltkamp, C.J. and **Samir, A.** (1997) Isotope data from Cretaceous chalks and foraminifera: environmental or diagenetic signals? *Geology*, **25**, 691–694.

Mitchell, A.J., Uličný, D., Hampson, G.J., Allison, P.A., Gorman, G.J., Piggott, M.D., Wells, M.R. and **Pain, C.C.** (2010) Modelling tidal current-induced bed shear stress and palaeocirculation in an epicontinental seaway: the Bohemian Cretaceous Basin, Central Europe. *Sedimentology*, **57**, 359–388.

Nagm, E., El-Qot, G. and **Wilmsen, M.** (2014) Stable-isotope stratigraphy of the Cenomanian-Turonian (Upper Cretaceous) boundary event (CTBE) in Wadi Qena, Eastern Desert, Egypt. *J. Afr. Earth Sci.*, **100**, 524–531.

Nishi, H., Takashima, R., Hatsugai, T., Saito, T., Moriya, K., Ennyu, A. and **Sakai, T.** (2003) Planktonic foraminiferal zonation in the Cretaceous Yezo Group, Central Hokkaido, Japan. *J. Asian Earth Sci.*, **21**, 867–886.

Obradovich, J. (1993) A Cretaceous time scale. In: *Evolution of the Western Interior Basin* (Eds W.G.E. Caldwell and E.G. Kauffman), *Geol. Assoc. Canada Spec. Pap.*, **39**, 379–396.

Oehlert, A.M. and **Swart, P.K.** (2014) Interpreting carbonate and organic carbon isotope covariance in the sedimentary record. *Nat. Comm.*, **5**, 4672. doi:10.1038/ncomms5672.

Oehlert, A.M., Lamb-Wozniak, K.A., Devlin, Q.B., Mackenzie, G.J., Reijmer, J.J.G. and **Swart, P.K.** (2012) The stable carbon isotopic composition of organic material in platform derived sediments: implications for reconstructing the global carbon cycle. *Sedimentology*, **59**, 319–335.

Ogg, J.G., Hinnov, L.A. and **Huang, C.** (2012) Cretaceous. In: *The Geological Time Scale 2012* (Eds F.M. Gradstein, J.G. Ogg, M.D. Schmitz and G.M. Ogg), **2**, 793–853. Elsevier, Amsterdam.

Olde, K., Jarvis, I., Pearce, M.A., Uličný, D., Tocher, B.A., Trabucho-Alexandre, J. and **Gröcke, D.** (2015a) A revised northern European Turonian (Upper Cretaceous) dinoflagellate cyst biostratigraphy: integrating palynology and carbon isotope events. *Rev. Palaeobot. Palynol.*, **213**, 1–16.

Olde, K., Jarvis, I., Uličný, D., Pearce, M.A., Trabucho-Alexandre, J., Čech, S., Gröcke, D.R., Laurin, J., Švábenická, L. and **Tocher, B.A.** (2015b) Geochemical and palynological sea-level proxies in hemipelagic sediments: a critical assessment from the Upper Cretaceous of the Czech Republic. *Palaeogeogr. Palaeoclimatol. Palaeoecol.*, **435**, 222–243.

Paces, T., Corcho Alvarado, J.A., Herrman, Z., Kodes, V., Muzak, J., Novak, J., Purtschert, R., Remenarova, D. and **Valecka, J.** (2008) The Cenomanian and Turonian aquifers of the Bohemian Cretaceous Basin, Czech Republic. In: *Natural Groundwater Quality* (Eds W.E. Edmunds and P. Shand), pp. 372–390. Blackwell, Oxford.

Parente, M., Frijia, G. and **Di Lucia, M.** (2007) Carbon-isotope stratigraphy of Cenomanian-Turonian platform carbonates from the southern Apennines (Italy): a chemostratigraphic approach to the problem of correlation between shallow-water and deep-water successions. *J. Geol. Soc. London*, **164**, 609–620.

Paul, C.R.C. and **Lamolda, M.A.** (2009) Testing the precision of bioevents. *Geol. Mag.*, **146**, 625–637.

Paul, C.R.C., Lamolda, M.A., Mitchell, S.F., Vaziri, M.R., Gorostidi, A. and **Marshall, J.D.** (1999) The Cenomanian-Turonian boundary at Eastbourne (Sussex, UK): a proposed European reference section. *Palaeogeogr. Palaeoclimatol. Palaeoecol.*, **150**, 83–121.

Pearce, M.A., Jarvis, I., Swan, A.R.H., Murphy, A.M., Tocher, B.A. and **Edmunds, W.M.** (2003) Integrating palynological and geochemical data in a new approach to palaeoecological studies: Upper Cretaceous of the Banterwick Barn Chalk borehole, Berkshire, UK. *Mar. Micropaleontol.*, **47**, 271–306.

Petrizzo, M.R. (2000) Upper Turonian–lower Campanian planktonic foraminifera from southern mid-high latitudes (Exmouth Plateau, NW Australia): biostratigraphy and taxonomic notes. *Cret. Res.*, **21**, 479–505.

Petrizzo, M.R. (2002) Palaeoceanographic and palaeoclimatic inferences from Late Cretaceous planktonic foraminiferal assemblages from the Exmouth Plateau (ODP Sites 762 and 763, eastern Indian Ocean). *Mar. Micropaleontol.*, **45**, 117–150.

Poulsen, C.J., Seidov, D., Barron, E.J. and **Peterson, W.H.** (1998) The impact of paleogeographic evolution on the surface oceanic circulation and the marine environment within the mid-Cretaceous Tethys. *Paleoceanography*, **13**, 546–559.

Prahl, F.G., De Lange, G.J., Scholten, S. and **Cowie, G.L.** (1997) A case of post-depositional aerobic degradation of terrestrial organic matter in turbidite deposits from the Madeira Abyssal Plain. *Org. Geochem.*, **27**, 141–152.

Pratt, L.M., Arthur, M.A., Dean, W.E. and **Scholle, P.A.** (1993) Paleoceanographic cycles and events during the Late Cretaceous in the Western Interior Seaway of North America. In: *Cretaceous Evolution of the Western Interior Basin of North America* (Eds W.G.E. Caldwell and E.G. Kauffman), *Geol. Assoc. Canada Spec. Pap.*, **39**, 333–353.

Premoli Silva, I. and **Sliter, W.V.** (1995) Cretaceous planktonic foraminiferal biostratigraphy and evolutionary trends from the Bottaccione section, Gubbio, Italy. *Palaeontogr. Ital.*, **82**, 1–89.

Rau, G.H., Froelich, P.N., Takahashi, T. and **Des Marais, D.J.** (1991) Does sedimentary organic $\delta^{13}C$ record variations in Quaternary ocean $[CO_2(aq)]$? *Paleoceanography*, **6**, 335–347.

Richardt, N. and **Wilmsen, M.** (2012) Lower Upper Cretaceous standard section of the southern Münsterland (NW Germany): carbon stable-isotopes and sequence stratigraphy. *Newsl. Stratigr.*, **45**, 1–24.

Robaszynski, F. and **Caron, M.** (1979a) Atlas de Foraminifères planctoniques de Crétacé moyen (Mer Boréal et Téthys). Première partie. *Cah. Micropaléontol.*, **1**, 1–185.

Robaszynski, F. and **Caron, M.** (1979b) Atlas de Foraminifères planctoniques de Crétacé moyen (Mer Boréal et Téthys). Deuxième partie. *Cah. Micropaléontol.*, **2**, 1–181.

Robaszynski, F. and **Caron, M.** (1995) Cretaceous planktonic foraminifera: comments on the Europe-Mediterranean zonation. *Bull. Soc. Géol. France*, **166**, 681–692.

Robaszynski, F., Donoso, J.M.G., Linares, D., Amedro, F., Caron, M., Dupuis, C., Dhondt, A.V. and **Gartner, S.** (2000) The Upper Cretaceous of the Kalaat Senan region, Central Tunisia. Integrated litho-biostratigraphy based on ammonites, planktonic foraminifera and nannofossils zones from Upper Turonian to Maastrichtian. Bull. Centre Rech. Explor.-Prod. *Elf Aquitaine*, **22**, 359–490.

Robaszynski, F., Zagrarni, M.F., Caron, M. and **Amédro, F.** (2010) The global bio–events at the Cenomanian-Turonian transition in the reduced Bahloul Formation of Bou Ghanem (central Tunisia). *Cret. Res.*, **31**, 1–15.

Rohling, E.J. and **Cooke, S.** (1999) Stable oxygen and carbon isotopes in foraminiferal carbonate shells. In: *Modern Foraminifera* (Ed. B.K. Sen Gupta), pp. 239–258. Kluwer, Amsterdam.

Sageman, B.B., Meyers, S.R. and **Arthur, M.A.** (2006) Orbital time scale and new C-isotope record for Cenomanian-Turonian boundary stratotype. *Geology*, **34**, 125–128.

Sageman, B.B., Singer, B.S., Meyers, S.R., Siewert, S.E., Walaszczyk, I., Condon, D.J., Jicha, B.R., Obradovich, J.D. and **Sawyer, D.A.** (2014) Integrating $^{40}Ar/^{39}Ar$, U-Pb, and

astronomical clocks in the Cretaceous Niobrara Formation, Western Interior Basin, USA. *GSA Bull.*, **126**, 956–973.

Saltzman, M.R. and **Thomas, E.** (2012) Carbon isotope stratigraphy. In: *The Geological Time Scale 2012* (Eds F.M. Gradstein, J.G. Ogg, M.D. Schmitz and G.M. Ogg), **1**, 207–232. Elsevier, Amsterdam.

Schlanger, S.O. and **Jenkyns, H.C.** (1976) Cretaceous oceanic anoxic events: causes and consequences. *Geol. Mijnb.*, **55**, 179–184.

Schlanger, S.O., Arthur, M.A., Jenkyns, H.C. and **Scholle, P.A.** (1983) Stratigraphic and paleo-oceanographic setting of organic carbon-rich strata deposited during the Cenomanian-Turonian oceanic anoxic event. *AAPG Bull.*, **67**, 545.

Schlanger, S.O., Arthur, M.A., Jenkyns, H.C. and **Scholle, P.A.** (1987) The Cenomanian–Turonian Oceanic Anoxic event, I. Stratigraphy and distribution of organic carbon-rich beds and the marine $d^{13}C$ excursion. In: *Marine Petroleum Source Rocks* (Eds J. Brooks and A.J. Fleet), *Geol. Soc. London. Spec. Publ.*, **26**, 371–399. Blackwell, Oxford.

Schlesinger, W.H. and **Berhardt, E.S.** (2013) *Biogeochemistry. An Analysis of Global Change*. Academic Press, Amsterdam, 672 pp.

Scholle, P.A. and **Arthur, M.A.** (1980) Carbon isotope fluctuation in Cretaceous pelagic limestones: potential stratigraphic and petroleum exploration tool. *AAPG Bull.*, **64**, 67–87.

Schrag, D.P., Depaolo, D.J. and **Richter, F.M.** (1995) Reconstrucing past sea-surface temperatures – correcting for diagenesis of bulk marine carbonate. *Geochim. Cosmochim. Acta*, **59**, 2265–2278.

Schrag, D.P., Higgins, J.A., Macdonald, F.A. and **Johnston, D.T.** (2013) Authigenic carbonate and the history of the global carbon cycle. *Science*, **339**, 540–543.

Schubert, B.A. and **Jahren, A.H.** (2013) Reconciliation of marine and terrestrial carbon isotope excursions based on changing atmospheric CO_2 levels. *Nat. Commun.*, **4**, 1653, doi:10.1038/ncomms2659.

Scopelliti, G., Bellanca, A., Erba, E., Jenkyns, H.C., Neri, R., Tamagnini, P., Luciani, V. and **Masetti, D.** (2008) Cenomanian-Turonian carbonate and organic-carbon isotope records, biostratigraphy and provenance of a key section in NE Sicily, Italy: palaeoceanographic and palaeogeographic implications. *Palaeogeogr. Palaeoclimatol. Palaeoecol.*, **265**, 59–77.

Shackleton, N.J. and **Kennett, J.P.** (1975) Paleotemperature history of the Cenozoic and the initiation of Antarctic glaciation: oxygen and carbon isotope analyses in DSDP sites 277, 279, and 281. (Eds J.P. Kennett and R.E. Houtz *et al.*), *Init. Rept. DSDP*, **29**, 743–755. US Government Printing Office, Washington, DC.

Sikora, P.J., Howe, R.W., Gale, A.S. and **Stein, J.A.** (2004) Chronostratigraphy of proposed Turonian–Coniacian (Upper Cretaceous) stage boundary stratotypes: Salzgitter-Salder, Germany, and Wagon Mound, New Mexico, USA. In: *Palynology and Micropalaeontology of Boundaries* (Eds A.B. Beaudoin and M.J.H. Head), *Geol. Soc. London. Spec. Publ.*, **230**, 207–242.

Sinninghe Damsté, J.S. and **Köster, J.** (1998) A euxinic southern North Atlantic Ocean during the Cenomanian/Turonian oceanic anoxic event. *Earth Planet. Sci. Lett.*, **158**, 165–173.

Sinninghe Damsté, J.S., Kuypers, M.M.M., Pancost, R.D. and **Schouten, S.** (2008) The carbon isotopic response of algae, (cyano)bacteria, archaea and higher plants to the late Cenomanian perturbation of the global carbon cycle: insights from biomarkers in black shales from the Cape Verde Basin (DSDP Site 367). *Org. Geochem.*, **39**, 1703–1718.

Sissingh, W. (1977) Biostratigraphy of Cretaceous nannoplankton. *Geol. Mijnb.*, **56**, 37–65.

Sprovieri, M., Coccioni, R., Lirer, F., Pelosi, N. and **Lozar, F.** (2006) Orbital tuning of a lower Cretaceous composite record (Maiolica Formation, central Italy). *Paleoceanography*, **21**, PA4212, doi:10.1029/2005PA001224.

Sprovieri, M., Sabatino, N., Pelosi, N., Batenburg, S.J., Coccioni, R., Iavarone, M. and **Mazzola, S.** (2013) Late Cretaceous orbitally-paced carbon isotope stratigraphy from the Bottaccione Gorge (Italy). *Palaeogeogr. Palaeoclimatol. Palaeoecol.*, **379**, 81–94.

Stoll, H.M. (2005) Limited range of interspecific vital effects in coccolith stable isotopic records during the Paleocene Eocene thermal maximum. *Paleoceanography*, **20**, PA1007, doi:10.1029/2004PA001046.

Stoll, H.M. and **Schrag, D.P.** (2000) High-resolution stable isotope records from the Upper Cretaceous rocks of Italy and Spain: glacial episodes in a greenhouse planet? *GSA Bull.*, **112**, 308–319.

Surlyk, F., Dons, T., Clausen, C.K. and **Higham, J.** (2003) Upper Cretaceous. In: *The Millennium Atlas: Petroleum Geology of the Central and Northern North Sea* (Eds D. Evans, C. Graham, A. Armour and P. Bathurst), pp. 213–233. The Geological Society of London, London.

Švábenická, L. (2012) Nannofossil record across the Cenomanian-Coniacian interval in the Bohemian Cretaceous Basin and Tethyan foreland basins (Outer Western Carpathians), Czech Republic. *Geol. Carpath.*, **63**, 201–217.

Swart, P.K. (2015) The geochemistry of carbonate diagenesis: the past, present and future. *Sedimentology*, **62**, 1233–1304.

Tajika, E. (1999) Carbon cycle and climate change during the Cretaceous inferred from a biogeochemical carbon cycle model. *Island Arc.*, **8**, 293–303.

Takahashi, A. (2005) Diversity changes in Cretaceous inoceramid bivalves of Japan. *Paleontol. Res.*, **9**, 217–232.

Takashima, R., Nishi, H., Yamanaka, T., Hayashi, K., Waseda, A., Obuse, A., Tomosugi, T., Deguchi, N. and **Mochizuki, S.** (2010) High-resolution terrestrial carbon

isotope and planktic foraminiferal records of the Upper Cenomanian to the Lower Campanian in the Northwest Pacific. *Earth Planet. Sci. Lett.*, **289**, 570–582.

Takashima, R., Nishi, H., Yamanaka, T., Tomosugi, T., Fernando, A.G., Tanabe, K., Moriya, K., Kawabe, F. and **Hayashi, K.** (2011) Prevailing oxic environments in the Pacific Ocean during the mid-Cretaceous Oceanic Anoxic Event 2. *Nat. Commun.*, **2**, 234, doi:10.1038/ncomms1233.

Tappan, H. (1980) Haptophyta, coccolithophores and other calcareous nannoplankton. *The Paleobiology of Plant Protista* (Ed. H. Tappan), pp. 678–803. Freeman, San Francisco.

Toshimitsu, S., Matsumoto, T., Noda, M., Nishida, T. and **Maiya, S.** (1995) Towards an integrated mega-, micro- and magneto-stratigraphy of the Upper Cretaceous in Japan. *J. Geol. Soc. Japan*, **101**, 19–29 (in Japanese with English abstract).

Tsikos, H., Jenkyns, H.C., Walsworth-Bell, B., Petrizzo, M.R., Forster, A., Kolonic, S., Erba, E., Premoli-Silva, I.P., Baas, M., Wagner, T. and **Sinninghe Damsté, J.S.** (2004) Carbon-isotope stratigraphy recorded by the Cenomanian – Turonian Oceanic Anoxic Event: correlation and implications based on three key localities. *J. Geol. Soc. London*, **161**, 711–719.

Tsuchiya, K., Hasegawa, H. and **Pratt, L.M.** (2003) Stratigraphic relationship between diagnostic carbon isotope profiles and inoceramid biozones from the Yezo Group, Hokkaido, Japan. *J. Geol. Soc. Japan*, **109**, 30–40 (in Japanese with English abstract).

Uličný, D., Hladíková, J. and **Hradecká, L.** (1993) Record of sea-level changes, oxygen depletion and the $\delta^{13}C$ anomaly across the Cenomanian-Turonian boundary, Bohemian Cretaceous Basin. *Cret. Res.*, **14**, 211–234.

Uličný, D., Laurin, J. and **Čech, S.** (2009) Controls on clastic sequence geometries in a shallow-marine, transtensional basin: the Bohemian Cretaceous Basin, Czech Republic. *Sedimentology*, **56**, 1077–1141.

Uličný, D., Jarvis, I., Gröcke, D.R., Čech, S., Laurin, J., Olde, K., Trabucho-Alexandre, J., Švábenická, L. and **Pedenychouk, N.** (2014) A high-resolution carbon-isotope record of the Turonian stage correlated to a siliciclastic basin fill: implications for mid-Cretaceous sea-level change. *Palaeogeogr. Palaeoclimatol. Palaeoecol.*, **405**, 42–58.

Uramoto, G.-I., Abe, Y. and **Hirano, H.** (2009) Carbon isotope fluctuations of terrestrial organic matter for the Upper Cretaceous (Cenomanian–Santonian) in the Obira area of Hokkaido, Japan. *Geol. Mag.*, **146**, 761–774.

Uramoto, G.-I., Tahara, R., Sekiya, T. and **Hirano, H.** (2013) Carbon isotope stratigraphy of terrestrial organic matter for the Turonian (Upper Cretaceous) in northern Japan: implications for ocean–atmosphere $\delta^{13}C$ trends during the mid-Cretaceous climatic optimum. *Geosphere*, **9**, 355–366.

Uramoto, G.I., Tahara, R. and **Hiranio, H.** (2015) Cretaceous carbon isotope stratigraphy and constraints on the sedimentary patterns of the Turonian forearc successions in Hokkaido, nothern Japan. In: *Chemostratigraphy: Concepts, Techniques, and Applications* (Ed. M. Ramkumar), pp. 173–183. Elsevier, Amsterdam.

Valečka, J. and **Skoček, V.** (1991) Late Cretaceous lithoevents in the Bohemian Cretaceous Basin, Czechoslovakia. *Cret. Res.*, **12**, 561–577.

Veizer, J., Ala, D., Azmy, K., Bruckschen, P., Buhl, D., Bruhn, F., Carden, G.A.F., Diener, A., Ebneth, S., Godderis, Y., Jasper, T., Korte, G., Pawellek, F., Podlaha, O.G. and **Strauss, H.** (1999) $^{87}Sr/^{86}Sr$, $\delta^{13}C$ and $\delta^{18}O$ evolution of Phanerozoic seawater. *Chem. Geol.*, **161**, 59–88.

Voigt, S. (1995) Palaeobiogeography of early Late Cretaceous inoceramids in the context of a new global palaeogeography. *Cret. Res.*, **16**, 343–356.

Voigt, S. (2000a) Cenomanian-Turonian composite $\delta^{13}C$ curve for Western and Central Europe: the role of organic and inorganic carbon fluxes. *Palaeogeogr. Palaeoclimatol. Palaeoecol.*, **160**, 91–104.

Voigt, S. (2000b) Stable oxygen and carbon isotopes from brachiopods of southern England and northwestern Germany: estimation of Upper Turonian palaeotemperatures. *Geol. Mag.*, **137**, 687–703.

Voigt, S. and **Hilbrecht, H.** (1997) Late Cretaceous carbon isotope stratigraphy in Europe: correlation and relations with sea level and sediment stability. *Palaeogeogr. Palaeoclimatol. Palaeoecol.*, **134**, 39–59.

Voigt, S. and **Wiese, F.** (2000) Evidence for Late Cretaceous (Late Turonian) climate cooling from oxygen-isotope variations and palaeobiogeographic changes in Western and Central Europe. *J. Geol. Soc. London*, **157**, 737–743.

Voigt, S., Gale, A.S. and **Flogel, S.** (2004) Midlatitude shelf seas in the Cenomanian-Turonian greenhouse world: temperature evolution and North Atlantic circulation. *Paleoceanography*, **19**, PA4020. doi:10.1029/2004PA001015.

Voigt, S., Gale, A.S. and **Voigt, T.** (2006) Sea-level change, carbon cycling and palaeoclimate during the Late Cenomanian of northwest Europe; an integrated palaeoenvironmental analysis. *Cret. Res.*, **27**, 836–858.

Voigt, S., Aurag, A., Leis, F. and **Kaplan, U.** (2007) Late Cenomanian to Middle Turonian high-resolution carbon isotope stratigraphy: new data from the Münsterland Cretaceous Basin, Germany. *Earth Planet. Sci. Lett.*, **253**, 196.

Voigt, S., Erbacher, J., Mutterlose, J., Weiss, W., Westerhold, T., Wiese, F., Wilmsen, M. and **Wonik, T.** (2008) The Cenomanian-Turonian of the Wunstorf section (North Germany): global stratigraphic reference section and new orbital time scale for Oceanic Anoxic Event 2. *Newsl. Stratigr.*, **43**, 65–89.

Voigt, S., Friedrich, O., Norris, R.D. and **Schoenfeld, J.** (2010) Campanian–Maastrichtian carbon isotope stratigraphy: shelf-ocean correlation between the European shelf sea and the tropical Pacific Ocean. *Newsl. Stratigr.*, **44**, 57–72.

Walaszczyk, I. and **Cobban, W.A.** (2000) Inoceramid faunas and biostratigraphy of the Upper Turonian–Lower Coniacian of the Western Interior of the United States. *Spec. Pap. Palaeontol.*, **64**, 1–118.

Walaszczyk, I. and **Peryt, D.** (1998) Inoceramid-foraminiferal biostratigraphy of the Turonian through Santonian deposits of the Middle Vistula Section, Central Poland. *Zent. Geol. Paläontol.*, **I, 11/12**, 1501–1513.

Walaszczyk, I., Wood, C.J., Lees, J.A., Peryt, D., Voigt, S. and **Wiese, F.** (2010) The Salzgitter-Salder Quarry (Lower Saxony, Germany) and Słupia Nadbrzeżna river cliff section (central Poland): a proposed candidate composite Global Boundary Stratotype Section and Point for the Coniacian Stage (Upper Cretaceous). *Acta Geol. Pol.*, **60**, 445–477.

Walaszczyk, I., Lees, J.A., Peryt, D., Cobban, W.A. and **Wood, C.J.** (2012) Testing the congruence of the macrofossil versus microfossil record in the Turonian-Coniacian boundary succession of the Wagon Mound-Springer composite section (NE New Mexico, USA). *Acta Geol. Pol.*, **62**, 581–594.

Walaszczyk, I., Shank, J.A., Plint, A.G. and **Cobban, W.A.** (2014) Interregional correlation of disconformities in Upper Cretaceous strata, Western Interior Seaway: biostratigraphic and sequence-stratigraphic evidence for eustatic change. *GSA Bull.*, **126**, 307–316.

Walker, J.C.G. (1986) Global geochemical cycles of carbon, sulfur and oxygen. *Mar. Geol.*, **70**, 159–174.

Wang, C.S., Hu, X.M., Jansa, L., Wan, X.Q. and **Tao, R.** (2001) The Cenomanian – Turonian anoxic event in southern Tibet. *Cret. Res.*, **22**, 481–490.

Wedepohl, K.H. (1971) Environmental influences on the chemical composition of shales and clays. In: *Physics and Chemistry of the Earth* (Eds L.H. Ahrens, F. Press, S.K. Runcorn and H.C. Urey), Vol. 8, pp. 307–333. Pergamon, Oxford.

Weissert, H., Lini, A., Föllmi, K.B. and **Kuhn, O.** (1998) Correlation of Early Cretaceous carbon isotope stratigraphy and platform drowning events: a possible link? *Palaeogeogr. Palaeoclimatol. Palaeoecol.*, **137**, 189–203.

Weissert, H., Joachimski, M. and **Sarnthein, M.** (2008) Chemostratigraphy. *Newsl. Stratigr.*, **42**, 145–179.

Wendler, I. (2013) A critical evaluation of carbon isotope stratigraphy and biostratigraphic implications for Late Cretaceous global correlation. *Earth-Sci. Rev.*, **126**, 116–146.

Wendler, J.E. and **Wendler, I.** (2016) What drove sea-level fluctuations during the mid-Cretaceous greenhouse climate? *Palaeogeogr. Palaeoclimatol. Palaeoecol.*, **441**, 412–419.

Wendler, I., Wendler, J., Graefe, K.U., Lehmann, J. and **Willems, H.** (2009) Turonian to Santonian carbon isotope data from the Tethys Himalaya, southern Tibet. *Cret. Res.*, **30**, 961–979.

Wendler, I., Willems, H., Graefe, K.-U., Ding, L. and **Luo, H.** (2011) Upper Cretaceous inter-hemispheric correlation between the Southern Tethys and the Boreal: chemo- and biostratigraphy and paleoclimatic reconstructions from a new section in the Tethys Himalaya, S-Tibet. *Newsl. Stratigr.*, **44**, 137–171.

Wendler, I., Huber, B.T., MacLeod, K.G. and **Wendler, J.E.** (2013) Stable oxygen and carbon isotope systematics of exquisitely preserved Turonian foraminifera from Tanzania – understanding isotopic signatures in fossils. *Mar. Micropaleontol.*, **102**, 1–33.

Werne, J.P. and **Hollander, D.J.** (2004) Balancing supply and demand: controls on carbon isotope fractionation in the Cariaco Basin (Venezuela) Younger Dryas to present. *Mar. Chem.*, **92**, 275–293.

Wiese, F. (1997) Das Turon und Unter-Coniac im nordkantabrischen becken (Provinz Kantabrien, Nordspanien): faziesentwicklung, bio-, event- und sequenzstratigraphie. *Berlin Geowiss. Abh. Reihe E*, **24**, 1–131.

Wiese, F. (1999) Stable isotope data ($\delta^{13}C$, $\delta^{18}O$) from the Middle and Upper Turonian (Upper Cretaceous) of Liencres (Cantabria, northern Spain) with a comparison to northern Germany (Söhlde & Salzgitter-Salder). *Newsl. Stratigr.*, **37**, 37–62.

Wiese, F. and **Kaplan, U.** (2001) The potential of the Lengerich section (Münster Basin, northern Germany) as a possible candidate Global boundary Stratotype Section and Point (GSSP) for the Middle/Upper Turonian boundary. *Cret. Res.*, **22**, 549–563.

Wiese, F. and **Voigt, S.** (2002) Late Turonian (Cretaceous) climate cooling in Europe: faunal response and possible causes. *Geobios*, **35**, 65–77.

Wiese, F., Čech, S., Ekrt, B., Košťák, M., Mazuch, M. and **Voigt, S.** (2004) The Upper Turonian of the Bohemian Cretaceous Basin (Czech Republic) exemplified by the Úpohlavy working quarry: integrated stratigraphy and palaeoceanography of a gateway to the Tethys. *Cret. Res.*, **25**, 329–352.

Wohlwend, S., Hart, M. and **Weissert, H.** (2015) Ocean current intensification during the Cretaceous oceanic anoxic event 2 – evidence from the northern Tethys. *Terra Nova*, **27**, 147–155.

Wonders, A.A.H. (1992) Cretaceous planktonic foraminiferal biostratigraphy, Leg 122, Exmouth Plateau, Australia. In: (Eds von Rad U. and B.U. Haq), *Proc. ODP Sci. Res.*, **122**, 587–599. Ocean Drilling Program, College Station, TX.

Wood, C.J., Ernst, G. and **Rasemann, G.** (1984) The Turonian–Coniacian stage boundary in Lower Saxony (Germany) and adjacent areas: the Salzgitter–Salder Quarry as a proposed international standard section. *Bull. Geol. Soc. Denmark*, **33**, 225–238.

Zhou, J., Poulsen, C.J., Pollard, D. and **White, T.S.** (2008) Simulation of modern and middle Cretaceous marine $\delta^{18}O$ with an ocean-atmosphere general circulation model. *Paleoceanography*, **23**, PA3223, doi:10.1029/2008PA001596.

Ziveri, P., Stoll, H., Probert, I., Klass, C., Geisen, M., Ganssen, G. and **Young, J.** (2003) Stable isotope 'vital

effects' in coccolith calcite. *Earth Planet. Sci. Lett.*, **210**, 137–149.

Zonneveld, K.A.F., Versteegh, G.J.M., Kasten, S., Eglinton, T.I., Emeis, K.C., Huguet, C., Koch, B.P., de Lange, G.J., de Leeuw, J.W., Middelburg, J.J., Mollenhauer, G., Prahl, F.G., Rethemeyer, J. and **Wakeham, S.G.** (2010) Selective preservation of organic matter in marine environments; processes and impact on the sedimentary record. *Biogeosciences*, **7**, 483–511.

Supporting Information

Additional Supporting Information may be found in the online version of this article:

Table S1. Macrofossil biostratigraphic markers in the Bch-1 borehole, Běchary, Czech Republic, according to S. Čech in Olde *et al.* (2015b).
Table S2. Age control points for the Bch-1 borehole.
Appendix S1. Biostratigraphy and age control.
Appendix S2. Analytical methods.
Appendix S3. Stable isotope and total organic carbon compositions of Bch-1 sediment samples.